Novel and Green Hypergolic Bi-Propellant System for Propulsion Application

P.A.W. van Dommelen

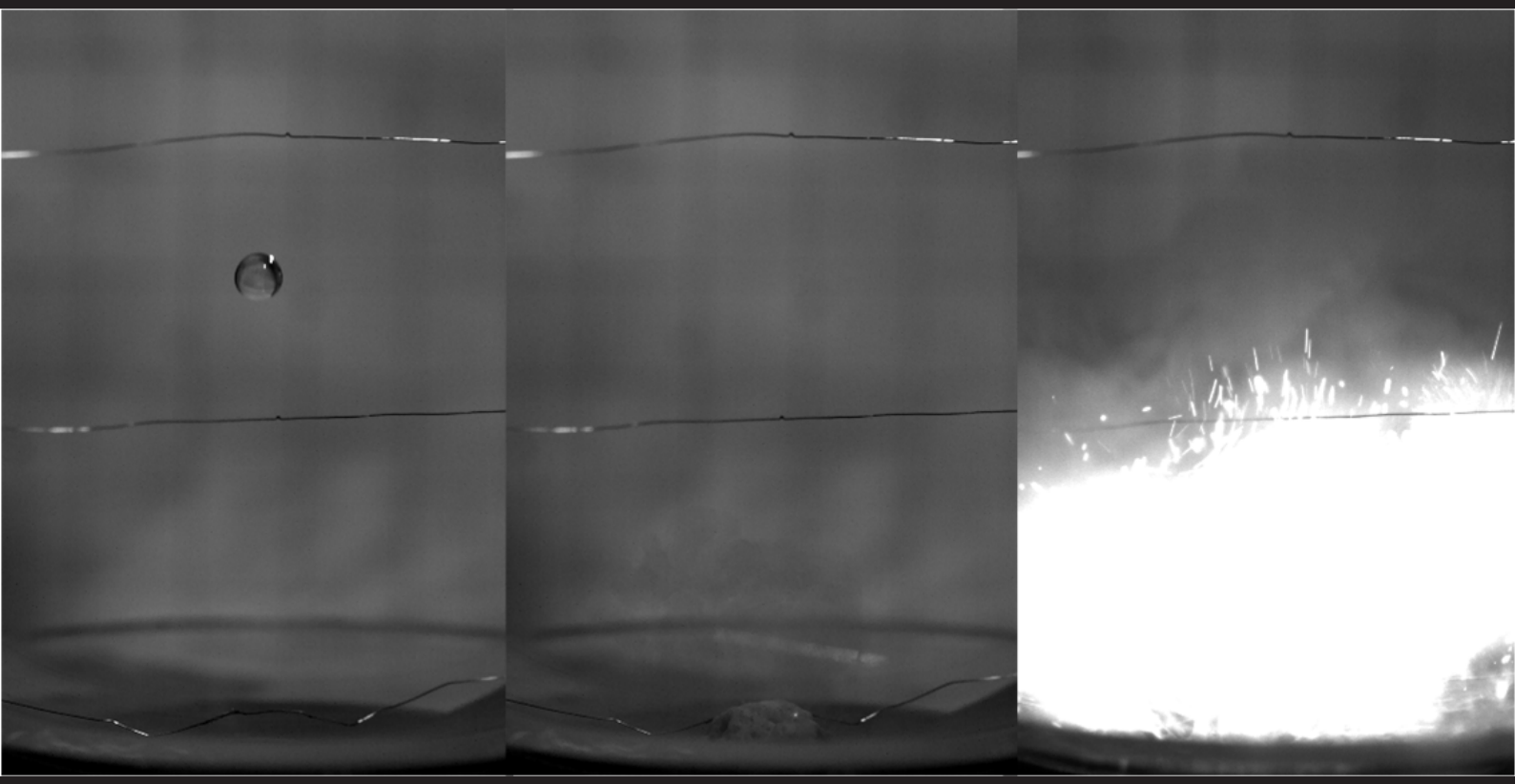

TU Delft

Novel and Green Hypergolic Bi-Propellant System for Propulsion Application

by

P.A.W. van Dommelen

to obtain the degree of Master of Science
at the Delft University of Technology,
to be defended publicly on Tuesday May 4, 2021 at 9:00 AM.

Student number:	4345673	
Project duration:	September 7, 2020 – May 4, 2021	
Thesis committee:	Prof. dr. E.K.A. Gill,	TU Delft, chairman of committee
	Dr. B.V.S. Jyoti,	TU Delft, supervisor
	Ir. R. Noomen,	TU Delft

This thesis is confidential and cannot be made public until November 4, 2021.

TU Delft

Preface

This report represents the work performed during my thesis to obtain the degree of Master of Science from the faculty of Aerospace Engineering at the Delft University of Technology. During the whole duration of the project, the world was facing the Covid crisis. This made it challenging to find motivation at times where human contact should be reduced to a minimum and working from home was the norm. Especially during these times I was enormously lucky to receive help and support from the people around me. To them I would like to show my gratitude.

Firstly, I would like to thank my supervisor and mentor B.V.S. Jyoti. Without her energy and dedicated involvement this thesis would not have been accomplished. I truely appreciate all the time she spend on this project and I have learned a whole lot from her input and feedback. I was fortunate to be one of the few people still allowed to visit the university during this time. The facilities made available to me by the university are the basis of this work. I want to extent my thanks to everyone at the DASM laboratory. Especially to Johan Bijleveld for helping me design my experiments and Durga Marineli for continuously supporting me during my lab work. Also the other people from the lab were always helpful when I needed or had trouble with some equipment. I would also like to thank Satya Ammu and Kunal Masania for the helpful discussions and input regarding the rheology part of my thesis as well as Armand Middeldorp for letting me use the rheometer in the Waterlab at the faculty of Civil Engineering and Geosciences. This thesis was performed as a part of SolvGE. They were able to provide me with an office at the university and a great working atmosphere. To the guys from SolvGE, Jaime, Pranav and Tommy, thanks for showing me around in the lab, supporting me where necessary, and being a great company.

Then I would like to thank my family and friends for supporting me during this last phase of my education. The evenings and weekends I spend with you helped me to relax and get my mind off work. It gave me all the energy and motivation I needed to keep moving forward. A special thanks goes out to my girlfriend Veronika for always supporting me, even when I am at my worst, and encouraging me to reach my goals.

P.A.W. van Dommelen
Eindhoven, March 2021

Abstract

Some propellants currently used in space propulsion have the disadvantage of being dangerous to humans and the environment. A well-known example of this are hydrazine and its derivatives which are toxic, corrosive, and carcinogenic. These disadvantages have led to a search for less hazardous storable liquid propellants, often referred to as green propellants. A green propellant is safer to use and handle and will therefore bring down the costs related to production, storage and handling. The main reason for the use of hydrazine is its hypergolicity with common oxidizers like NTO and nitric acid. Hypergolicity is the property that a fuel and oxidizer ignite spontaneously when brought in contact without the need for an external source. This property is beneficial since it eliminates the need for an ignition system, thereby making the propulsion system more simple, reliable, and cheaper. It is therefore desired that a replacement propellant also shows this property with common oxidizers.

During this thesis two methods are explored with the goal of creating a green hypergolic propellant combination. One based on catalytically enhanced ethanol and high concentration hydrogen peroxide. The other based on a pyrophoric liquid that is added to ethanol. There have already been efforts made before by adding catalyst particles or a strong reducer to a hydrocarbon fuel like kerosene or ethanol. The problem with using catalyst or strong reducer particles is the difficulty of creating a homogeneous mixture. Due to the liquid nature of the parent fuel, the particles will start to separate from the fuel and sink to the bottom of the container. To overcome this problem an organic gelling agent is added to the fuel to increase its viscosity, thereby increasing the sedimentation time. This will not only increase the shelf life of the fuel but also decrease the vapor pressure, making it less flammable and safer to work with, and reduce storage problems like propellant sloshing and spilling. Increasing the viscosity also makes it more difficult to transfer the fuel through the feed system and achieve proper atomization. However, by applying shear force on the fuel it shows shear thinning behavior, decreasing the viscosity close to that of the parent properties making it easy to use in existing propulsion systems designed for liquids. A second effect of the organic gelling agent is that due to its energetic nature it participates in the combustion. Therefore, the amount of catalyst needed can be reduced to a negligible amount while still achieving good performance properties like ignition delay time. This is verified by means of a drop test.

As a second approach, instead of adding solid catalyst particles a pyrophoric liquid is added to ethanol. A liquid allows for easier mixing and creating of a homogeneous mixture resulting in a longer shelf life compared to using catalyst particles. The pyrophoric liquid also fully participates in combustion resulting in increased performance compared to catalyst particles that do not combust. Due to the reactive nature of the pyrophoric liquid this propellant formulation is expected to be able to achieve hypergolicity with multiple common oxidizers. This results in a versatile system which can be used in current propulsion systems without extensive modification required. By eliminating the need for an ignition system, the propulsion system is simplified and its reliability is increased.

Contents

List of Figures

List of Tables

List of Abbreviations and Symbols

Abbreviations

Abbreviation	Description
CoAcac	Cobalt (II) Acetylacetonate
CuCl	Copper (II) Chloride
CuClH	Copper Chloride Hydrous
DASML	Delft Aerospace Structures and Materials Laboratory
DAQ	Data Acquisition system
DEZ	Diethylzinc
EtOH	Ethanol
HEX	Hexane
HSC	High Speed Camera
HTP	High Test Peroxide
JP-10	Jet Propellant-10
MMH	Monometlylhydrazine
MnAcac	Manganese (II) Acetylacetonate
NI	National Instruments
NTO	Nitrogen Tetroxide
PD	Photodiode
PFV	Photron Fastcam Viewer
PPE	Personal Protection Equipment
TEA	Triethylaluminum
TEB	Triethylborane
TC	Thermocouple
TMA	Trimethylaluminum
UDMH	Unsymmetrical dimethylhydrazine
Visc. Eth.	Viscous Ethanol

Symbols

Symbol	Description	Unit
A	Pre-exponential factor	[-]
E_a	Activation Energy	[J/mol]
G	Modulus	[Pa]
GMW	Gram Molecular Weight	[g]
ID	Ignition Delay	[ms]
k	Reaction rate constant	[-]
K_γ	Strain constant	[-]
K_τ	Stress constant	[-]
M	Torque	[N.m]
R	Universal gas constant	[J/K.mol]
T	Temperature	[K]
wt%	Weight percent	[%]
γ	Shear strain	[-]
$\dot{\gamma}$	Shear rate	[1/s]
ΔH	Standard enthalpy	[kJ/mol]
η	Viscosity	[Pa.s]
Θ	Angular displacement	[rad]
$\dot{\Theta}$	Angular velocity	[rad/s]
ρIsp	Density specific impulse	[Kg.s/m^3]
τ	Shear stress	[Pa]

1 Introduction

This Chapter will provide an introduction to the research topic of this thesis. Some background information is given on ignition in a rocket engine with a focus on hypergolic ignition in section 1.1. Then in section 1.2 the importance of propellant choice is discussed in terms of safety for humans and the environment. This thesis is written in collaboration with the start-up company SolvGE. A short introduction of SolvGE will be given in section 1.3. Based on the background information a research objective is formulated is section 1.4 accompanied by some research questions. Finally, section 1.5 presents the structure of this report.

1.1. Hypergolicity

To start the combustion of propellants in a combustion chamber of a rocket engine the propellants usually require an external stimulus. The ignition system consists of the hard- and software necessary to give this stimulus and initiate combustion of the fuel and oxidizer. It can achieve this by raising the propellant temperature high enough to allow for self-sustained combustion. The amount of energy required for this temperature raise depends on the properties of the propellants used and on the size of the combustion chamber. Once combustion is achieved the ignition system is no longer active since the heat released from the combustion will keep itself going. Only when a restart is necessary the ignition system is used again. Various methods exist that can be used for ignition. Some of the most used include pyrotechnic, pyrogen, spark plug, catalyst bed, hypergolic, or a laser ignition system. Out of these ignition options hypergolic ignition is the most favorable for a number of reasons. Hypergolic ignition can be achieved by specific combinations of fuel and oxidizer. Here an external source is not needed to ignite the mixture. Instead it ignites spontaneously at room temperature when brought in contact with each other. Since no external ignition force is required, hypergolic mixtures only need a simple valve to mix the fluids and start ignition. Using only a valve as ignition system is a very low complexity method since it requires only very few parts. Other ignition methods achieve ignition in multiple steps (pyrotechnic and pyrogen), require an electrical circuit (pyrotechnic, pyrogen, spark plug, and laser), or are based on a complex geometrical structure (catalyst bed). Having additional steps or components increases the parts of the ignition system that can fail, thus decreasing its reliability. The simplicity of hypergolic ignition makes it very reliable, enables mass savings over other ignition methods, and makes it cheap [1, 2]. Another advantage is the ability to have unlimited restarts. Some ignition methods like pyrotechnic and pyrogen igniters can only be used once. For some uses, like a rocket stage, this is sufficient. For attitude control or orbit maneuvers a propulsion system is usually required to be restarted multiple times, thus eliminating the use of some ignition methods.

1.2. Green propellants

Unfortunately, hypergolicity is a property of the propellants used and can therefore not be applied in all cases. Some propellant combinations which are known to be hypergolic are listed in Table 1.1. Of these, hydrazine based propellants are the most widely used [1, 3].

Table 1.1: Common hypergolic propellant combinations [4, 5].

Oxidizer	**Fuel**
Oxygen	Triethylaluminum, Analine
Nitrogen tetroxide (NTO), Nitric acid	Hydrazine, monomethylhydrazine (MMH), Unsymmetrical dimethylhydrazine (UDMH)
Hydrogen peroxide (>60%)	Hydrazine-hydrate
Fluorine, chlorine trifluoride, and diflouroxide	Almost all fuels

A big disadvantage of these propellants is that they are toxic, corrosive, and carcinogenic [6]. To handle these toxic propellants excessive safety measures like personal protection equipment and special storage containers have to be used, see Figure 1.1. These measures add extra costs to the production and handling of the propellants. More environmentally friendly propellants already exist, like hydrogen, kerosene, or methane, but they do not have the property of being hypergolic with common oxidizers. Hydrazine does have this property and it is one of the main reasons for its use. Developing propellants with performance comparable to those of commonly used propellants while being non-toxic and environmentally benign is one of the main goals of current space science [7, 8].

Figure 1.1: Personal protection equipment and storage container required for handling toxic propellants [9].

In terms of oxidizers NTO and nitric acid are most often used in hypergolic systems. Like hydrazine, these propellants are corrosive and require special safety measures during storage and handling. Liquid oxygen is an excellent green oxidizer but it has the problem of having a very low boiling point. This induces additional challenges like cryogenic handling and storage. Hydrogen peroxide seems to have the best potential as a green oxidizer. It is non-toxic, has

environmentally friendly exhaust products, and is liquid at normal temperatures and pressures. Unfortunately, no single green fuel has been found to be hypergolic with hydrogen peroxide. Instead hydrocarbon fuels are enhanced with a catalyst or strong reducer to induce hypergolicity. This, however, also comes with challenges like stability and aging of the fuel. A less researched topic is the use of a pyrophoric liquid to induce hypergolicity. Due to the nature of a pyrophoric liquid it has the potential to ignite with many known oxidizers. During this thesis a new catalyst based fuel is developed that is hypergolic with hydrogen peroxide. Next to this an effort is made to create a hypergolic fuel using a pyrophoric liquid.

1.3. SolvGE

This thesis is performed in collaboration with SolvGE. This start-up company was founded by Dr. B.V.S. Jyoti who is an assistant professor at the Delft University of Technology and daily supervisor for this thesis. SolvGE is currently producing worlds first hydrogen peroxide printer. It is a device capable of producing very high concentrations hydrogen peroxide, also called high test peroxide (HTP), of up to >99,5%, on location. The portability of this device eliminates the need for transportation of HTP which is bound by strict regulations and is joined by high costs. The prototype available at the University of Delft made it possible for HTP to be used during this thesis, which would otherwise be impossible.

Although the founders of SolvGE have a background in space engineering, the company focuses on all potential markets related to hydrogen peroxide. The research performed during this thesis acts as an initial study for the development of a novel green hypergolic propellant combination. Eventually the goal of SolvGE is to develop a versatile propulsion system based on this novel propellant and HTP.

1.4. Research objective and questions

During this thesis, research will be performed in search for a novel green fuel that is hypergolic with hydrogen peroxide. To do this two approaches will be explored; through the use of a catalyst and a pyrophoric liquid. Although hypergolic fuels have been formulated in the past with the use of a catalyst, here an emphasis is laid on the reduction of the catalyst concentration to a negligible amount. This is done in an effort to reduce the negative effects of a catalyst. The research objectives are as follows:

- *To develop a novel hypergolic bipropellant system by adding a negligible amount of catalyst to ethanol and its characterization.*
- *To develop a novel hypergolic bipropellant system by adding a pyrophoric liquid to ethanol and its characterization.*

Based on these objectives four main research questions are defined. These questions including subquestions are listed below:

1. What available catalyst can be used to induce hypergolicity between ethanol and hydrogen peroxide?
   (a) What is the minimum catalyst concentration required to achieve hypergolicity?
   (b) What concentration of thickening agent is required to keep the catalyst particles suspended in ethanol?
   (c) Can the catalyst concentration be further reduced by addition of a thickening agent, while still achieving hypergolicity?

   (d) Can the catalyst concentration be further reduced by addition of metal particles, while still achieving hypergolicity?

2. To what extend does the addition of a thickening agent change the rheological properties of ethanol?

   (a) What is the effect of a thickening agent on the viscosity of ethanol?

   (b) How does a thickening agent affect the yield point, time dependent and temperature dependent behavior of ethanol?

3. Which pyrophoric liquid can be used to induce hypergolicity between ethanol and hydrogen peroxide?

   (a) What is the minimum concentration of pyrophoric liquid required to achieve hypergolicity?

   (b) Does the addition of a thickening agent aid in the stability of an ethanol fuel enhanced with a pyrophoric liquid?

4. What is the ignition delay for the developed propellants and how can the ignition be characterized?

   (a) What is the effect of parameters like catalyst or HTP concentration on the ignition delay?

   (b) What is the effect of a thickening agent on the ignition delay and ignition characterization?

   (c) What is the effect of aging on the ignition delay?

1.5. Report structure

To reach the objectives and answer the research questions defined for this thesis several steps are taken. First, in Chapter 2, findings in literature are presented which are relevant to the research topic. Here a focus is laid on previous research in creating a green hypergolic fuel, the use of hydrogen peroxide as an oxidizer, and the gellation of propellants. Then, in Chapter 3, fuels are formulated using catalysts available at the university and their hypergolicity with hydrogen peroxide is tested through experimentation. An effort is made to reduce the catalyst concentration by addition of a thickening agent or metal particles. The addition of a thickening agent changes the rheological properties of the fuel. The characterisation of this is performed in Chapter 4. Here the effect of a thickening agent on the viscosity, yield point, and time and temperature dependence of ethanol is analysed. In Chapter 5 an effort is made to formulate a fuel that is hypergolic with hydrogen peroxide by adding a pyrophoric liquid to ethanol. Due to the nature of pyrophoric liquids a dedicated experimental setup is developed for the transfer of these substances. Finally, in Chapter 6, drop tests are performed using the developed propellants to measure the ignition delay and maximum temperature during combustion. For these experiments also a dedicated test setup was developed.

2

Literature study

This Chapter contains a summary of the literature study performed for this thesis. Starting off, research was done into creating a green hypergolic propellant. Several methods have been studied which are presented in Section 2.1. Then in Section 2.2 a closer look will be given into the use of hydrogen peroxide as an oxidizer. Finally, the effects of gelling a propellant will be discussed in Section 2.3.

2.1. Green hypergolic research

A single green propellant which is hypergolic with common oxidizers has yet to be found. Instead research is performed on the addition of energetic particles to a hydrocarbon fuel to make it hypergolic with oxidizers such as hydrogen peroxide. Adding catalyst particles has been the topic of some studies [10, 11, 12, 13], as well as adding a strong reducer [14, 15, 16] or a pyrophoric liquid [17, 1, 18, 19]. In this Section some relevant results of these researches are described which are used as a basis for this thesis.

2.1.1. Catalyst particles

A catalyst can make a fuel hypergolic with hydrogen peroxide by speeding up its decomposition reaction. Since this reaction is exothermic the energy released can increase the temperature to above the auto-ignition point of the fuel. In a research by Cong et al. [10] small amounts of Mn(II), Mn(III), Co(II), Co(III), Fe(III), and Pd(II) salts were added to kerosene as an effort to make it hypergolic with H_2O_2. By performing open-cup tests it was found that Mn(II), Mn(III), and Co(II) salts exhibit the highest energy levels needed for ignition. Unfortunately, the salts have a low solubility in kerosene and thus did not create a homogeneous mixture. In case of all three catalysts hypergolic ignition was achieved with 96% hydrogen peroxide. Mixture ratios and delay times were not mentioned in this study. However, it was noted that after a storage period of 3 months the hypergolic fuel did not show any degradation.

Next to kerosene also ethanol has been the subject of some studies. Florczuk et al. [16] achieved hypergolic ignition between ethanol and 98% H_2O_2 by the addition of 2-ethylohexanoate cobalt (II). They reported ignition delays between 53 and 83 ms. Even though an adequate ID was achieved, it required 15% catalyst content. Such a large catalyst content significantly reduces the part of the fuel that actually undergoes combustion. This can result in a low performance since less energy is being released per kg of fuel. A study by M.S. Naseem et al. [13] shows that the ignition delay time for gelled ethanol containing 1 wt% of Copper chloride hydrous (CuClH) or Manganese (II) acetylacetonate (MnAcac) with hydrogen peroxide ranges

from 10 to 50 ms when multiple droplets of oxidizer are added. When only one droplet was added only the MnAcac sample showed ignition. The samples contained between 6% and 8% of gelling agent. The use of only 1% catalyst is already a great improvement compared to the fuel developed by Florczuk et al. However, the high percentage of gelling agent can cause some issues when pumping the propellant.

In an effort to improve the hypergolicity of ethanol with H_2O_2 without increasing the wt% of catalyst, energetic particles can be added to the mixture. In a study by B.V.S. Jyoti et al. [20] a comparison was made between pure and energized ethanol gel. All fuels here contained 4 wt% gelling agent and 1 wt% catalyst, which is either CuClH or MnAcac. In case of the energized fuels 4 wt% of either Aluminum (Al), Boron (B) or Carbon (C) nanoparticles were added. Drop test results show that generally mixtures containing MnAcac have a lower ignition delay time compared to mixtures containing CuClH. Overall, the observed ignition delay was between 1 and 30 ms which is comparable to existing hypergolic bipropellant systems [20]. The lowest ignition delay of 1.33 ms was achieved by combining gelled ethanol with 1 wt% MnAcac and 4 wt% B particles. From comparing these studies can be concluded that adding metal nanoparticles can have a positive effect on the hypergolicity of the system. Unfortunately, there is also a downside. In the combustion chamber the liquid part of the fuel will vaporize first. This leaves the solid particles which can agglomerate into larger particles [2]. Since the combustion of these large particles takes such a long time, they are frequently only partially combusted when they exit the combustion chamber. Next to this the particles can stick to the wall, thereby changing the dimensions of the combustion chamber and affecting its performance.

The use of adding a catalyst to a hydrocarbon fuel to make it hypergolic has also been investigated for hybrid rocket engines. In a study by J. John et al. [21] organic gellants have been added to liquid ethanol to solidify it. By solidifying the ethanol, it can be used for hybrid rocket applications while at the same time providing better mixing conditions with the catalyst. Three different catalysts were tested in this study: Copper (II) chloride (CuCl), manganese (III) acetylacetonate (MnAcac) and cobalt (II) acetylacetonate (CoAcac). During the fuel formulation phase both CuCl and CoAcac showed degradation of the gellant network and are therefor not suitable catalyst for this use. Adding MnAcac however showed to result in a stable fuel. The catalytically promoted ethanol was then tested on hypergolicity with 90% H_2O_2 by means of drop tests. Results showed an ignition delay time ranging from 49 to 307 ms depending on the catalyst concentration. 16 wt% of catalyst resulted in the lowest delay time where 9 wt% of catalyst showed the highest ignition delay time. In both cases 13 wt% of the fuel sample was made up of gellant.

2.1.2. Strong reducer

Instead of using catalyst particles to make a propellant combination hypergolic it is also possible to use a strong reducer, typically metal hydrides. When a strong reducer comes in contact with a strong oxidizer it can easily combust thereby igniting the main fuel. In an article by Kang et al. [14] a strong reducing agent is added to a hydrocarbon fuel to make it hypergolic with hydrogen peroxide. Focusing on performance, metal hydrides like lithium or beryllium compounds can be used as a reducing agent which, due to their low molecular weight, enhance rocket performance. Unfortunately, they are extremely expensive and difficult to handle which makes them not suitable to use in a green propellant. As an alternative sodium borohydride ($NaBH_4$) is used which has a lower performance but is safe to store, use and handle, and is the least expensive commercially available metal hydride [14]. Drop tests with a hydrocarbon

fuel containing 5 wt% $NaBH_4$ and hydrogen peroxide, ranging from concentrations of 90 wt% to 98 wt%, were performed. This resulted in ignition delay times varying with the concentration of hydrogen peroxide. The lowest ignition delay time, of 4 ms, was achieved by using 98 wt% hydrogen peroxide. 90 wt% H_2O_2 resulted in an ignition delay time of 13 ms. In a similar study by B. Natan et al. [15] sodium borohydride was added to gelled kerosene to make it hypergolic with 92% hydrogen peroxide. This resulted in an ignition delay time of less than 8 ms when using 7% $NaBH_4$ and 4% gelling agent. The main drawback of using strong reducers is their water sensitivity. Contact with water can neutralize their activity [16]. Therefore propellants containing strong reducing agents have to be stored under special water free conditions.

2.1.3. Pyrophoric liquid

A pyrophoric liquid has the property that it ignites spontaneously in air. This high reactivity with oxygen makes it a potential candidate to induce hypergolicity. In a research by T.W. Ryan et al. [17] the effect of pyrophoric additives on ignition delay, heat of combustion and reaction rates was studied. The pyrophoric liquids used were triethylaluminum (TEA) and trimethylaluminum (TMA) which were selected due to their high energy density and reactivity. TEA and TMA were mixed with a propellant called JP-10 (cyclopentadiene) in various ratios and subjected to ignition tests. It was found that in all cases the ignition delay and total reaction time were significantly reduced in comparison to neat JP-10. Also the temperature dependence of the ignition delay was lowered by two orders of magnitude resulting in a more reliable ignition independent of temperature. By performing drop and flow studies T.W. Ryan et al. also showed that the pyrophoric/JP-10 blends are much easier to handle than pure pyrophoric liquids.

Later in a study by S.M. Davis and N. Yilmaz [1] the thermochemical behaviour of TEA in combination with various hydrocarbons and oxidizers was studied. These include solvents like hexane, methanol, aniline, nitromethane, and nitropropane and oxidizers like liquid oxygen, nitrogen tetroxide, nitrous oxide, nitric acid, and liquified air. Fuels were formulated by adding a range of mass fractions TEA to a hydrocarbon after which a reaction was simulated with each oxidizer. Performance results showed that the addition of TEA to a hydrocarbon fuel has a very small effect on the ρIsp, suggesting that the wt% of TEA in the fuel has little influence on the thrust characteristics. This in turn allows for a small amount of TEA to be used, while still achieving a proper performance.

An effort to make kerosene hypergolic with hydrogen peroxide was made by A.A. Kozlov et al. [18]. Here a 'starter fuel' was used which is a mixture of two pyrophoric liquids; TEA and triethylborane (TEB). In a reaction with 84.5% hydrogen peroxide it was found that a minimum concentration of 13% starter fuel was required to achieve hypergolic ignition. With an increase in temperature the concentration starter fuel required for ignition will decrease. For ignition in vacuum conditions a higher concentration of starter fuel is required than for ignition in air. B.M. Melof et al. [19] performed a research on finding new hypergolic combinations with hydrogen peroxide. Most of the fuels studied were non-pyrophoric or enhanced with a catalyst, however, one pyrophoric liquid was used. Hypergolic ignition was achieved using a fuel consisting of 25% TEA in hexane with 90% hydrogen peroxide. No quantitative parameters were measured, although the reaction was indicated as very fast and with a very high ignition potential.

2.2. Hydrogen peroxide

In this section a closer look is given into hydrogen peroxide. Firstly a brief history is presented on its use, after which the most important properties are summarized. Then some information is given on its availability, storage and handling.

2.2.1. History

The use of hydrogen peroxide in rocketry dates back to the mid 1930's. German scientist Hellmuth Walter developed both mono- and bi-propellant rocket engines based on the use of hydrogen peroxide [22]. The most notable example from this time is the V-2 rocket developed by Germany during the second world war. Here H_2O_2 was used as a monopropellant gas generator to drive the turbo pumps of the V-2 [4]. Walter has experimented with various methods to decompose H_2O_2 like mixing it with a liquid catalyst (potassium permanganate), spraying it onto a lining containing a solid catalyst (manganese dioxide), or pumping it through a bed containing catalyst impregnated pellets [22]. Later, also the British employed H_2O_2 in their Black Arrow satellite launcher, where sliver was used as a catalyst. It was found that stabilisers present in the H_2O_2 contaminate the catalyst surface thereby reducing its effectiveness [22]. This effect is known as catalyst poisoning. Stabilisers were added to H_2O_2 to reduce its decomposition rate during storage. But even under favorable conditions H_2O_2 will still decompose at a slow rate, about 1% per year [23]. With the discovery of hydrazine as a propellant the use of H_2O_2 was reduced. In the period from 1985 to 1990 H_2O_2 was almost entirely unused in the space industry [24]. Hydrazine was favored due to its improved performance and since it does not suffer from the stability issues that H_2O_2 has. Only recently hydrogen peroxide has gained popularity due to its 'green' nature. As hydrazine is very toxic and corrosive it poses significant hazards when used. Hydrogen peroxide offers reduced risks during handling and storage which is seen as more and more important in the space industry.

2.2.2. Properties

Hydrogen peroxide is similar to water in its chemical formula (H_2O_2) but also in many physical properties like melting point, dielectric constant, and hydrogen bonding [25]. Its density is with 1.45 g/cm^3 about 1.5 times higher than that of water and it also has a higher viscosity and boiling point of $1.245 \cdot 10^{-3}$ Pa.s and 150^oC respectively [26]. At ambient conditions hydrogen peroxide is a colorless, transparent liquid with a slightly acidic odor in high concentrations. It is not flammable in any concentration [25]. The oxygen present in the peroxide group exists in an unstable oxidation state making H_2O_2 an excellent oxidizing agent [25]. Hydrogen peroxide almost always exists as a solution in water. Therefore hydrogen peroxide is usually given as a concentration (wt%) in water. Commercially available hydrogen peroxide has a concentration of around 30% [23] which has a too low energy content to be used for propulsion application. At a concentrations above approximately 67% the heat released during the decomposition of hydrogen peroxide is large enough to completely vaporize all the liquid. From this concentration, an increase in concentration results in an increased temperature of the generated gasses from decomposition. For propulsion applications it is therefore desired that the concentration of hydrogen peroxide is as high as possible. General concentrations used range from 85% to >99% and are known as high test peroxide (HTP). Figure 2.1 shows both the liquid-vapor and solid-liquid phase diagrams of hydrogen peroxide solutions in water. It shows that at concentrations above 74% violent decomposition can be triggered by raising the temperature. For higher concentrations a lower temperature is required. This effect can be dangerous and the HTP temperature during storage has to be maintained at a low level. On the other hand, this effect can also be used to initiate rapid decomposition of HTP for propulsion applications without the need for a catalyst, as has been explored in a thesis by J. Quesada [5]. When

examining the solid-liquid phase diagram it can be seen that the addition of one component to the other causes a decrease in the freezing point of the mixture. The minimum freezing point lies around -55^{o}C at a concentration of about 62%. However, since only high concentrations are suitable for use in propulsion applications the freezing point remains around 0^{o}C.

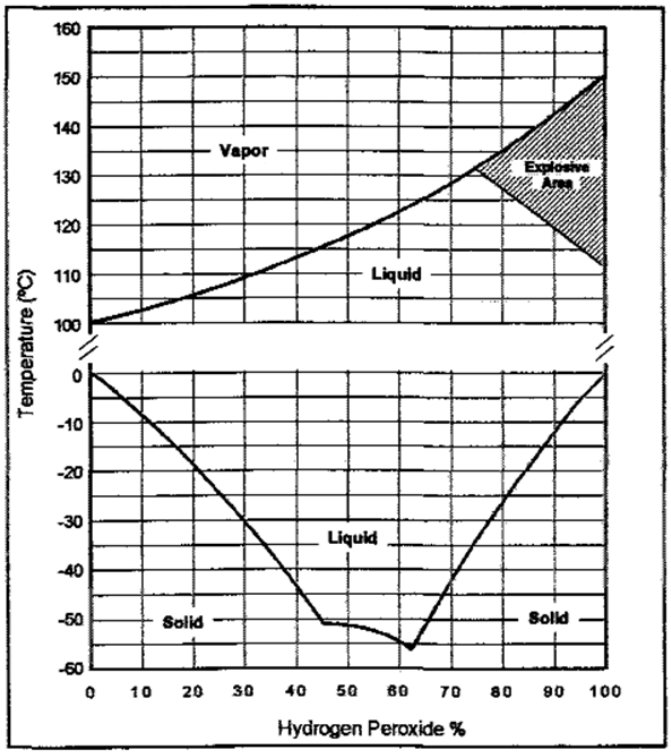

Figure 2.1: Liquid-vapor and solid-liquid phase diagrams for H_2O_2 solutions in water [25].

2.2.3. Availability, storage and handling

High test peroxide is only available for qualified buyers where lower concentrations can be purchased privately. Also in terms of transportation does the concentration play an important role. For concentrations below 8% no regulations apply, however for increasing concentrations the regulations become increasingly strict [27]. Over 40% hydrogen peroxide cannot be transported by plane. For road transport the regulations are a bit less strict, however for concentrations above 60% a dedicated transport is required. Because of these strict regulations it can be expensive and difficult to acquire high concentrations of hydrogen peroxide. Fortunately, for this thesis high test peroxide could be produced in-house by SolvGE.

During storage and handling of hydrogen peroxide an important consideration is the material selection. Many materials like brass, copper, nickel, iron, bronze, zinc, synthetic rubbers, and polypropylene are incompatible with hydrogen peroxide [28]. Some aluminum alloys and stainless steels can be used as well as Teflon. All surfaces that are in contact with hydrogen peroxide should be non-porous, smooth, and as free of impurities as possible to keep the decomposition reaction at a minimum. Containers used to store hydrogen peroxide should contain a vent through which gasses generated by decomposition can escape. When handling HTP personal protection equipment should be used. Hydrogen peroxide is non-toxic but is corrosive when it comes into contact with skin. By immediately pouring water over the affected area this effect can be stopped.

2.3. Gelling

Since often catalysts are not soluble in the parent fuel, mixing them does not result in a homogeneous mixture. This leads to poor performance due to the mixture having different properties at different locations. Another issue that comes with the use of liquid propellants is sloshing in the propellant tanks [29]. This results in asymmetrical load forces on the tank structure as well as difficulties in keeping the tank outlet covered with propellant at all times. Next to this, liquid propellants come with the possibility of leakage and spills during handling. Especially when hazardous propellants are used this is a big safety concern. To address these problems the propellant can be gelled thereby changing the visco-elastic properties of the fuel. A gel is a state of matter somewhere in between a liquid and a solid, depending upon the level of shear [30]. It can be created by the combination of a liquid solvent and a gelling or thickening agent. When mixed, the gelling agent forms a three-dimensional solid network structure which encloses the liquid phase [31] giving the fuel an increased viscosity. This enables the catalyst particles to be suspended in the fuel with a uniform distribution, without compromising on the energetic performance of the system [15]. An increased viscosity also reduces propellant sloshing, leaking and spilling, making the propellant safer to handle. Furthermore, propellants in a gelled form have a lower vapor pressure compared to their liquid form [32]. This makes them less flammable and therefore again safer and easier to handle. Various gelling agents exist which can be divided into two groups; organic and non-organic. In a study by G. Nachmoni and B. Natan [33] a non-organic gelling agent was used to make kerosene-based gel fuels. Here it was found that an increase in gelling agent resulted in an increase of heat of vaporization. This led to an increased ignition delay time and more heat required to achieve ignition. On the other hand, if an organic gelling agent is used it participates in the combustion and thereby releases energy which improves the performance of the gel system [13].

In general, a gel forms by following four steps; adding the gelling agent to the solvent, de-agglomeration of the gellant particles, swelling, and cross-linking. Figure 2.2 gives a schematic illustration of these four steps. When the gelling agent is introduced to the solvent it is still clumped together. By applying a shear force, by means of mechanical stirring or temperature increase, the gellant particles start to de-agglomerate. The result is a solution of homogeneously distributed gellant particles in the solvent. During rest, the gellant particles swell by absorbing liquid and clustering together. Between these clusters cross-links can be formed generating even bigger clusters and a network structure. These cross-links can be based on covalent, coulombic, hydrogen, coordination bonds or physical interactions, depending on the type of gellant used [30].

Based on the type of cross-linking bonds between the gellant clusters the gel can either have a reversible or irreversible nature. Gels formed by covalent bonding are irreversible due to its strong interaction. Weaker interactions like hydrogen or coordination bonds and physical interactions are reversible. The reversibility also means that the gel is less stable, which is a relevant property for storage and shelf life. Low stability of a gel could lead to evaporation of the fuel, separation of suspended particles, and the formation of decomposition products [30]. On the other hand, a low stability is very well suited for atomization of the propellant. Depending on the propellant requirements a trade-off has to be made here.

The most important properties of a gel are its rheological properties which include; viscosity, yield stress, thixotropy, and visco-elasticity. Gels can be categorized as non-Newtonian fluids, meaning it does not follow Newton's law of viscosity. This law states that a fluid has a constant viscosity independent of stress, gels thus do not have this property. The most direct way of

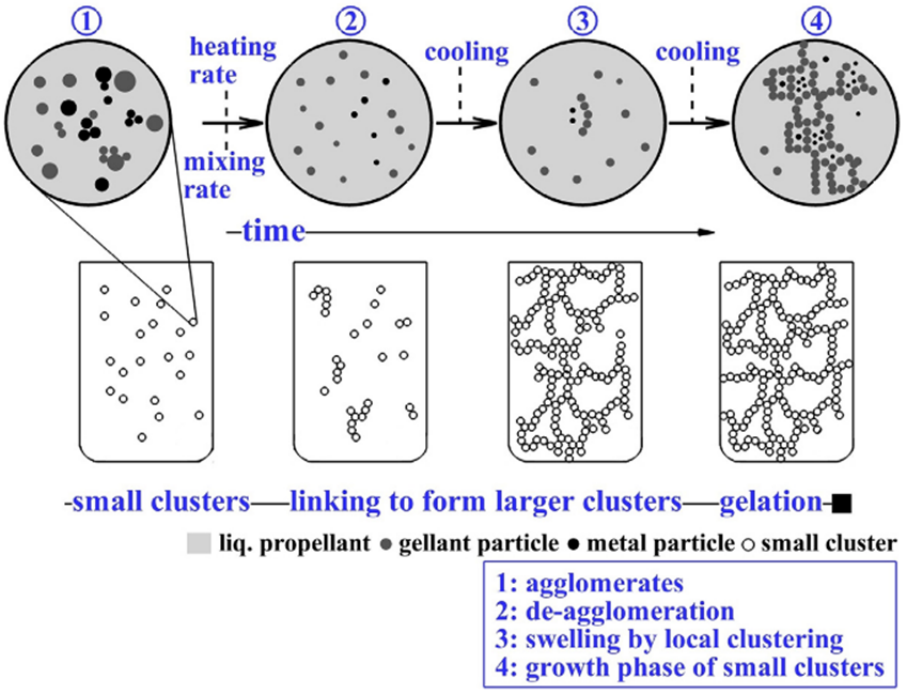

Figure 2.2: Steps in gel formation [30].

comparing the rheological properties of fluids is through the use of flow curves. These curves present the relationship between viscosity (η), shear stress (τ), and shear rate ($\dot{\gamma}$). Figure 2.3 shows an example of possible flow curves for Newtonian and non-Newtonian fluids. If the viscosity of a fluid decreases with increasing shear rate it is called 'shear thinning', where the opposite effect is called 'shear thickening'. Gels show a shear thinning behavior [30]. This means that at rest (e.g. in a propellant tank) the gel shows a high viscosity which is favorable since it allows the suspension of particles and counteracts sloshing. But when a shear rate is applied (e.g. during pumping) the viscosity decreases making it easier to pump the propellant. This effect can be explained by the way a gel is formed. As was mentioned before a gelling agent forms a 3D network structure in the solvent which gives it an increased viscosity. When a shear force is applied this network structure will break down, thereby decreasing the viscosity.

The properties of a gel that give it its advantages also come with some disadvantages. Even though gels can show good stability during storage, this stability can reduce gradually over long storage times [30]. The high stability can also pose challenges during pumping and injection of the fuel. An increased viscosity of the fuel leads to an increased pressure drop when pumping and counteracts the atomization process that should occur during injection. This can cause a loss of combustion stability [35]. The network structure of a gel traps the liquid propellant resulting in a delayed vaporization of the fuel, and thus a reduced burning rate. If an inorganic, non-combustible gelling agent is used the burning rate is even further reduced. Due to the reduced burning rate a longer combustion chamber is required to achieve a complete combustion, adding mass to the system. On top of this a non-combustible gellant can cause solid residue, injector clogging, combustion losses, and restart problems [30]. To minimize the negative effects of a gel propellant a minimum concentration of organic, combustible gelling agent should be used. A small concentration will result in less drastic changes in the rheolog-

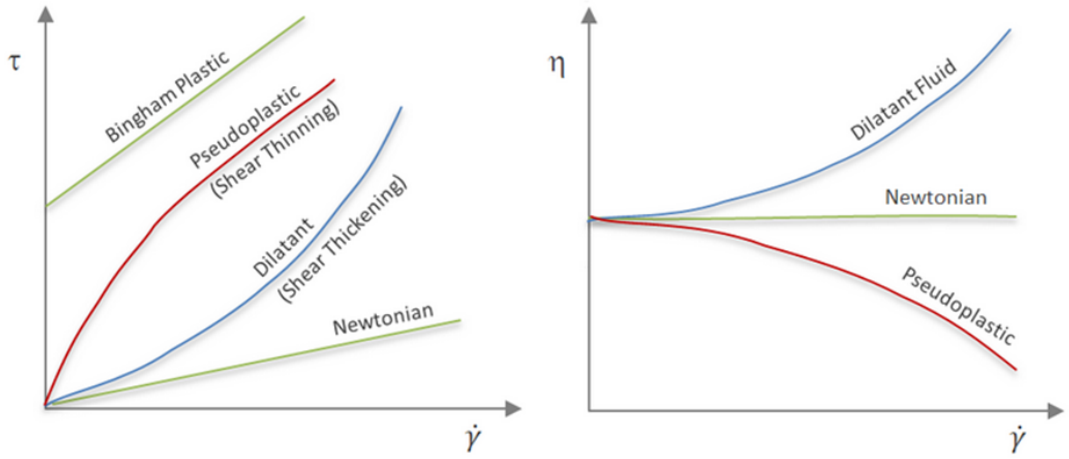

Figure 2.3: Flow curves for different classifications of fluids [34].

ical properties of the fuel and thus limit the negative effects while at the same time enabling suspension of particles in the fuel.

3

Hypergolicity investigation

In this Chapter an effort is made to make ethanol hypergolic with hydrogen peroxide. This is done by adding catalyst particles to ethanol which speed up the decomposition rate of hydrogen peroxide. Thirteen different catalyst candidates are considered and their hypergolic potential in ethanol with hydrogen peroxide is tested in section 3.2. Then to improve energetic content and mixing quality a thickening agent is added to ethanol. Section 3.3 goes into determining the optimal concentration of thickening agent. Using the most promising catalyst candidates and optimal concentration of thickening agent a number of experiments are performed in section 3.4. Here the concentration of catalyst is reduced until no or very slow ignition is observed. Finally in section 3.5 an effort is made to further reduce the catalyst concentration by adding energetic particle to the fuel.

3.1. Theory

When mixing hydrogen peroxide with ethanol no reaction occurs. Only when an external ignition source is available the mixture will ignite. The purpose of this thesis is, however, to create a hypergolic propellant combination based on hydrogen peroxide and ethanol. The key to achieving this is through the decomposition of hydrogen peroxide. Equation 3.1 shows this decomposition reaction. It has two important characteristics which are required for achieving hypergolicity. Firstly, the reaction is exothermic, meaning it releases heat. For 100% hydrogen peroxide the heat released through decomposition (ΔH) is -2884.5 kJ/kg at ambient pressure and a temperature of 25^{o}C [36]. The released heat increases the temperature of the hydrogen peroxide that is still present which increases the rate of decomposition making the reaction self-sustaining. When hydrogen peroxide is decomposing in the presence of ethanol, its temperature will also increase. To achieve ignition the temperature of ethanol has to be increased to above its auto-ignition point of 363^{o}C [37]. Then, once the ethanol is ignited, it undergoes a combustion reaction with oxygen to form water and carbon dioxide. The heat of combustion of this reaction is -29666 kJ/kg [38] which will further cause the temperature to increase, resulting in a self-sustaining combustion.

$$2H_2O_2 \rightarrow 2H_2O + O_2 + \Delta H \tag{3.1}$$

The second important characteristic noticed in Equation 3.1 is that when hydrogen peroxide decomposes it creates oxygen. The presence of oxygen is crucial since it is a vital component in combustion reactions. In Earth's atmosphere oxygen is naturally present, which is enough for a sustained combustion of ethanol. For space applications, however, this is not the case.

Here hydrogen peroxide can act as the oxidizing component of a bi-propellant system.

Since no reaction occurs when mixing hydrogen peroxide with ethanol a method has to be used to increase the decomposition rate of H_2O_2. Typically one of two approaches is used: increasing the temperature or adding a catalyst. How either of these approaches affects the reaction rate is expressed using the Arrhenius equation, shown below.

$$k = A \cdot exp(\frac{-E_a}{RT}) \tag{3.2}$$

In this equation k is the rate constant [-], A is the pre-exponential factor [-] which is a constant for each chemical reaction, E_a is the activation energy [J/mol] required for the reaction, R is the universal gas constant [8.3145 J/K mol], and T is the temperature [K]. Equation 3.2 shows that temperature has a direct effect on the reaction rate. At an increased temperature the molecules will have a higher energy and move faster. This increases the probability of collisions between molecules which can result in a decomposition reaction. How a catalyst can affect the reaction rate is expressed through the activation energy E_a. A catalyst is a substance that, when added to the reactants, can lower the activation energy. It does this by providing an alternative reaction mechanism that has a lower activation energy than the original reaction mechanism. Graphically this can be represented as in Figure 3.1. The catalyst, however, only acts as an intermediate step in the reaction process and thus remains unchanged. This means that the catalyst can be reused and the amount of catalyst required is usually low.

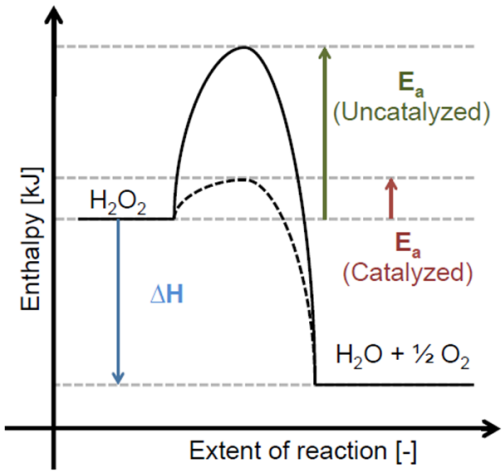

Figure 3.1: The effect of a catalyst on the activation energy required for the decomposition reaction of hydrogen peroxide [5].

In a propulsion system a catalyst is usually implemented in the form of a catalytic bed which consists of either pellets or screens. Here the goal is to have a large surface area in a small volume. Disadvantages of this implementation are that it requires complex adaptations to the combustion chamber and increases its size and mass. On top of that, a catalytic bed often causes a large pressure drop [4]. To compensate for this drop the propellants have to be stored at a higher pressure or the pressure has to be increased by the use of a pump. Both of these options increase the complexity of the system since components have to be designed to withstand an increased pressure. Instead of using a bed the catalyst can also be directly implemented by mixing it with either the fuel or oxidizer. In this case, since the catalyst speeds

up the decomposition of the oxidizer, it could be mixed with the fuel. Then, when both the fuel and oxidizer are injected into the combustion chamber, the catalyst particles present in the fuel will cause decomposition of the oxidizer resulting in ignition. This method has the advantage that it does not require any additional components or external ignition source and thus results in a less complex, more reliable combustion engine.

3.2. Liquid fuel

In an effort to make ethanol hypergolic with hydrogen peroxide a number of different catalysts were explored. Catalysts can be divided into three categories: heterogeneous, where the phase of the catalyst differs from that of the reactants, homogeneous, where the catalyst and reactants exist in the same phase, or enzymes, which are biological catalysts. All of these types can be used for the decomposition of hydrogen peroxide [39], however, this thesis will focus only on the use of heterogeneous catalysts. All catalysts used are in powder form and selected based on their availability in the Chemical lab of the DASML. This option is chosen since it does not require the purchase of new chemicals which costs time and money, and because a large number of catalyst candidates was already available in the lab. The catalysts selected are mainly coming from the transition metal family. Transition metals have the ability to form five or more chemical bonds, often have multiple accessible oxidation states, and have the tendency to accept electron pairs which makes them excellent catalysts [40]. Catalysts used are based on Fe, Cu, Zr, La, Ni, Zn, Mn, and Br. To determine the most promising candidate a screening is performed based on a number of steps. This section describes the first step of this process.

One fuel sample is created for each catalyst by mixing it with ethanol. For initial formulations a weight ratio is used of 90% ethanol to 10% catalyst. The eventual goal of the study is to find a formulation that shows hypergolicity while having the smallest possible concentration of catalyst. 10% catalyst is used as a starting point since it should give a good indication into which catalysts can be disregarded immediately. To formulate a fuel sample first 0.1 g of catalyst powder is transferred into a small container. This is done on a scale with a resolution of 10^{-4} g. Then, using a syringe, ethanol is added until the scale registers a weight of 1 gram. The sample is manually stirred to obtain a homogeneous mixture, and then labelled. This process is repeated for each of the selected catalysts. Some of the resulting fuel samples can be seen in Figure 3.2. After formulation of the fuel samples some important differences are already noticed. The two samples depicted on the left hand side of Figure 3.2 show a homogeneous solution where the catalyst has completely dissolved in the ethanol. Samples shown on the right hand side did not mix properly and catalyst particles quickly started to sink to the bottom of the container. For propulsion applications it is important that the fuel is a homogeneous mixture with equal properties irregardless of location in the fuel. If this is not the case it can lead to instabilities during pumping and combustion.

Now all fuel samples have been formulated, their hypergolicity with HTP can be tested simply by mixing the two together. First, however, the concentration of HTP has to be determined. As was already explained in Chapter 2 the concentration of HTP has a large influence on its performance as a propellant. Hydrogen peroxide used in these experiments is offered by SolvGE and is concentrated from 30% to around 90%. Every day before using HTP its concentration is measured using a refractometer. This device measures the refractive index of a liquid in ^{o}Brix. To transform the ^{o}Brix value to refractive index a table by ICUMSA is used [41]. Then based on data collected by P.A. Giguere and P.Geoffrion [42] on the refractive index of various concentrations of hydrogen peroxide the concentration can be determined. Data used

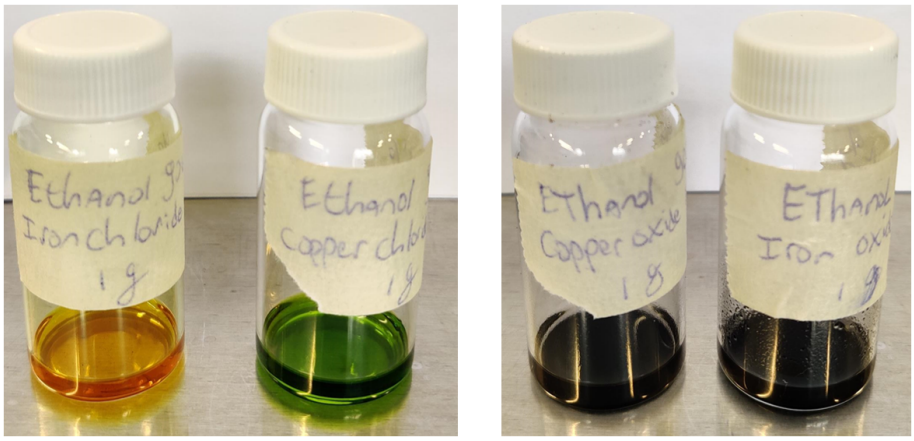

Figure 3.2: Examples of fuel samples created by mixing 90% ethanol with 10% catalyst.

and relations based on it can be found in Appendix C.1.

Now all preparations are done the tests are ready to be performed. 10 droplets of a fuel sample were transferred into a smaller reaction vessel using a syringe. Then, drop by drop the 90% HTP was added to the sample while recording everything with a mobile phone for later analysis. This process was repeated for each formulated fuel sample and the results can be found in Table 3.1. In this Table the potential of the catalyst is represented by a number ranging form 0 to 4. With 0 = no reaction, 1 = slow decomposition, 2 = fast decomposition, 3 = slow ignition, and 4 = fast ignition. Furthermore, the concentration HTP is noted and the mixing quality is indicated.

Table 3.1: Hypergolicity test results with 88-92% HTP and ethanol mixed with 10% catalyst.

#	Base	Potential	Observation	Notes
1	Fe	0	No reaction	92% HTP, Poor mixing
2	Fe	2	Fast decomposition	92% HTP, Good mixing
3	Cu	0	No reaction	92% HTP, Poor mixing
4	Cu	1	Slow decomposition	92% HTP, Good mixing
5	Cu	2	Fast decomposition	92% HTP, Saturated mixture
6	Cu	0	No reaction	92% HTP, Saturated mixture
7	Zr	0	No reaction	88% HTP, Saturated mixture
8	La	0	No reaction	88% HTP, Saturated mixture
9	Ni	0	No reaction	88% HTP, Saturated mixture
10	Mn	1	Slow decomposition	92% HTP, Poor mixing
11	Mn	4	Fast ignition	92% HTP, Poor mixing
12	Zn	0	No reaction	88% HTP, Good mixing
13	Br	1	Slow decomposition	88% HTP, Poor mixing

Quickly it becomes clear that most of the catalysts that were used can be discarded. Only three out of thirteen tested samples showed a high enough potential and will be used for further study. These include sample number 2, 5, and 11 and will from now on be indicated as FCAT, CCAT, and MCAT respectively. For comparison these tests are repeated using 1-butanol as main component instead of ethanol. Butanol is chosen since it has an auto ignition temperature of 314^{o}C which is lower than ethanol [43]. For these tests only the three most

promising candidates are used. Results can be found in Table 3.2. When looking at these results it is noticed that nothing has changed in terms of mixing conditions. In terms of hypergolic potential, however, some differences are observed. FCAT shows a higher potential with butanol than with ethanol. After adding HTP the mixture ignites after about 3 seconds, achieving slow ignition. CCAT again shows fast decomposition. MCAT seems to perform worse in combination with butanol. When a drop of HTP is added to this mixture fast decomposition is observed in combination with fumes and a spark. Then, when adding the fourth droplet HTP, the mixture ignites. MCAT still has a lower potential than FCAT since there only one drop was required for ignition.

Table 3.2: Hypergolicity test results with 88% HTP and butanol mixed with 10% catalyst.

Catalyst	Potential	Observation	Notes
FCAT	3	Slow ignition	88% HTP, Good mixing
CCAT	2	Fast decomposition	88% HTP, Saturated mixture
MCAT	2	Fast decomposition / Slow ignition	88% HTP, Poor mixing

3.3. Adding a thickening agent

Results presented in the previous section where liquid ethanol was used, showed some points of improvement. First of all there was only one out of thirteen catalyst candidates that showed fast ignition. With the goal to reduce the catalyst concentration as far as possible, while still achieving hypergolic ignition within a reasonable time, the results using liquid ethanol do not look very promising. The concentration catalyst used of 10% is relatively high and should, for a promising candidate, show ignition. On the other hand, mixing quality is also an issue. Only three out of thirteen candidates resulted in a good mixture with ethanol. Out of these three only one showed a high enough hypergolic potential. The other two candidates with a high potential did not mix properly or resulted in a saturated mixture with ethanol. If a fuel is not homogeneous this can result in instabilities in pumping and combustion, thus mixing has to be improved.

In an effort to address both these issues a thickening agent is added to ethanol. As discussed in Section 2.3 an organic gelling agent can participate in the combustion of the fuel. This means that it can make the fuel more energetic. Adding a gelling agent can have a positive effect on the performance of the fuel in terms of hypergolicity and ignition delay [44, 13]. On the other hand, the main reason of adding a thickening agent is to affect the visco-elastic properties of the fuel. Due to the network structure created by the thickening agent the fuel will have an increased viscosity. An advantage of this is that catalyst particles will be suspended in the fuel, resulting in a homogeneous mixture. A disadvantage is that an increase in viscosity also makes the fuel harder to be pumped through the feed system. More on this topic will be covered in Chapter 4. In an effort to achieve an increase in viscosity high enough to suspend particles but low enough that the fuel still acts as a liquid only a negligible amount of thickening agent is used.

Three different samples with a thickening agent added to ethanol were formulated. Since the goal is to add only a negligible amount it was chosen to use concentrations of 0.5%, 1%, and 1.5% thickening agent in ethanol. In total 20 grams of each sample was formulated. This was done by first measuring out the correct weight of thickening agent which was placed on

a plastic dish. Afterwards the same was done for ethanol which was placed in a 50 ml glass container. A magnetic stirring bar was added to the ethanol, and the container was placed on a magnetic stirrer. It was turned on and set to a velocity of 500 rpm. Then slowly the thickening agent was added. It is important to perform this step slowly to prevent the thickening agent from forming clumps. After all thickening agent was added the rpm was increased to 1000 and the sample was stirred for several hours. Stirring was completed when the sample showed a homogeneous mixture, without visible clumps. The three resulting samples can be found in Figure 3.3. Visually they are hard to distinguish from pure ethanol but the difference is noticed when tilting the containers.

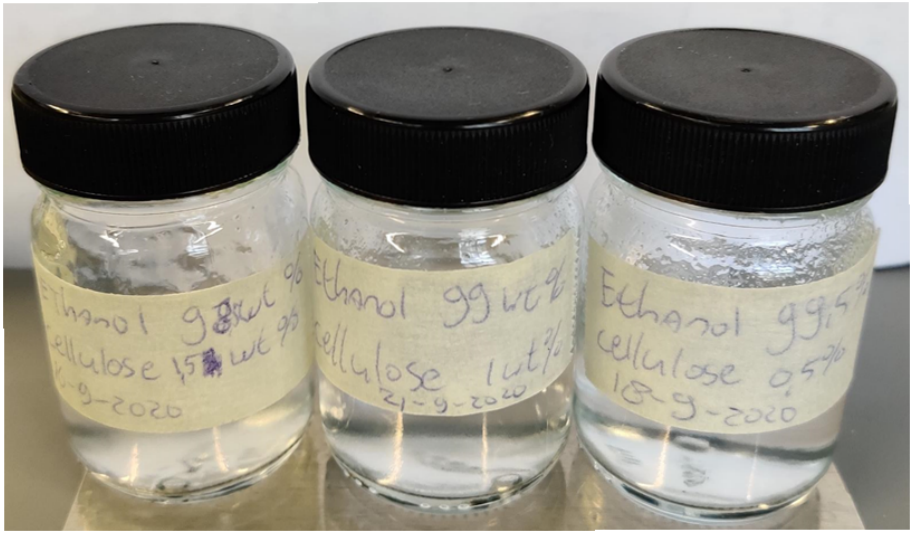

Figure 3.3: Samples created by mixing ethanol with 1.5%, 1%, and 0.5% thickening agent.

Now the same procedure as described in Section 3.2 is followed. Here, however, only the three catalyst candidates are used which showed promising behavior in the liquid ethanol experiments. FCAT, CCAT, and MCAT are used to create a fuel sample in combination with the three ethanol samples resulting in a total of nine samples to be tested. Formulation of these samples is done similarly to the liquid case, only a metal stirring rod was used to create a proper mixture since swirling did not suffice. Each fuel sample contained 10% catalyst. Then a hypergolicity study with HTP was performed for each sample. Results of this study are presented in Table 3.3.

These results show that adding the thickening agent has the desired effect. With increasing concentration of thickening agent both FCAT and CCAT move from fast decomposition to slow ignition. In case of FCAT the increase in HTP concentration is also a contributor in the increased hypergolic performance. When looking at the mixing quality it is noticed that for MCAT the quality increases with an increase in concentration thickening agent. Based on these results it is chosen to do further experimentation using ethanol containing 1% thickening agent. This concentration is high enough to result in a good mixture of fuel and catalyst while offering a performance boost and keeping the viscosity as close to liquid ethanol as possible. Throughout this thesis report the combination of ethanol with 1% thickening agent will be referred to as viscous ethanol, where ethanol will be referred to as liquid ethanol. This is done to prevent confusion.

Table 3.3: Hypergolicity test results with viscous ethanol created by adding 1.5%, 1%, or 0.5% thickening agent. The viscous ethanol is mixed with catalyst according to 90% viscous ethanol and 10% catalyst.

Catalyst	Potential	Observation	Notes
	1.5% Thickening agent		
FCAT	3	Slow ignition	92% HTP, Good mixing
CCAT	3	Slow ignition	92% HTP, Saturated mixture
MCAT	4	Fast ignition	92% HTP, Good mixing
	1% Thickening agent		
FCAT	2	Fast decomposition	88% HTP, Good mixing
CCAT	3	Slow ignition	88% HTP, Saturated mixture
MCAT	4	Fast ignition	88% HTP, Good mixing
	0.5% Thickening agent		
FCAT	2	Fast decomposition	88% HTP, Good mixing
CCAT	2	Fast decomposition	88% HTP, Saturated mixture
MCAT	4	Fast ignition	88% HTP, Poor mixing

3.4. Viscous fuel

The first two steps of the screening process have been completed. Three promising catalyst candidates have been identified and a sample with desirable visco-elastic properties has been formulated. In the next step the goal is to reduce the concentration of catalyst in the viscous ethanol to determine the minimum concentration required for hypergolic ignition. To do this a sample is formulated containing 5% catalyst, after which the sample is tested on hypergolicity with 88% HTP. If the test shows ignition within a reasonable amount of time the concentration is further lowered and the test is repeated. This is done until no or very slow ignition is observed. Results of these experiments can be found in Table 3.4. Figure 3.4 shows how such an experiment looks like. Using a syringe one droplet of HTP is dropped in a small amount of fuel. Here it resulted in fast ignition which means the catalyst concentration can be further reduced.

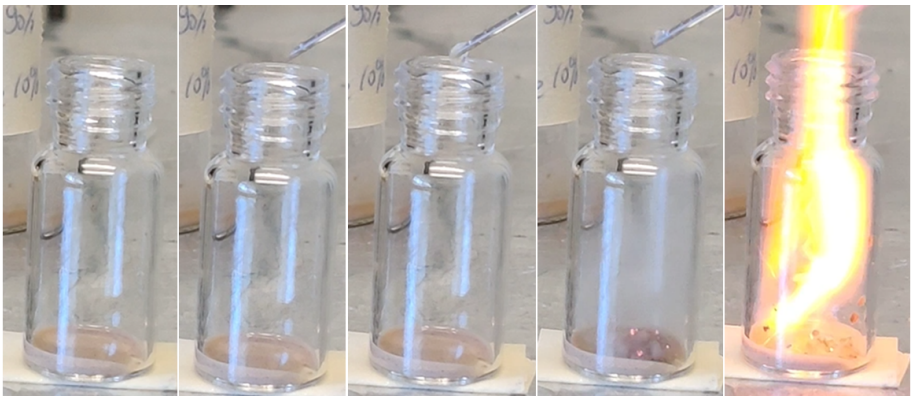

Figure 3.4: Hypergolicity experiment using a fuel consisting of 90% viscous ethanol and 10% MCAT with an 88% HTP droplet.

For both FCAT and CCAT a concentration of 5% was already too low to show hypergolic ignition with 88% HTP. MCAT showed more promising results with ignition still occurring at a concentration of 2%. This sample showed fast decomposition when adding one drop of 88% HTP, when adding a second drop fast ignition was observed. Later this round of experiments was repeated since a higher concentration of HTP, 96%, was made available by SolvGE. This

is expected to show better results since an increased concentration of HTP is more energetic and less energy is taken up by the water present in the HTP. The same procedure as with 88% HTP was followed, starting from the concentration catalyst that did not show ignition with 88% HTP. Results from experiments with 96% HTP are also presented in Table 3.4. In case of FCAT a major improvement is seen. Where 88% HTP led to fast decomposition, 96% HTP results in fast ignition. This means the concentration can further be decreased. At a concentration of 3% FCAT the sample showed slow ignition. After adding a drop of 96% HTP the mixture changes color from yellow/brown to a slightly darker tone. No violent decomposition or fumes are observed. Then after about 15 seconds the mixture suddenly ignites. Ignition is achieved here but the delay is so long that it is decided not to further decrease the concentration FCAT. CCAT also shows some improvement but not as much as FCAT. At 5% catalyst, two drops of 96% HTP resulted in ignition after about 3 seconds. Then when the concentration CCAT is further reduced to 3% only fast decomposition is observed. MCAT showed by far the most promising results. After switching to 96% HTP this sample showed fast ignition at 2% and slow ignition at 1% catalyst concentration. In this last case the first droplet of 96% HTP resulted in fast decomposition and the second drop in fast ignition. These results were good enough to further decrease the MCAT concentration. At a value of 0.5% the sample did not show ignition anymore. Here fast decomposition was observed for each drop.

Table 3.4: Hypergolicity experiments with viscous ethanol and various concentrations of catalyst in combination with 88% or 96% HTP.

wt% Catalyst	Potential	Observation	Notes
		FCAT	
10%	2	Fast decomposition	88% HTP, Good mixing
5%	2	Fast decomposition	88% HTP, Good mixing
5%	4	Fast ignition	96% HTP, Good mixing
3%	3	Slow ignition	96% HTP, Good mixing
		CCAT	
10%	3	Slow ignition	88% HTP, Saturated mixture
5%	2	Fast decomposition	88% HTP, Saturated mixture
5%	3	Slow ignition	96% HTP, Saturated mixture
3%	2	Fast decomposition	96% HTP, Saturated mixture
		MCAT	
10%	4	Fast ignition	88% HTP, Good mixing
5%	4	Fast ignition	88% HTP, Good mixing
3%	3	Slow ignition	88% HTP, Good mixing
2%	3	Slow ignition	88% HTP, Good mixing
2%	4	Fast ignition	96% HTP, Good mixing
1%	2	Fast decomposition	88% HTP, Good mixing
1%	3	Slow ignition	96% HTP, Good mixing
0.5%	2	Fast decomposition	96% HTP, Good mixing

As was done for the liquid case these experiments are repeated with butanol instead of ethanol. The same concentration of 1% thickening agent was added to butanol making it more viscous. This viscous butanol was then used to create fuel samples with FCAT, CCAT, and MCAT in a similar manner as was done for viscous ethanol. Results on hypergolicity with 88% and 96% HTP can be found in Table 3.5. FCAT shows slightly better results with viscous butanol than it did with viscous ethanol, as was also the case when no thickening agent was used. At a

concentration of 3% FCAT it took around 35 seconds after impact of the HTP droplets before the mixture ignited. This was the case for both 88% and 96% HTP. A difference should be expected here due to the increase in HTP concentration. The lack of a difference can be explained by the amount of HTP added which was 8 droplets for the 88% case and 5 droplets for the 96% case. Overall the performance is poor due to the extremely long delay time. CCAT also shows poor performance in combination with viscous butanol. In none of the tested cases ignition was achieved. Even when switching to 96% HTP this only resulted in fast decomposition. MCAT again shows the most potential out of the three candidates, even though its performance with viscous butanol is worse than with viscous ethanol. At a concentration of 3% and 1% it takes 3 to 4 droplets of HTP before the mixture ignites, where viscous ethanol showed fast ignition at a MCAT concentration of 2%. Again the critical concentration is somewhere between 0.5% and 1% since at 0.5% only fast decomposition is observed.

Table 3.5: Hypergolicity experiments with viscous butanol and various concentrations of catalyst in combination with 88% or 96% HTP.

wt% Catalyst	Potential	Observation	Notes
		FCAT	
10%	3	Slow ignition	88% HTP, Good mixing
5%	3	Slow ignition	88% HTP, Good mixing
3%	3	Slow ignition	88% HTP, Good mixing
3%	3	Slow ignition	96% HTP, Good mixing
		CCAT	
10%	2	Fast decomposition	88% HTP, Saturated mixture
5%	2	Fast decomposition	88% HTP, Saturated mixture
5%	2	Fast decomposition	96% HTP, Saturated mixture
		MCAT	
10%	4	Fast ignition	88% HTP, Good mixing
5%	3	Slow ignition	88% HTP, Good mixing
5%	4	Fast ignition	96% HTP, Good mixing
3%	3	Slow ignition	96% HTP, Good mixing
1%	3	Slow ignition	96% HTP, Good mixing
0.5%	2	Fast decomposition	96% HTP, Good mixing

3.5. Adding energetic particles

The final step in the screening process is to try to reduce the catalyst concentration required for hypergolic ignition by addition of energetic particles. Metallization of a propellant has the potential to enhance performance due to the added energetic potential of the metal powder [45, 46, 47]. In general aluminum particles are used which have already shown to be able to reduce ignition delay [48]. Therefore, also in this step an aluminum powder will be added to the formulated fuels. At the time of performing these experiments only 88% HTP was available. The fuels used are therefore based on the results obtained with 88% HTP in section 3.4. Here the lowest catalyst concentration tested was 5% for FCAT and CCAT and 1% for MCAT which all resulted in fast decomposition. In an effort to achieve ignition a small amount of aluminum powder is added to these fuel formulations. Here the aluminum powder replaces some amount of viscous ethanol as shown in this example; 95% visc.eth. + 5% FCAT becomes 92% visc.eth. + 5% FCAT + 3% Al. The newly formulated fuels containing aluminum are then tested on hypergolicity with 88% HTP similarly as was done in previous steps. The

results for samples based on viscous ethanol can be found in Table 3.6. FCAT showed a small improvement compared to when no aluminum powder was added. When one droplet of 88% HTP is added the mixture changes from light green to a brown color, then a small moment later decomposition is observed. Only when adding the fourth droplet ignition is achieved. Then, when adding subsequent droplets again only decomposition is seen. There was a slight improvement since ignition occurred, but it still does not look very promising. In case of CCAT and MCAT where 3% and 1% aluminum powder was added, respectively, no changes in reaction were observed. Both cases led to fast decomposition which was also achieved without the use of aluminum powder.

Table 3.6: Hypergolicity experiments with viscous ethanol, catalyst and aluminum particles in combination with 88% HTP.

Catalyst	Al	Potential	Observation	Notes
5% FCAT	3% Al	3	Slow ignition	88% HTP, Good mixing
5% CCAT	3% Al	2	Fast decomposition	88% HTP, Saturated mixture
1% MCAT	1% Al	2	Fast decomposition	88% HTP, Good mixing

As was done in previous steps also here the same experiment is repeated for viscous butanol instead of viscous ethanol. Fuel formulations used are based on the results from section 3.4 with 88% HTP. Again the samples that did not show good performance are attempted to be improved by adding a small amount of aluminum powder. Results of hypergolicity tests with 88% HTP and viscous butanol samples energized with aluminum powder can be found in Table 3.7. For FCAT a 2% catalyst concentration was used since a 3% concentration resulted in ignition. This sample did not show ignition but rather slow decomposition. After adding 88% HTP the same color change as before was observed. Only after about 50 seconds a violent decomposition occurred. The aluminum powder did not show a noticeable effect here. Also in case of CCAT no improvement was noticed. After adding 3% aluminum powder the sample still showed only fast decomposition when 88% HTP was added. MCAT did show a small improvement. Where in the original case 4 drops were required to achieve ignition, here only 1 was necessary. Even though ignition was achieved in both cases, the addition of aluminum powder seemed to have sped up the reaction.

Table 3.7: Hypergolicity experiments with viscous butanol, catalyst and aluminum particles in combination with 88% HTP.

Catalyst	Al	Potential	Observation	Notes
2% FCAT	1% Al	1	Slow decomposition	88% HTP, Good mixing
5% CCAT	3% Al	2	Fast decomposition	88% HTP, Saturated mixture
5% MCAT	3% Al	4	Fast ignition	88% HTP, Good mixing

For the remainder of this thesis the addition of aluminum powder is not pursued as an option anymore. Results from hypergolicity tests did not show any improvement in most cases and only minor improvements for 2 out of 6 samples. On top of that, the addition of aluminum powder can have other negative effects like residuals and a decrease in combustion efficiency [49].

3.6. Conclusion

In this Chapter an effort was made to make ethanol hypergolic with hydrogen peroxide. Based on a literature study it was chosen to add catalyst particles to ethanol which, when brought into contact with hydrogen peroxide, increase the decomposition rate of hydrogen peroxide. The heat released by this decomposition can increase the temperature of ethanol to above its auto-ignition point, resulting in ignition. In the first step a screening was performed using transition metal based catalysts that were available in the Chemical lab of DASML. These catalyst were mixed with ethanol in the ratio 1:9 and tested on hypergolicity with 88% HTP. Resulting from these test were three candidates that showed promising behavior; FCAT, CCAT, and MCAT. Then, in order to further improve performance and mixing quality, a small amount of thickening agent was added. The negligible amount of 1% thickening agent was concluded to show the best balance in increased performance and low increase in viscosity.

In section 3.4 viscous ethanol was used as a base to formulate new fuel samples. Fuels were created using the aforementioned FCAT, CCAT, and MCAT. The goal here was to reduce the catalyst concentration as far as possible until no or very slow ignition is observed when 96% HTP was added. Results showed that a minimum of 3% FCAT, 5% CCAT, or 1% MCAT were required to achieve ignition. The same experiments were repeated while using viscous butanol instead of viscous ethanol. In this case a minimum of 3% FCAT or 1% MCAT were required for ignition. This is similar to samples based on viscous ethanol, but these samples showed a slightly longer ignition delay. Samples containing CCAT did not show ignition in any case. Finally an effort was made to further reduce the catalyst concentration required for hypergolic ignition by addition of aluminum powder. This only resulted in minor improvement for 2 out of 6 tested samples and thus aluminum powder will not be pursued as an option for the remainder of this thesis.

4

Rheology study

This Chapter will focus on the rheology study which has been performed on the sample containing 99% ethanol and 1% thickening agent. First, a short introduction is given on rheology and its key parameters, as well as the different setups which are possible. Then, the chosen setup is described. Section 4.2 contains the test plan. Four different studies were performed including a viscosity study, yield point study, time dependent study, and temperature dependent study. The results of these studies are then presented in Section 4.3.

4.1. Theory

Rheology is the study of the flow and deformation of matter. Materials can behave in a range from purely viscous or liquid like to purely elastic or solid like. However, an ideal liquid or solid does not exist and all materials lie somewhere in between of these extremes. The flow behavior of a liquid can be expressed by its viscosity and the deformation behavior of a solid by its modulus. Ethanol is used as the main component of the fuel. Because it is a liquid, viscosity will be the most important parameter in this study. A thickening agent has been added to liquid ethanol with the goal of increasing its viscosity. Through a rheology study insight can be gained into the effect of the added thickening agent on the viscosity of the fuel. A rotational rheometer is the ideal tool to measure viscosity. In this type of rheometer the liquid is placed between a stationary and a rotational surface. More information on types of rheometer setups is given later in this section. To perform a measurement the rheometer will apply or measure the torque (M), angular displacement (θ), and angular velocity ($\dot{\theta}$). Then, from these base parameters, all other properties can be calculated. The shear stress is calculated according to Equation 4.1,

$$\tau = M \cdot K_\tau \tag{4.1}$$

where τ is the shear stress in Pa, M is the torque in N·m and K_τ is the stress constant which is dependent on the measurement geometry. Strain is determined using the angular displacement as follows:

$$\gamma = \theta \cdot K_\gamma \tag{4.2}$$

Here γ is the shear strain, θ the angular displacement in radians, and K_γ the strain constant which also depends on the measurement geometry. Finally, shear rate is calculated using Equation 4.3,

$$\dot{\gamma} = \dot{\theta} \cdot K_\gamma \tag{4.3}$$

with $\dot{\gamma}$ being the shear rate in s^{-1} and $\dot{\theta}$ the angular velocity in radians/s. Using these three base parameters the modulus and viscosity of the material can be calculated according to Equations 4.4 and 4.5 respectively.

$$G = \frac{\tau}{\gamma} \tag{4.4}$$

$$\eta = \frac{\tau}{\dot{\gamma}} \tag{4.5}$$

Here G is the modulus in Pa and η the viscosity in Pa·s. From the parameters mentioned in above equations only the strain and stress constants K_γ and K_τ are still unaccounted for as they are dependent on the measurement geometry. In general there are three types of geometries that can be used: parallel plate, cone and plate, and concentric cylinder. Figure 4.1 shows these configurations.

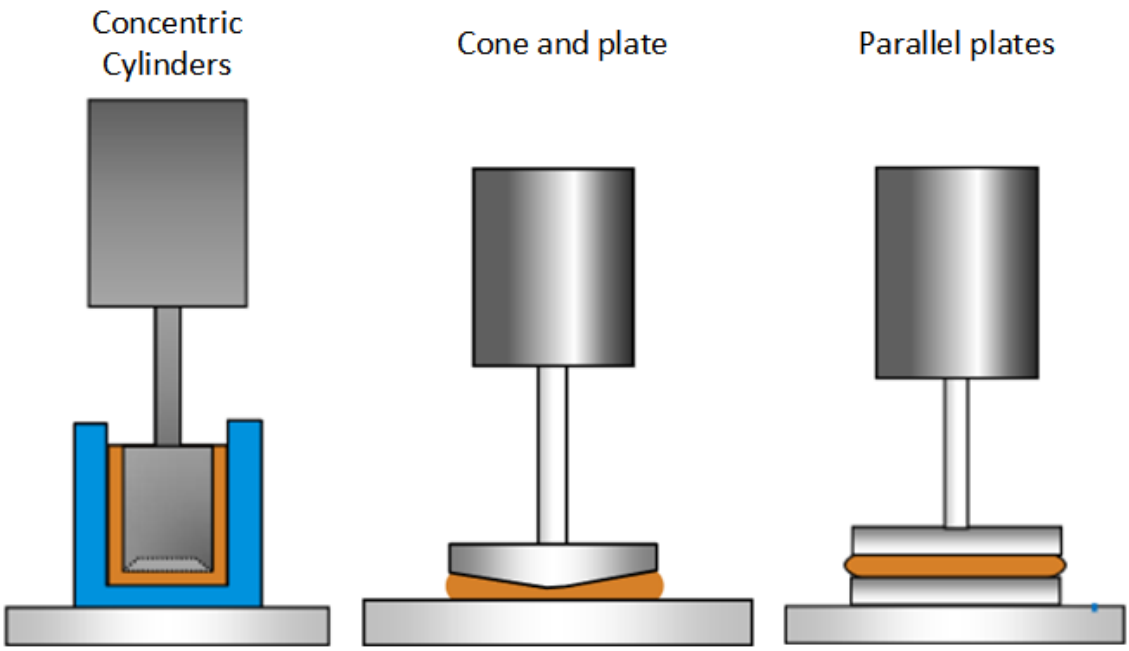

Figure 4.1: A schematic representation of the concentric cylinder, cone and plate, and parallel plate setup for a rotational rheometer. Figure is adapted from [50].

The concentric cylinder setup is often used for very low to medium viscosity liquids. It has the advantage that it minimizes the evaporation, which is beneficial when using ethanol since it evaporates at room temperature. Next to this it is also suitable for high shear rates. The cone and plate setup can be used for a viscosity ranging from very low to high. It can also measure at a high shear rate, and it requires only a small volume of sample. It is, however, more prone to evaporation. Parallel plates can be used for low to high viscosity liquids as well as soft solid materails. The effective shear rate varies across the parallel plate as it depends on the gap between the plates and the distance from the center. In case of the cone the shear rate is normalized due to the variable distance between the cone and plate. This results in slightly more accurate results when using a cone setup in comparison to a parallel plate setup [50].

Before a setup could be selected, it had to be checked which setups are available in the DASML. Unfortunately only a parallel plate setup was available here. Also the temperature stage was difficult to work with and took a long time to reach the desired temperature. To find a better setup other faculties were contacted. Eventually a concentric cylinder setup was

made available for the use of this thesis by the Waterlab of the faculty of civil engineering and geosciences. It was chosen to use this setup since it is better suited for very low viscosity, it minimizes evaporation, and had an excellent temperature stage. The rheometer used was an Anton Paar MCR 302 in combination with a C-PTD 170/Air peltier temperature control device which has a range of 0 to 170 C. Figure 4.2 shows this rheometer before and after sample loading including indications for the cylinders, temperature controller and insulation.

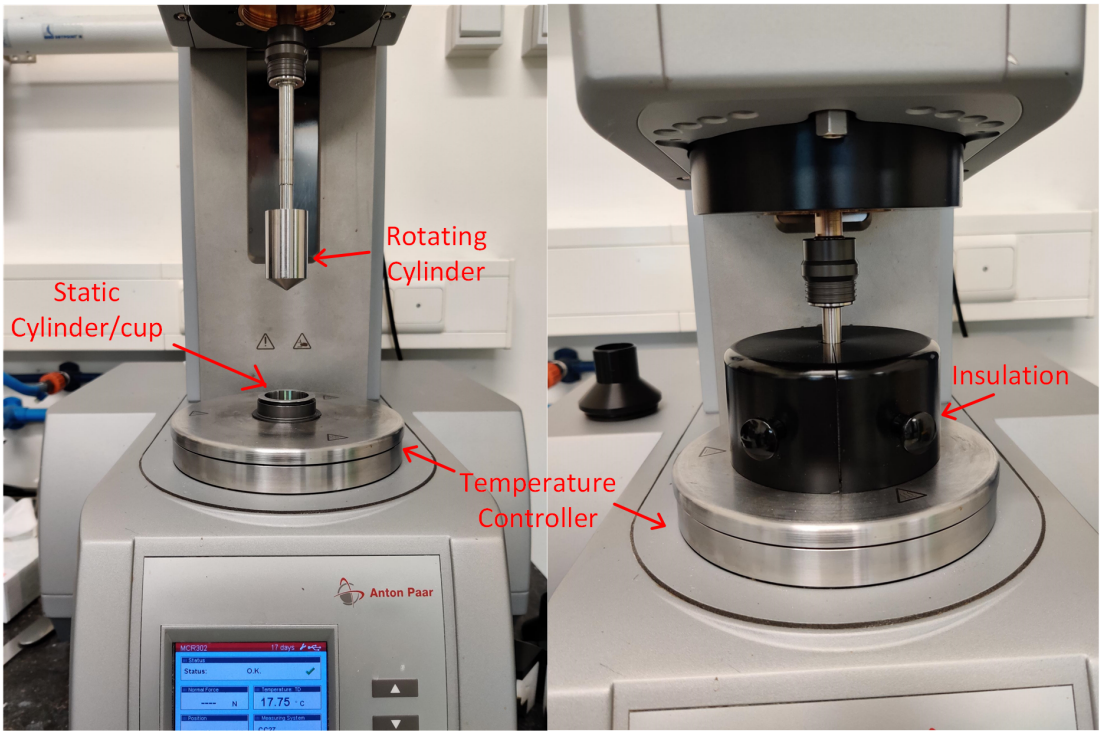

Figure 4.2: A picture of the rheometer before sample loading (left) and after sample loading (right).

4.2. Test plan

This section describes the measurements performed with the Anton Paar MCR 302 rheometer on the viscous ethanol sample. All samples used are taken from the same batch and consist of 99% ethanol and 1% thickening agent. With exception of the temperature dependent study, all tests were performed at ambient pressure and room temperature around 20^{o}C. For each test 15 ml of sample was used, which was just enough to completely submerge the rotating cylinder. Every measurement was repeated at least three times to get reliable data. The following studies were performed:

- **Viscosity study:** This study is performed to determine the viscosity of the sample over a large range of shear rates. To do this the shear rate is increased following a continuous ramp starting from 0.001 to 3860 s^{-1}, which is the maximum shear rate achievable by the rheometer. Within this range 100 data points are collected which have a logarithmic distribution. This distribution is chosen since a viscosity curve is generally plotted on a logarithmic scale. One test has a duration of 250 seconds. The viscosity curve gives insight on how the viscosity of a sample varies with varying shear rate or stress. For Newtonian liquids the viscosity is equal, irregardless of shear rate or stress. Ethanol

is an example of a Newtonian liquid, an should thus show this behavior. By adding a thickening agent it is expected that the resulting sample does not show Newtonian behavior anymore. This is expected since the viscosity is influenced by the network structure created by the thickening agent. The more bonds are present in this network, the higher the viscosity. A change in shear rate or stress is expected to influence the number of bonds in the network structure. In order to compare the viscosity of viscous ethanol to that of liquid ethanol, both are used in this study.

- **Yield point study:** A yield point study is very similar to a viscosity study. The difference is that it is performed at lower shear rates. In this case the shear rate is increased starting from 0.0001 to 10 s^{-1}. Here again 100 data points are used which follow a logarithmic distribution over a duration of 250 seconds. The yield point is defined as the lowest shear-stress value above which the material will start to flow. Below this value the material will act like a solid and above it, it will act like a liquid. The yield stress indicates the minimum amount of pressure required to make the material flow. In a propulsion application the fuel has to be pumped through the feeding lines. The pressure required to make the fuel flow is therefore of great importance. Since only a negligible amount of thickening agent is added to ethanol it is expected that the yield stress is very low. Also, through visual observation it is noticed that just by tilting the sample container, the sample starts to flow. This shows that only a small pressure is required to make the sample flow.

- **Time dependent study:** To determine time dependent effects on the viscosity of the fuel sample, two different tests are performed. First, a similar test is performed as was done in the viscosity study. Again the shear rate was increased from 0.001 to 3860 s^{-1} with 100 logarithmically distributed data points. Here, however, the time it takes to complete one test is varied. For the viscosity study this time was 250 seconds. Three more tests are performed with a duration of 80, 40, and 20 seconds. By increasing the shear rate over time, the shear stress is also increasing. In this study the effect of the rate of change of the shear stress on the viscosity of the fuel sample is tested. In the 250 seconds test the shear rate is increased very slowly, where in the 20 seconds test this occurs very rapidly. It is expected that a rapid change in shear rate results in a lower viscosity since the network structure is quickly ripped apart and does not have any time to recover itself, which might be the case for the long duration test. The second time dependent study measures a different effect. Here the shear rate is not increased over time but remains constant. A constant shear rate of 100 s^{-1} is applied to the fuel sample for a duration of 250 seconds. This shows the effect of applying a constant pressure for a longer amount of time. It is expected that the viscosity will gradually decrease over time and will go towards an asymptotic value.

- **Temperature dependent study:** This study is again very similar to the viscosity study. The shear rate is increased from 0.001 to 3860 s^{-1} over a duration of 250 seconds with 100 data points that follow a logarithmic distribution. Here, however, the temperature at which this test is performed is varied. For all other tests the temperature was set at 20 ^{o}C. In this study the temperature is varied from 0 ^{o}C to 50 ^{o}C in steps of 10 ^{o}C. This will result in 6 independent viscosity curves. It is expected that an increased temperature results in a decreased viscosity.

4.3. Results

This section presents the results found in the studies described in Section 4.2.

4.3.1. Viscosity study

Figure 4.3 shows the viscosity curve for (liquid) ethanol as well as for the viscous ethanol sample containing 1% thickening agent. Since ethanol is a Newtonian fluid it should show a constant viscosity, independent of shear rate. Measurements confirm this statement, except for low shear rates. Here the viscosity measured is higher than the actual viscosity. An explanation could be that the surface tension of ethanol causes this apparent increase in viscosity at low shear rates [50]. The viscosity of ethanol at 20 ^{o}C is about 1.2 mPa·s [51]. The measured viscosity of ethanol is about 1.35 mPa·s which is fairly close to the real value.

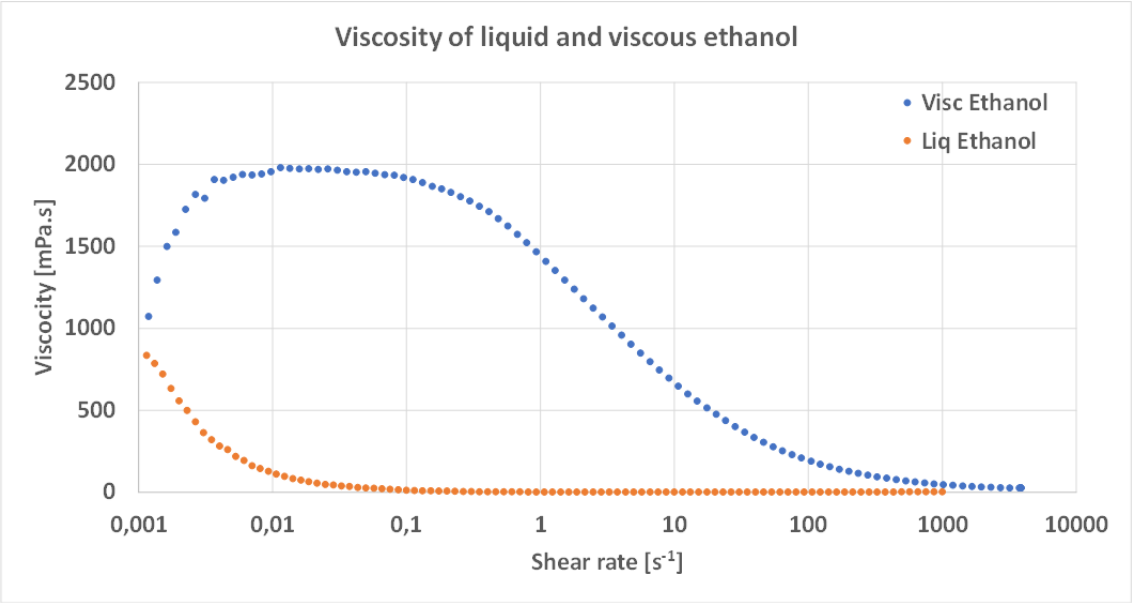

Figure 4.3: Viscosity of ethanol and a sample consisting of 99% ethanol and 1% thickening agent as a function of shear rate.

When examining the viscosity curve of the viscous ethanol sample it shows a much higher viscosity at low shear rates, when compared to liquid ethanol. This increase in viscosity is caused by the network structure created by the thickening agent. Bonds in the network inhibit the flow of the sample. This high viscosity is beneficial for a number of reasons. First of all, when a catalyst is added to viscous ethanol a high viscosity will counteract sedimentation. The process of sedimentation typically occurs at shear rates between 10^{-5} and 10^{-2} s^{-1} [50], where the viscosity is highest. This means that the catalyst will stay homogeneously distributed in the ethanol for a longer time, as compared to liquid ethanol. Another advantage of a high viscosity is that it reduces vapor pressure, making the ethanol less flammable and safer to work with. Finally, an increased viscosity also reduces propellant sloshing in a propellant tank. This then reduces forces exerted by the propellant on the tank resulting in a lower structural requirement.

As the shear rate increases also the shear stress increases. Stress applied to the sample causes the bonds in the network to break down, thereby decreasing the viscosity. As can be seen in Figure 4.3, the viscosity of viscous ethanol decreases as shear rate increases. This effect is known as shear thinning. Eventually, at a high enough shear rate, there are only little bonds left in the network structure. This results in a flattening of the viscosity curve towards a

value of 26 mPa·s, which is about one order of magnitude larger than that of liquid ethanol. It seems a large difference, however, it is a viscosity comparable to liquids like milk and coffee [50]. This low viscosity makes it easier to pump the fuel through the feed system and inject it into the combustion chamber. Pumping and injection typically occurs at shear rates in the range of 10^2 to 10^5 s^{-1} [50], where the viscosity is at a minimum. This means that when pumping the viscous ethanol, it will show a viscosity close to that of liquid ethanol. Overall, by adding a negligible amount of thickening agent to ethanol, it shows benefits at low shear rates while showing properties close to liquid ethanol at high shear rates.

4.3.2. Yield point study

Results of the yield point study are presented in Figure 4.4. It was expected that at a low shear rate the viscosity would be low and that it would increase as shear rate increases until the yield point is reached. Here, however, the viscosity curve shows a different effect. The viscosity starts high, then decreases as shear rate increases until a plateau is reached. After this plateau the viscosity continues to decrease. This shows that for low shear rates the behavior is different than was expected. The curve leaves two possibilities for the yield point; either it occurs at a shear rate below 0.0001 s^{-1} and was not captured by this measurement or it is located on the plateau. When this first option would be correct the shear stress corresponding to the yield point would be lower than 0.001 Pa, which is negligible. The second option, however, seems more probable. The plateau approximately ranges from a shear rate of 0.01 to 0.1 s^{-1}, which corresponds to the plateau seen in the viscosity curve shown in Figure 4.3. Since Figure 4.3 shows an increase in viscosity between a shear rate of 0.001 to 0.01 s^{-1} it is assumed that the yield point must lay somewhere on the plateau. The maximum viscosity measured on this plateau corresponds to a shear stress of 0.078 Pa, which is assumed to be the yield stress. After this point the viscosity starts to decrease and the viscous ethanol sample starts to behave like a liquid.

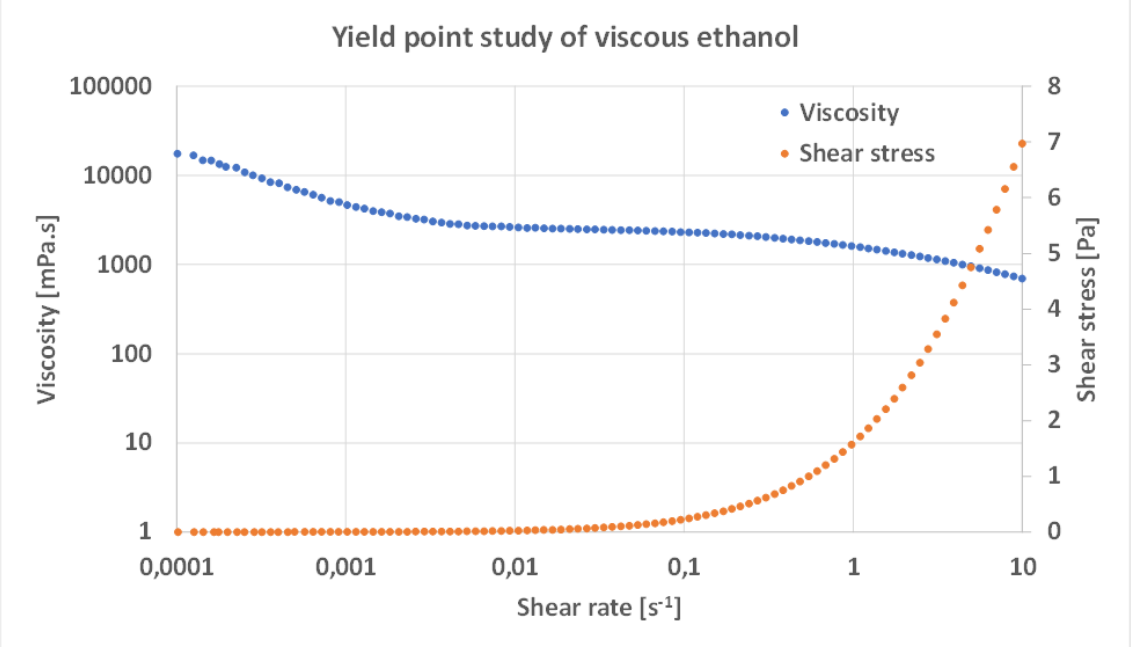

Figure 4.4: Yield point study of a sample consisting of 99% ethanol and 1% thickening agent.

It is unsure why the viscosity curve presented in Figure 4.4 shows a high viscosity at low shear rates. Since yield point measurements are a comparison between the internal and external forces it would be better to perform a measurement using a controlled shear stress instead of shear rate [52]. Also, samples with a very low yield stress require the rheometer to operate close to the low-end torque specification. At these conditions the yield stress cannot be easily determined using the stress sweep method [53]. Instead a test can be performed where the shear rate starts high and then logarithmically decreases. The yield point is then indicated by the yield stress which reaches a plateau at low shear rates [53].

4.3.3. Time dependent study

As was mentioned in Section 4.2 the time dependent study consists of two separate tests. First, the results of the duration study are presented in Figure 4.5. From this figure can be derived that for low shear rates, a long duration results in a higher viscosity. However, as the shear rate increases the viscosity measured in each case merges towards a similar trend. This means that a fast increase in shear rate results in a lower viscosity. A possible explanation could be that for the short duration measurements the network structure in the ethanol is broken so quickly that it hardly has any time to recover. This results in a low viscosity. For long duration measurements the network structure is broken at a slower rate meaning that there is some time for the network to recover and restore bonds, resulting in a higher viscosity. This effect can be beneficial if the propellant is used in pulse mode operation. This mode is characterized by fast switching on and off of the propellant feeding. A certain mass flow has to be reached within a very short duration. Since the propellant shows the lowest viscosity in these conditions it is very suitable for pulse mode operation. Then, at high shear rate the network structure is broken down so fast that even in the long duration measurement there is not enough time to recover the network. This results in a similar viscosity independent of duration.

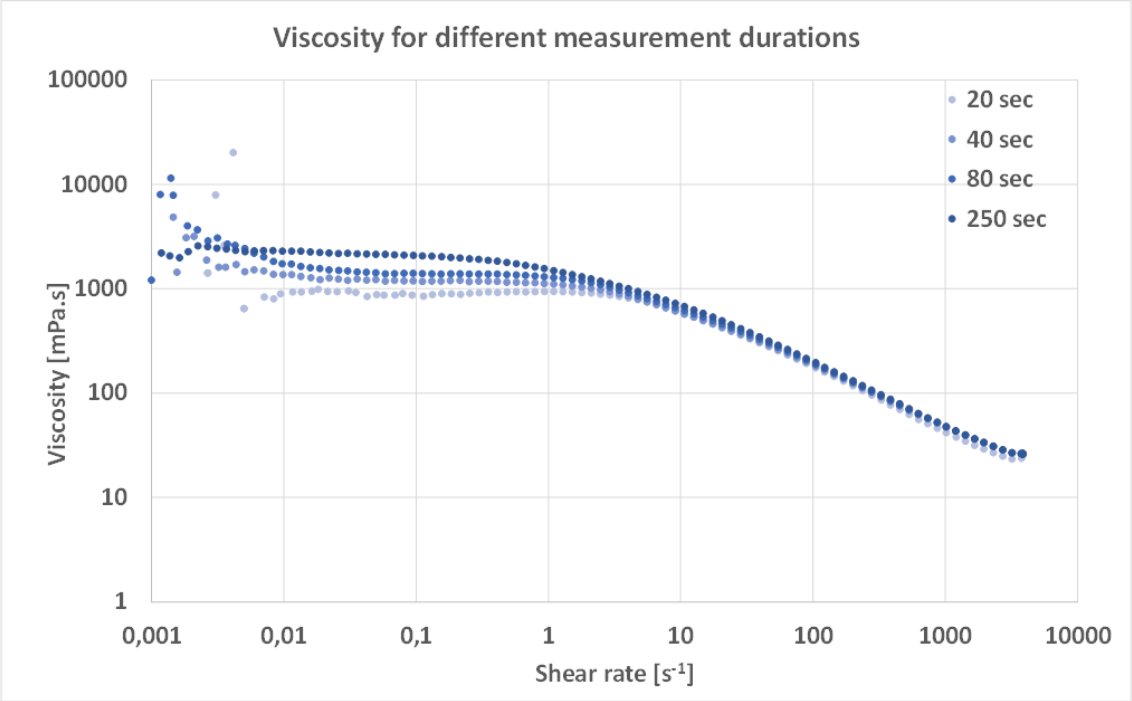

Figure 4.5: Viscosity of a sample consisting of 99% ethanol and 1% thickening agent, measured for a shear rate ranging from 0.001 to 3860s^{-1}. Measurement duration was varied between 20, 40, 80, and 250 seconds.

Results of the second time dependent study can be found in Figure 4.6. From this figure can be concluded that the viscosity will decrease over time at a constant shear rate. The viscosity decreases rapidly within the first few seconds, after which the decrease in viscosity slows down. This might suggest that the viscosity is heading towards an asymptotic value. For Newtonian liquids the viscosity is independent of shear rate. Next to that it is also independent of time. In case of viscous ethanol, however, the viscosity changes with time at a constant shear rate. This can be explained by the effect that the network structure is being broken by the shear stress applied thereby decreasing the viscosity over time. Since the amount of bonds in the network will decrease over time, also the amount of bonds broken per second will decrease over time. The amount of bonds recovered per second is assumed to increase if the total amount of bonds decreases. This results in a break even point which is reached over time. Here the amount of bonds broken per second is equal to the amount of bonds recovered per second. In a propulsion application this effect is more important for long burn times. If there is a constant mass flow for a long duration of time the viscosity of the propellant will decrease over time thereby lowering the pressure required to pump the propellant.

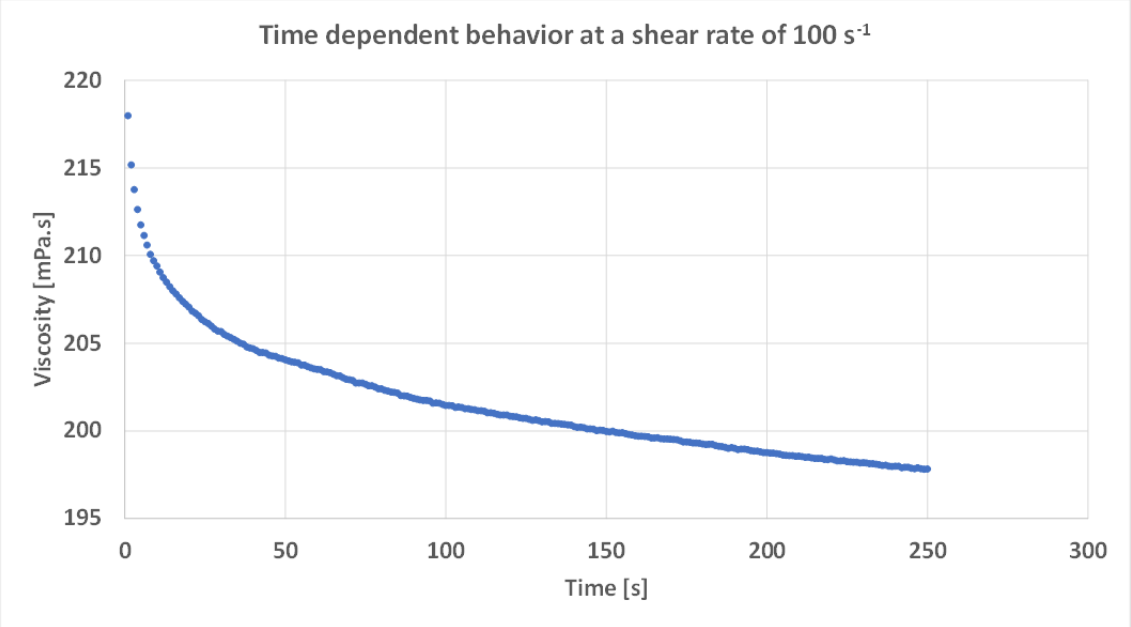

Figure 4.6: Viscosity of a sample consisting of 99% ethanol and 1% thickening agent, measured at a constant shear rate of 100s^{-1} for a duration of 250 seconds.

4.3.4. Temperature dependent study

The effect of temperature on the viscosity of viscous ethanol is shown in Figures 4.7 and 4.8 which show the viscosity as a function of shear rate and shear stress respectively. As was expected, and is also known for liquid ethanol, an increase in temperature results in a decrease in viscosity. This effect is more noticeable at low shear rates, where the difference is larger. At a shear rate of 0.1 s^{-1} the 0 ^{o}C sample has a viscosity of 3940 mPa·s where the 50 ^{o}C sample shows a viscosity of 490 mPa·s, which is about an order of magnitude difference. Then, at a higher shear rate of 3860 s^{-1} the viscosities have been reduced to 30 and 20 mPa·s for the 0 ^{o}C and 50 ^{o}C sample, respectively. This means that when the viscous ethanol experiences a high shear rate, during pumping and injection for example, the temperature only has a small effect on the viscosity. This low temperature sensibility makes for a robust system. At low shear rate the viscous ethanol is at rest and the exact viscosity is thus insignificant.

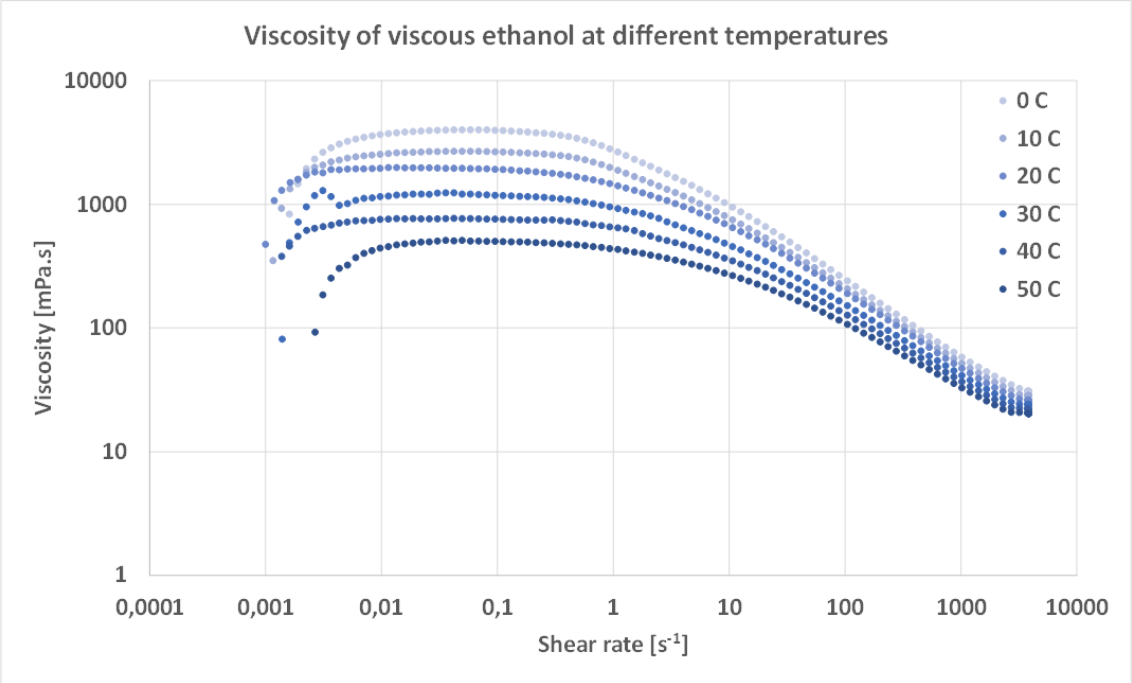

Figure 4.7: Viscosity of a sample consisting of 99% ethanol and 1% thickening agent as a function of shear rate. Measured at a temperature ranging from 0 to 50^{o}C in steps of 10^{o}C.

Figure 4.8 gives more insight into the effect of temperature on the yield point. The yield point corresponds to the maximum viscosity before the viscosity starts to decrease. When looking at the maximum viscosity at each temperature it can be seen that for increasing temperature the maximum viscosity shifts to the left. Since the viscosity is plotted against the shear stress, a shift to the left indicates a decrease in shear stress. The table in the upper left corner of Figure 4.8 gives an overview of the yield stress at the measured temperatures. These numbers confirm that an increase in temperature results in a decrease in yield stress. A typical propellant tank has a pressure in the order of bars or 10^5 Pa. Compared to this the yield stress at any measured temperature is negligible. For any temperature the tank pressure should be high enough to easily get past the yield point of the fuel, thereby decreasing its viscosity and making it easy to flow.

4.4. Conclusion

In this Chapter a rheology study has been performed using a sample consisting of 99% ethanol and 1% thickening agent. This study was split into four parts including viscosity study, yield point study, time dependent study and temperature dependent study. From the viscosity study can be concluded that the sample shows a shear thinning behavior. At low shear rates the viscosity is high which counteracts the sedimentation of particles in the sample. This means that when a catalyst is mixed with the sample the particles will stay distributed homogeneously for a much longer time than when a catalyst is added to pure (liquid) ethanol. This effect increases the life time of the catalytically enhanced ethanol fuel. Then at higher shear rates the viscosity decreases starting from the yield point. The yield point study shows a yield stress of about 0.078 Pa. By applying a shear stress of 0.078 Pa or higher the viscosity of the sample will decrease, causing the sample to flow and behave like a liquid. With increasing shear rate the sample will eventually reach a viscosity very close to that of pure (liquid) ethanol. For a

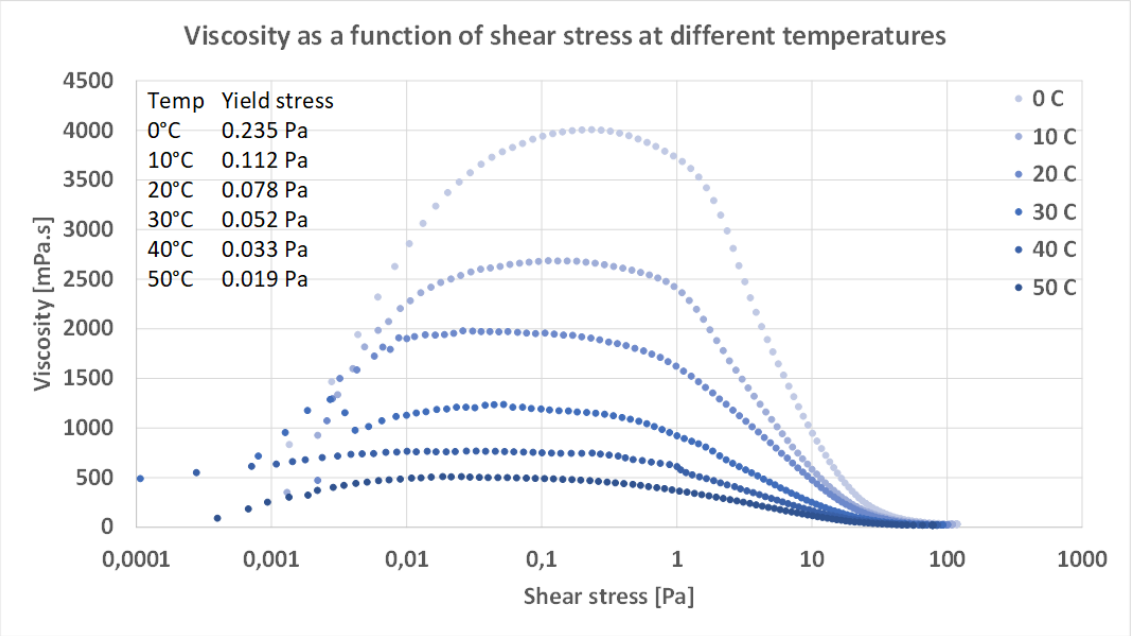

Figure 4.8: Viscosity of a sample consisting of 99% ethanol and 1% thickening agent as a function of shear stress. Measured at a temperature ranging from 0 to 50^{o}C in steps of 10^{o}C.

propulsion application this means that by applying enough pressure the viscous ethanol will act like liquid ethanol and can be easily pumped through a feed and injection system.

Results from the time dependent study showed that if the shear rate is increased in a short amount of time it results in a lower viscosity than when the same increase of shear rate is done over a longer duration. This effect makes the sample very suitable for use in pulse mode operation of a propulsion system. Here the propellant flow is started and stopped within a short duration of time. Under these conditions the sample shows the lowest viscosity. The second time dependent study showed that if a constant shear rate is applied, the viscosity decreases over time. This effect is more beneficial for propulsion applications with a longer burn time. Overall, the sample shows promising effects in both short and long burn time propulsion modes. Finally a temperature dependent study was performed. From the results can be concluded that an increase in temperature leads to a decrease in viscosity as well as a decrease in yield stress.

5

Pyrophoric liquid

In this Chapter a different approach is taken, instead of a catalyst, to make ethanol hypergolic with hydrogen peroxide. Based on a literature study indications are found that pyrophoric liquids can have a hypergolic reaction with hydrogen peroxide or other common oxidizers. Therefore, the use of a pyrophoric liquid as a substitute for a catalyst is researched in this thesis. Due to the risks associated with pyrophoric liquids a dedicated experimental setup is build, which is described in section 5.2. Then in section 5.3 the procedure followed to transfer a pyrophoric liquid is described. Observations made during sample formulation and during hypergolic experiments with hydrogen peroxide can be found in section 5.4.

5.1. Theory

As was proven in Chapter 3 catalyst particles can be added to ethanol in order to make it hypergolic with high concentrations of hydrogen peroxide. In this Chapter an alternative route is discussed which makes use of a pyrophoric liquid instead of a catalyst. A pyrophoric liquid has the property that it ignites spontaneously in air. This high reactivity and ignition potential makes it for a possible candidate to induce hypergolicity between ethanol and hydrogen peroxide. Next to this a pyrophoric liquid also has the potential to react with other oxidizers like liquid oxygen, nitrogen tetroxide, nitric acid, or nitrous oxide [54]. Where catalysts are specifically suitable for the decomposition of hydrogen peroxide they do not aid the ignition when another oxidizer is used. Since pyrophoric liquids do have this potential it can make for a more versatile system. A fuel containing pyrophoric liquid could be formulated in such way that it does not only show hypergolicity with hydrogen peroxide but also with other common oxidizers. This fuel can then be applied in various different use cases and propulsion systems.

Triethylaluminum (TEA) is one of the most studied pyrophoric liquids for use in propulsion applications. Unfortunately, still not much is known about its reaction mechanism with common oxidizers. In a study performed by Gonçalves et al. [55] an initial reaction mechanism is proposed for the combustion reaction between TEA and oxygen. It mainly consists of two pathways which are shown in Figure 5.1. Firstly, through collision with oxygen, hydrogen atoms can easily be abstracted resulting in the generation of HO_2, OH, H_2, and H_2O. The OH radicals are very reactive and aid in the propagation of the reaction. The flammable hydrogen gas H_2 can combust with oxygen. Secondly, the bond between the aluminum and carbon atoms is prone to break. This results in aluminum that can oxidize to aluminum oxide, and C_2H_5 groups that can form flammable hydrocarbon gasses like C_2H_6 and C_2H_4, or react with oxygen to form CO_2 and H_2O. By simulating the combustion reaction between TEA and oxygen

its activation energy was estimated to be around 1.2 kJ/mol. In comparison, the activation energy for the decomposition of uncatalyzed H_2O_2 is 75 kJ/mol which can be brought down to 49 kJ/mol when using a platinum catalyst [5]. This shows the reactivity of TEA. Although this is just a preliminary analysis it gives some insight into the pyrophoric nature of TEA.

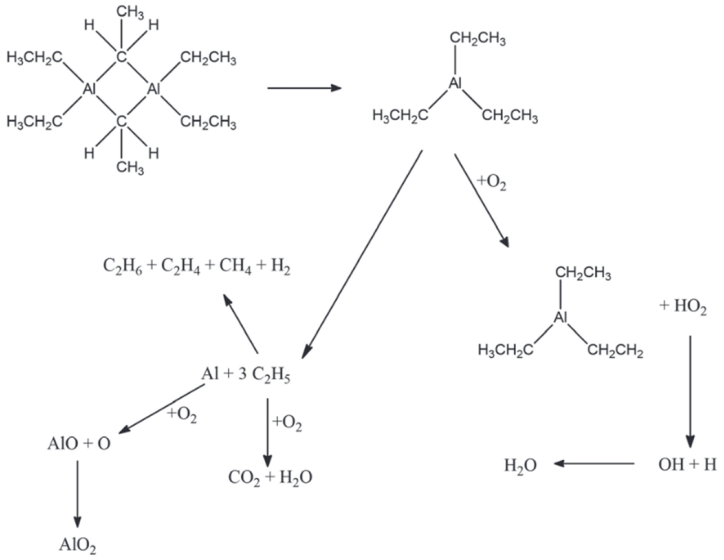

Figure 5.1: Main pathways for TEA combustion as proposed by [55].

Based on this and findings in literature from Chapter 2 pyrophoric liquids are thought to have a high enough potential to be studied in this thesis. All cases found have in common that TEA is used, which is therefore also taken as a starting point. As a secondary option also diethylzinc (DEZ) is considered. Similarly as was done with various catalysts, fuels will be formulated using ethanol and TEA. Then after formulation their hypergolicity with high concentrations of HTP will be tested. However, due to the nature of pyrophoric liquids they have to be handled with great care and under an inert atmosphere. To do this a special experimental setup is required which is described in section 5.2. Furthermore, due to safety and funding considerations a 1.0M solution of TEA and DEZ in hexane is used instead of pure TEA or DEZ.

5.2. Experimental setup

Due to their reactivity with air, pyrophoric liquids have to be kept under an inert atmosphere at all times. The first solution that then comes to mind is to use a glovebox. This is a sealed container with a controlled environment inside. It contains two gloves which allow someone to manipulate objects that are inside while remaining on the outside themselves. Unfortunately, no proper glovebox is available in the DASML. Only a self-made glovebox was present from a previous project. This glovebox, however, had some issues which could not be resolved within the time span of this thesis. Thus, an alternative method of transferring a pyrophoric liquid under an inert atmosphere had to be used. Based on literature, the use of a Schlenk line was considered the best alternative. It consists of two manifolds, one connected to an inert gas source and one connected to a vacuum pump. A setup was created around the use of a Schlenk line which will be described below. Equipment used in this setup is listed in Table 5.1.

Preferably the pure form of TEA or DEZ would be used since it has the highest energetic content and reactivity, resulting in a higher ignition potential. For initial studies, however, the following solutions are used:

Table 5.1: A list of equipment required for the transfer of a pyrophoric liquid.

Inventory			
ID	**Item**	**ID**	**Item**
ETOH	Ethanol	SL	Schlenk line
DEZ	Diethylzinc 1.0M	BBL	Bubbler
TEA	Triethylaluminum 1.0M	DC	Drying column
HEX	Hexane	NS	Nitrogen supply
CL	Clamps	VP	Vacuum pump
RBF	Round bottom flask	FH	Fume hood
Seal	Seal	NDL	Needle
MS	Magnetic stirrer	SYR	Syringe
MSB	Magnetic stirring bar	DS	Dry sand

- Triethylaluminum (CAS number 97-93-8) as a 1.0M solution in hexanes from Sigma Aldrich.
- Diethylzinc (CAS number 557-20-0) as a 1.0M solution in hexanes from Sigma Aldrich.

A 1.0M (Molar) solution means that 1 liter of solution contains 1 gram molecular weight (GMW) of the dissolved substance. A GMW is equal to the sum of the combined atomic weights of all atoms in the molecule expressed in grams. For TEA the GMW is for example equal to $1 \cdot Al + 6 \cdot C + 15 \cdot H = 1 \cdot 26.98 + 6 \cdot 12.01 + 15 \cdot 1.01 = 114.16g$. Now using the density of TEA, 832 kg/m^3, and hexane, 655 kg/m^3, the mass fraction of TEA in the 1.0M solution can be determined and is equal to 16.8%. The same process is repeated for DEZ resulting in a mass fraction of 17.4% DEZ in a 1.0M solution in hexanes. These compounds are very reactive, however, when diluted with a hydrocarbon solvent to concentrations of 10-20% they do not ignite immediately when in contact with air [56].

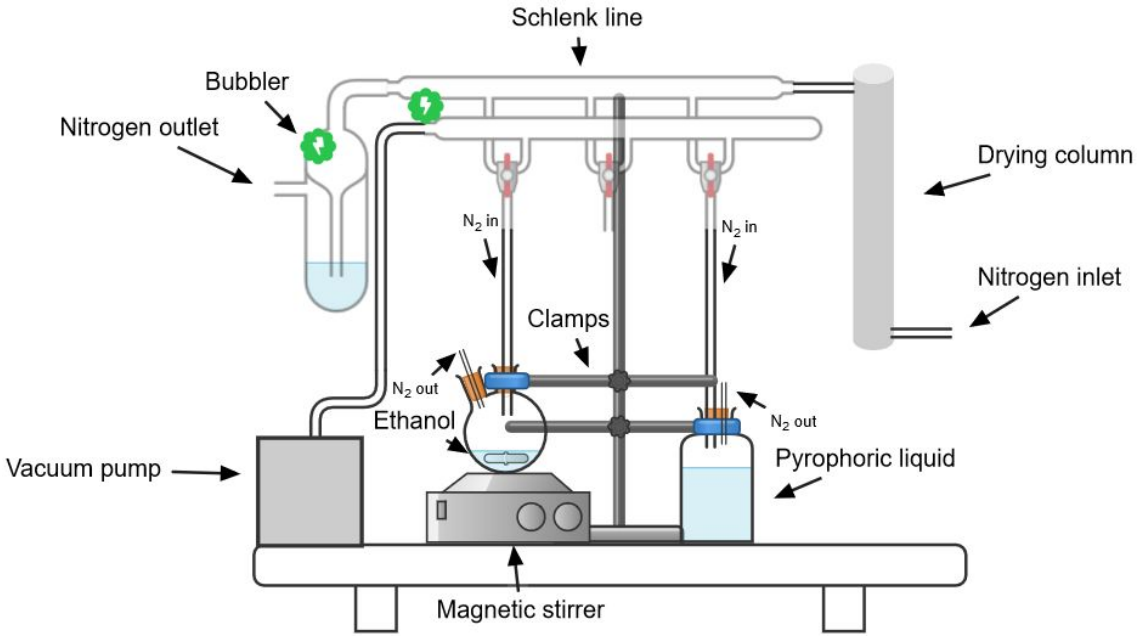

Figure 5.2: A schematic representation of the setup used for transferring a pyrophoric liquid.

Even though the pyrophoric liquids are diluted, they should still be shielded from contact with

air. The containers in which they are provided have a special seal cap. This cap makes sure that no air can enter the container. By puncturing the cap with a needle the pyrophoric solution can be accessed. Figure 5.2 shows a schematic overview of the setup used to transfer this pyrophoric solution. The inert gas part of the Schlenk line is on one end connected to a nitrogen supply. Before entering the manifold the nitrogen passes through a drying column to ensure a minimal amount of moisture in the nitrogen. Pyrophorics are often water reactive and their contact with water should thus be avoided. The other end of the inert gas manifold connects to a bubbler which acts as a gas outlet. The oil present in the bubbler prevents air from flowing back into the manifold and therefore ensures there is only nitrogen present inside. The second manifold of the Schlenk line has only an outlet. This is connected to a vacuum pump, creating a vacuum in this manifold. Between the two manifolds several glass taps are situated. Two separate parallel channels run diagonally through these taps allowing access to either manifold separately. This system can be used to create an inert atmosphere in a sealed flask by connecting a tube from the Schlenk line to the flask and alternating it between a vacuum and nitrogen gas.

Both the pyrophoric liquid container as the receiving bottle are clamped firmly in place. The receiving container is placed on a magnetic stirrer with a stirring bar inside and then sealed off. The seals can be punctured by a needle allowing access to the inside of the containers without allowing air to flow in. A magnetic stirrer is used to thoroughly mix the ethanol and pyrophoric solution in the receiving container to create a homogeneous mixture. The whole setup is placed inside a fume hood for safety considerations. The continuous ventilation gets rid of any fumes that may be released in the process by accident and the glass screen serves as protection for any splashing. For fire safety a container of dry sand is present inside the fume hood. A full safety plan approved by the head of DASML, Dr. J.C. Bijleveld, can be found in Appendix A.

5.3. Transfer procedure

Before transferring a pyrophoric liquid some preparations have to be made. First of all, all glassware used is thoroughly cleaned after which it is placed in an oven at 120^{o}C for at least 4 hours to remove any moisture. Then the glassware is placed in a desiccator where it can cool down to room temperature. The fume hood is cleaned and all unnecessary materials are removed. Extra care is taken to remove anything flammable. Then the availability and location of safety equipment like dry sand, a fire extinguisher, and an (eye) shower is checked. Other people present in the lab will be notified that an experiment with pyrophorics is being performed. Finally, the glassware is taken out of the desiccator and clamped into position. A magnetic stirring bar is placed inside and all openings are sealed using rubber septa. Also the pyrophoric solution container will be clamped into position. During these steps the adequate personal protection equipment (PPE) is worn including gloves, safety glasses, and a lab coat.

When using a Schlenk line there still exist two methods of transferring a pyrophoric liquid; using a syringe or a cannula (double-tipped needle). In case of small quantities, <20 ml, a syringe is safe to use [57]. The transfer procedure was always carried out under supervision of Dr. B.V.S. Jyoti and Ir. D.P. Mainali Sharma. The following procedure for transferring a pyrophoric was strictly followed:

- Flush the receiving bottle with alternating nitrogen and vacuum at least three times using the Schlenk line to create an inert atmosphere in the bottle.
- Insert a needle with dry nitrogen from the Schlenk line into the receiving bottle.

- Insert a venting needle in the receiving bottle to prevent over pressurization. Nitrogen is now continuously flowing in and out of the bottle.
- Flush a new syringe several times with nitrogen, ensuring it is free of air.
- Use this syringe to transfer the desired amount of ethanol into the receiving bottle.
- Turn on the magnetic stirrer.
- Insert a needle with dry nitrogen from the Schlenk line into the bottle containing the pyrophoric solution.
- Insert a venting needle into the bottle containing the pyrophoric solution to prevent over pressurization.
- Flush a new syringe several times with nitrogen, ensuring it is free of air.
- Insert the needle of the syringe through the rubber of the bottle containing the pyrophoric solution.
- Gently pull liquid in the syringe. Never fill the syringe more than 50%. Only use small quantities <1ml. Extract slightly more than required. The inflow of nitrogen and venting needle should prevent the syringe from creating a vacuum.
- While keeping the needle in the bottle containing the pyrophoric solution turn the syringe so the needle end points up. Slowly push out the gas bubbles and excess liquid until the desired amount is still left in the syringe.
- Pull in some inert gas so the needle does not contain any pyrophoric liquid.
- Remove the needle from the bottle containing the pyrophoric solution and insert it through the rubber septum of the receiving bottle.
- Deposit the desired amount of pyrophoric solution into the receiving bottle.
- Remove the needle from the receiving bottle.
- Flush the syringe in hexane at least three times to clear it from the pyrophoric chemical.
- Remove the nitrogen supply and venting needle from the bottle containing the pyrophoric solution. Close it and store it.
- Remove the nitrogen supply and venting needle from the receiving bottle.
- Properly dispose the used syringes and needles.

After completing these steps the pyrophoric solution is safely transferred into the bottle containing the ethanol. The mixture is carefully observed and when a homogeneous mixture is thought to be reached the magnetic stirrer is turned off. Observations on these experiments are described in Section 5.4.

5.4. Results

In this Section the observations during fuel formulation using a pyrophoric solution are presented. A difference is made between fuels formulated with viscous ethanol and liquid ethanol. As a reference, experiments have also been performed where the pyrophoric solution was the only content of the fuel.

5.4.1. Viscous ethanol

An effort is made to formulate a fuel that is hypergolic with hydrogen peroxide. Based on the results from Chapter 3 viscous ethanol is used as a basis of the fuel. Instead of using a catalyst here a small amount of pyrophoric liquid is added to viscous ethanol. Here the increased viscosity should again help to form a homogeneous mixture, but on the other hand also trap the pyrophoric liquid to make it stable in air. Due to the nature of the pyrophoric solution, at first only a very small quantity is used. Then, when the system is stable and some experience and confidence has been build up in handling a pyrophoric liquid the quantity can slowly be increased. It is expected that for very low concentrations of pyrophoric liquid the fuel will not show a hypergolic reaction with hydrogen peroxide. However, by slowly increasing the concentration the goal is to find the critical point where hypergolic ignition occurs.

Using the setup and procedure described in Sections 5.4 and 5.3 0.1 ml of TEA solution is added to 2 ml of viscous ethanol. Since the pyrophoric solution only contains 16.8% of actual pyrophoric substance the total weight fraction of TEA in the formulated fuel is only 0.69%. When the TEA solution was added to the viscous ethanol no reaction was observed. To create a proper mixture the magnetic stirrer was left on for about three hours, stirring at an rpm of 200. Then, when the stirring was stopped, it was noticed that the viscosity of the formulated fuel had changed. Figure 5.3 (Left) shows a picture of the formulated fuel sample. It clearly shows an increase in viscosity. The sample no longer has a liquid appearance but can be classified better as a gel. It is unknown if this is due to the reaction between either of the components or due to the long stirring time. It is, however, an undesired effect since the formulated propellant should be a liquid. Carefully the flask in which the mixture was formulated is unsealed and air is let in. No reaction is observed between the fuel and the air, meaning that the TEA is diluted thus far that it does not show pyrophoric behaviour anymore. The fuel sample is then transferred in a container as shown in Figure 5.3. Similar as was done in Chapter 3 the fuel sample is tested on hypergolicity with 97% HTP. A small amount of sample is placed in a reaction container and a few drops of HTP are added. No reaction is observed. Then the same sample is tested with 30% hydrogen peroxide. Due to the water reactivity of TEA a reaction might occur here, however, this is not observed.

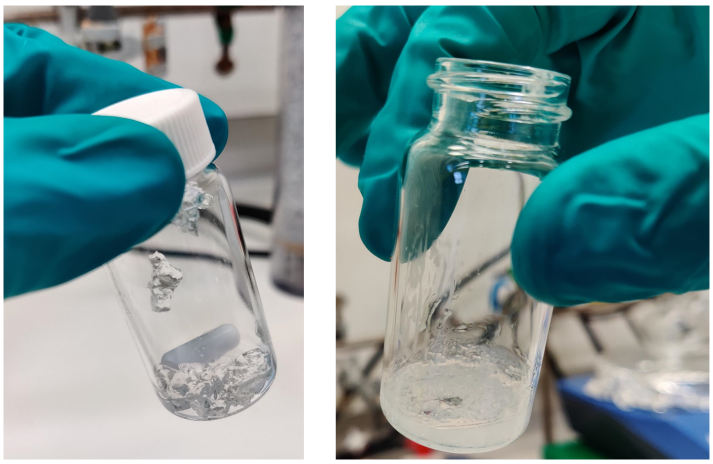

Figure 5.3: (Left) The result of mixing 2ml of viscous ethanol with 0.1ml of 1.0M TEA solution in hexanes for three hours on 200rpm. (Right) The result of mixing 2ml of viscous ethanol with 0.1ml of 1.0M DEZ solution in hexanes.

In an effort to achieve hypergolicity the concentration of TEA in the fuel sample is increased. A fuel is formulated using 2 ml viscous ethanol and 0.2 ml of TEA solution which corresponds

to a concentration of 1.33% TEA in the fuel. Instead of stirring for three hours the mixture is now only stirred for 10 minutes at 200rpm. After these 10 minutes no observable change has occurred in the viscosity of the sample. Then, after waiting for one hour without stirring, the viscosity had again increased to form a gel. It is therefore suspected that this is due to a reaction between the thickening agent and the pyrophoric solution. The formulated sample is again stable in air and does not react with 97% or 30% hydrogen peroxide.

Next to using TEA a fuel was also formulated using DEZ. The sample consisted of 2 ml viscous ethanol mixed with 0.1 ml 1.0M DEZ solution in hexanes. This translates to a concentration of 0.75% DEZ in the final fuel sample. When the DEZ solution was added to the mixing flask some white smoke was observed. This has to be a reaction between the DEZ solution and the atmosphere inside the flask since it occurred before contact with the viscous ethanol. Some leftover air had to be in the flask which reacted with the DEZ. The air can be caused by a leak in the system, a leaking seal for example, or by flushing the flask too few times with alternating vacuum and nitrogen. When the DEZ solution comes in contact with the viscous ethanol is almost instantly increases in viscosity and forms a gel. The resulting fuel sample can be seen in Figure 5.3 (Right). It has a white opaque color which is expected to be due to the formation of zinc-oxide caused by the reaction between DEZ and oxygen which was still left in the flask. When removing the seal, no further reaction with air was observed. Also adding 97% or 30% hydrogen peroxide did not result in any reaction. Due to the reaction between the pyrophoric solution and the thickening agent resulting in gel formation the current thickening agent is not suitable for fuel formulation with the tested pyrophoric solutions. For further study other thickening agents can be explored which might be more compatible with pyrophoric liquids. During the scope of this thesis this is not pursued due to time limitations.

5.4.2. Liquid ethanol

Since the pyrophoric solutions showed to be incompatible with viscous ethanol some fuels are formulated using liquid ethanol instead. The same procedure is followed as was done with viscous ethanol. A fuel sample was formulated using 2 ml ethanol and 0.1 ml TEA solution, corresponding to a TEA concentration of 0.69%. During mixing no reaction is observed and no changes in viscosity occurred. The final mixture seems to be homogeneous and does not separate, however it is hard to see since both components are colorless transparent liquids. When removing the seal no reaction is observed between the sample and air. A hypergolicity test is performed using 96% hydrogen peroxide. Some gas bubbles are generated when the HTP is added indicating decomposition of hydrogen peroxide. The decomposition rate is very slow. In an effort to increase this effect a new sample is formulated using 2 ml ethanol and 0.2 ml TEA solution, corresponding to a TEA concentration of 1.33%. No significant differences are found in any step with respect to the fuel sample containing 0.69% TEA. Then a sample is formulated which contains 2.98% TEA. No reaction was observed during the formulation phase. When adding 96% HTP again some bubbles are generated, and on top of that also white solid particles start to appear in the sample. It is thought that these particles are aluminum oxide as a result from the reaction between TEA and oxygen coming from the decomposition of hydrogen peroxide. As a final effort to create a fuel hypergolic with hydrogen peroxide a sample is formulated with 10.63% TEA. During the mixing phase a reaction was observed between the TEA solution and ethanol. It is unknown which reaction is occurring here, but some bubbles are formed. The reaction stopped after a short period of time. The final sample was stable in air and showed a similar reaction with 96% HTP as the previous samples. When holding the reaction vessel no significant temperature increase was noticed.

This process was repeated using the DEZ solution instead of the TEA solution. First a sample was formulated using 2 ml ethanol and 0.1 ml DEZ solution, corresponding to a DEZ concentration of 0.75%. When transferring the DEZ solution into the mixing flask a reaction with the atmosphere is observed which releases white fumes. Presumably, this is a reaction between DEZ and oxygen which is still present inside the flask. When the smoke settles an opaque white liquid is left due to the formation of zinc oxide. This mixture is stable in air and does not show any reaction when 96% HTP is added. Probably all DEZ had already reacted with the oxygen and the pyrophoric liquid had thus lost its effect. For the formulation of the next sample, in an effort to remove as much oxygen from the mixing flask as possible it was flushed with alternating nitrogen and vacuum 6 times instead of the usual 3 times. It is unknown at what pressure the vacuum pump operates, but in a worst case scenario it is assumed to be 1 torr [58] which is equal to 1/760 atm or 133.3 Pa. This means that when the vacuum pump is connected to the mixing flask after some time the pressure inside the flask should be about 1/760 atm. Based on the ideal gas law, assuming the temperature does not change, this means that the number of air molecules inside the flask is 1/760th of what it was at atmospheric pressure. After filling the flask with nitrogen the pressure is back to 1 atm and the process is repeated. When repeating this 6 times it means that the fraction of air left is only $(\frac{1}{760})^6 = \frac{1}{192 \cdot 10^{15}}$ which is basically nothing. The test was performed again and 0.1 ml of DEZ solution was transferred to the mixing flask. Again a reaction with the atmosphere was observed and white fumes were created. The only reason that air could still be present inside the flask is due to a leak. It is unknown in which part of the system this leak is exactly but it is assumed to be in one of the septa. All septa available in the right size were already used before and it is therefore hard to tell if they actually prevent air from entering the flask. For further study better equipment should be used to create a 'leak free' setup to transfer pyrophoric liquids. If too much air leaks in all pyrophoric liquid will react before the actual fuel is formulated, making it useless.

5.4.3. TEA solution

As a reference case some experiments are also performed using only the 1.0M TEA solution in hexanes without first mixing it with ethanol. First a small quantity of the solution is transferred into an open empty container to observe the reaction with air. As soon as the TEA solution leaves the syringe white fumes are starting to be generated, but no ignition occurs. After a short time all TEA is reacted and an opaque white liquid is left which is hexanes with aluminum oxide. For a second experiment the reaction vessel is filled with 97% HTP. When adding a small quantity of TEA solution first the TEA reacts with the oxygen in the air forming white fumes. But not all TEA reacts and some of it comes into contact with the hydrogen peroxide resulting in ignition with a short delay. Figure 5.4 shows the steps of this experiment. In frame 2 the formation of white fumes can be seen, which are still visible in frame 3. Only a small quantity resulted in a relatively large flame as can be seen in frame 4. The reaction created some aluminum oxide which can be seen in frame 5 as it colors the reaction vessel white.

These experiments were performed to prove that TEA is in fact hypergolic with high concentrations of hydrogen peroxide. Even though the TEA was diluted to a concentration of 16.8% hypergolicity was still achieved. For further study it would be interesting to use TEA in a less diluted form to use it to its full potential.

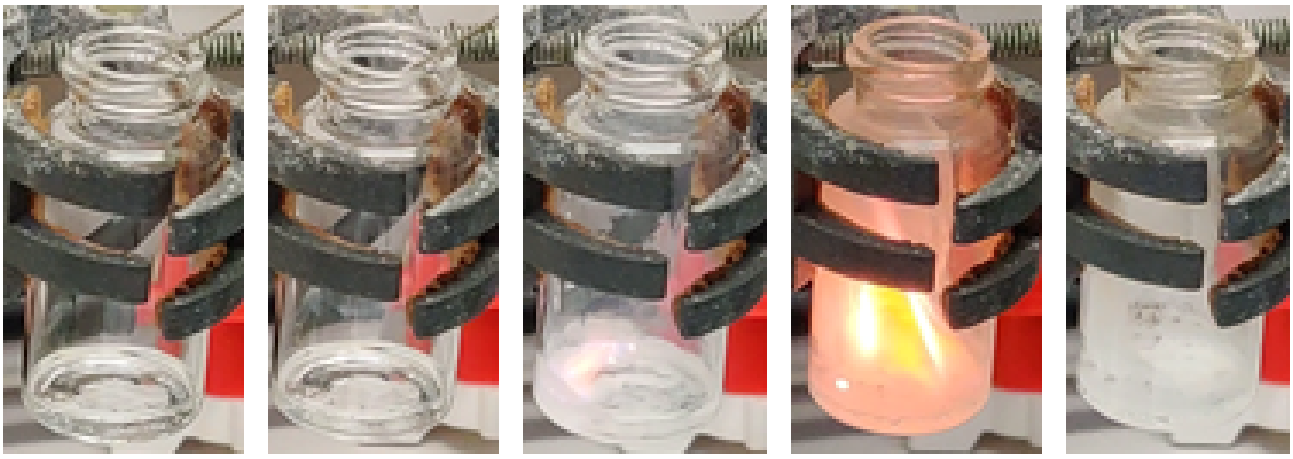

Figure 5.4: The reaction between 97% HTP and 1.0M TEA solution in hexanes in open air. *Frame 1:* reaction vessel filled with 97% HTP. *Frame 2:* white fumes as TEA solution is added. *Frame 3:* start of ignition. *Frame 4:* full combustion. *Frame 5:* leftover aluminum oxide from the reaction.

5.5. Conclusion

In this Chapter experiments were performed to assess the possibility of using a pyrophoric liquid to induce hypergolicity between ethanol and hydrogen peroxide. Based on literature pyrophoric liquids have shown to be hypergolic with high concentrations of hydrogen peroxide. For this study a 1.0M solution of triethylaluminum in hexanes and a 1.0M solution of diethylzinc in hexanes was used. For safe transfer of these liquids an experimental setup was build based on the use of a Schlenk line and a strict transfer procedure was developed. Using this fuel samples were formulated using first viscous ethanol and various concentrations of TEA solution. This resulted in a reaction between the thickening agent in the ethanol and the TEA solution causing the viscosity to increase, thereby forming a gel. The formulated gels were stable in air and did not show any reaction with high or low concentrations of hydrogen peroxide. Adding DEZ solution to viscous ethanol resulted in a similar effect. On top of that zinc oxide was formed giving the gel an opaque white appearance. The gellation effect is undesired since the goal of this thesis is to formulate a liquid fuel. For further study other thickening agents should be explored.

Due to the incompatibility with viscous ethanol, fuel samples are formulated using liquid ethanol. Various concentrations of TEA solution were added to ethanol resulting in a seemingly homogeneous mixture. The mixtures were stable in air and a slow decomposition reaction occurred when 96% hydrogen peroxide was added. With higher concentrations of TEA in the fuel, around 10%, aluminum oxide particles started to appear in the reaction vessel when 96% HTP was added. No significant temperature increase was noticed. The same experiment was then repeated for DEZ solution. Here, however, a problem occurred where the DEZ would react with oxygen still left in the mixing flask making the fuel useless. This oxygen was present due to an unknown leak in the system. For further study better equipment has to be used and more care has to be put into the creation of the transfer setup to mitigate this problem.

Finally some experiments were performed using only the TEA solution, without mixing it with ethanol. The solution was transferred into an open empty vessel to study the reaction with air. Only white fumes were observed and no ignition occurred. Aluminum oxide was left behind as a product of the reaction. Then the same experiment was repeated, only now 97% HTP was present in the reaction vessel. The mixture of TEA solution and 97% HTP ignited with a short

delay, proving that TEA is in fact hypergolic with high concentrations of hydrogen peroxide. For further study it is advised to use a less diluted form of TEA to use the full potential of this pyrophoric liquid.

6

Ignition delay study

This Chapter will focus on the study that has been carried out to determine the ignition delay of the developed propellants. First a literature review is done where various methods are explored to determine ignition delay. Then a method is chosen and the equipment and experimental setup required is described. Following this a test plan is presented which lists all performed tests including the test procedure. Finally the results of these tests are presented. Here, first the ignition will be characterized, after which the ignition delay is determined for each developed sample. Based on these results the effect of various parameters on the ignition delay is determined as well as their effect on temperature.

6.1. Literature review

The screening of various propellant formulations in Chapter 3 already gave some insight in which candidates show hypergolicity with HTP. To better characterize the candidates and to be able to compare them to already existing alternatives, their hypergolicity has to be expressed quantitatively. The key parameter in this case is the ignition delay time (ID). It is defined as the time between oxidizer and fuel contact and ignition [1]. The ID time can be split up into physical and chemical delay times. Here physical delay indicates the time between contact of the oxidizer and fuel and achieving proper mixing and vaporisation. Chemical delay is the time between the achievement of vaporisation and ignition. Figure 6.1 gives a graphical representation of the relationship between these parameters.

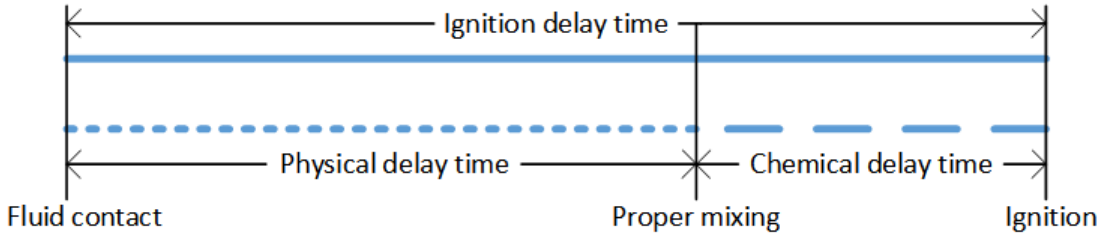

Figure 6.1: A graphical representation of physical, chemical and ignition delay time.

There are 3 types of tests which are typically used to determine the ID time of a hypergolic propellant combination. These include drop test, impinging jet test, and engine test. A short description of each is given below.

Drop test: In a drop test a droplet of fuel is dropped on a pool of oxidizer, or vice-versa. The ID can be measured by filming the reaction with a high speed camera that has a high enough frame rate to capture the different stages of ignition, or by use of sensors like photodiodes or thermocouples. Drop tests are performed at ambient pressure and temperature and therefore are a bad representation of a reaction in a real combustion engine. This, in combination with the poor mixing of fuel and oxidizer, results in an ID time higher than those measured with an impinging jet or engine test where conditions are much closer to a real engine [59]. Drop test do, however, give a good indication of ID and allow for comparison between different propellant candidates. Since drop tests only require a small amount of propellant and a relatively simple setup they are ideal for initial screening and can quickly and cheaply provide insight in the potential of a certain hypergolic propellant combination.

Impinging jet test: Like the name already suggests, in an impinging jet test the fuel and oxidizer are brought into contact by injection through an impinging jet injector. An example of an impinging jet test setup is shown in Figure 6.2. The injector is placed in a vessel closely resembling a combustion chamber. Using a vessel like this enables the researcher to control temperature and pressure and is therefore able to create conditions much closer to those in a real engine, as compared to drop tests. Since an injector is used also the mixing of fuel and oxidizer closely resembles the effects seen in a combustion engine. An impinging jet test allows for researching the effect of ambient temperature and pressure, mixture ratio, and injection velocity on the ID time. The disadvantage of this type of test is its complexity and higher cost compared to performing a drop test.

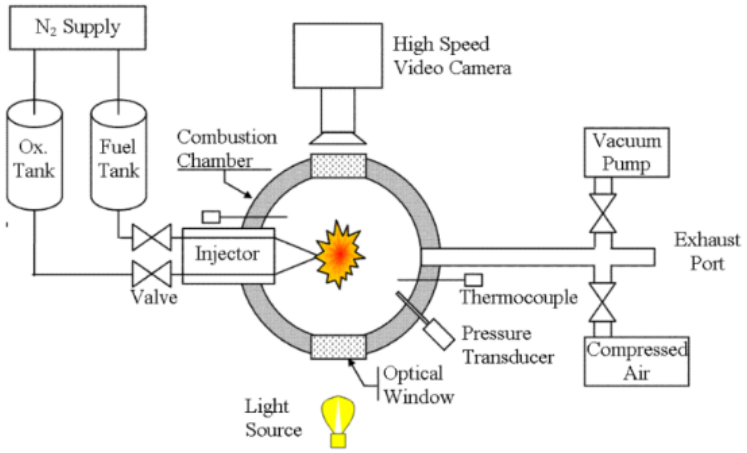

Figure 6.2: A schematic of an impinging jet test setup [60].

Engine test: Engine tests are the last step in assessing the ID time of a propellant combination. Here a real rocket engine is used which gives conditions as close as possible to application conditions. Engine tests are very similar to impinging jet tests but differ on some key aspects. Measuring of the ID time is not performed by visual observation but instead the chamber pressure is used. The ignition point is defined as the time the combustion chamber reaches 90% of the steady-state pressure [61]. In addition to this, in an engine test multiple injector elements can be used, where only one is used in an impinging jet test. Engine tests are the most complex and expensive of the 3 types described here. They require a complete engine design based on the chosen propellant combination. Engine tests are therefore only performed with very promising candidates resulting from the impinging jet tests.

As part of this thesis several new fuels have been formulated with a potential to show hypergolicity with high concentrations of hydrogen peroxide. During the screening phase hypergolicity was observed for some of these newly developed fuels. There is however no data yet on the ID time of any of these fuels. Therefore, as a first indication of performance, it is chosen to perform drop tests. Looking at the resources available for this thesis, in terms of time and funds, performing drop tests is the only realistic option. Due to the relatively simple experimental setup required it is possible to test a high number of samples within a short amount of time. In order to create a drop test setup for this thesis a literature review is performed, comparing experimental setups developed in the past.

Table 6.1: An overview of the equipment used in drop test setups found in literature.

Reference	[21]	[62]	[14]	[63]	[64]	[20]	[65]
Computer system	X	X	X	X	X	X	X
Diffuse light source				X	X		
High-speed camera	X	X	X	X	X	X	
Laser	X		X	X			X
Microphone	X		X				
Oscilloscope			X	X			
Photodiode	X		X	X			X
Photomultiplier tube			X				
Reaction vessel	X	X	X	X	X	X	X
Syringe	X	X	X	X	X	X	X
Syringe actuator		X	X	X			X
Thermocouple						X	X

Table 6.1 shows an overview of the equipment used in drop tests found in literature. Quickly it becomes clear that some of the equipment is absolutely necessary since it is used in all cases. These include a computer system, a reaction vessel and a syringe. Then, there are several options for measuring the ID time. The option used in almost all cases is the high speed camera. By filming the reaction with a high enough frame rate, it is possible to capture the moment of contact and the moment of ignition. Additionally, chemical and physical phenomena which occur between first contact and ignition can also be observed. A second option is the use of a laser in combination with a photodiode. The laser is positioned in a way that the beam horizontally crosses the reaction vessel. At the opposite side of the vessel a photodiode is placed which acts as a target for the laser. Figure 6.3 from H. Kang et al [14] shows very clearly how a laser/photodiode combination can be used to detect the different stages of ignition. Here it is divided into 6 stages:

1. A droplet is generated by the syringe and falls until it reaches the top of the laser beam.

2. When the droplet crosses the laser beam it scatters the light. This results in less light reaching the photodiode, causing a drop in the signal.

3. The distance between the bottom of the laser beam and the top of the fuel is measured beforehand. Using the drop height, the velocity of the droplet can be calculated. Combining these two parameters the time it takes for the droplet to travel from the bottom of the laser beam to the surface of the fuel can be determined.

4. When the oxidizer droplet comes in contact with the fuel it initiates liquid phase reactions. Due to the high impact velocity, violent sloshing will occur and droplets will be expelled in all directions. Some of these droplets will cross the laser beam and can thus be detected by the photodiode.

5. Resulting from the liquid phase reactions are gaseous products. A cloud of gaseous reactants will quickly expand. These gases will scatter the laser beam, and can thus as well be detected by the photodiode.

6. When the exothermic reactions have resulted in a temperature increase above that of the auto-ignition temperature of the mixture, the gases will ignite. The ignition will release energy in the form of heat and light. The sudden increase in luminosity can again be detected by the photodiode.

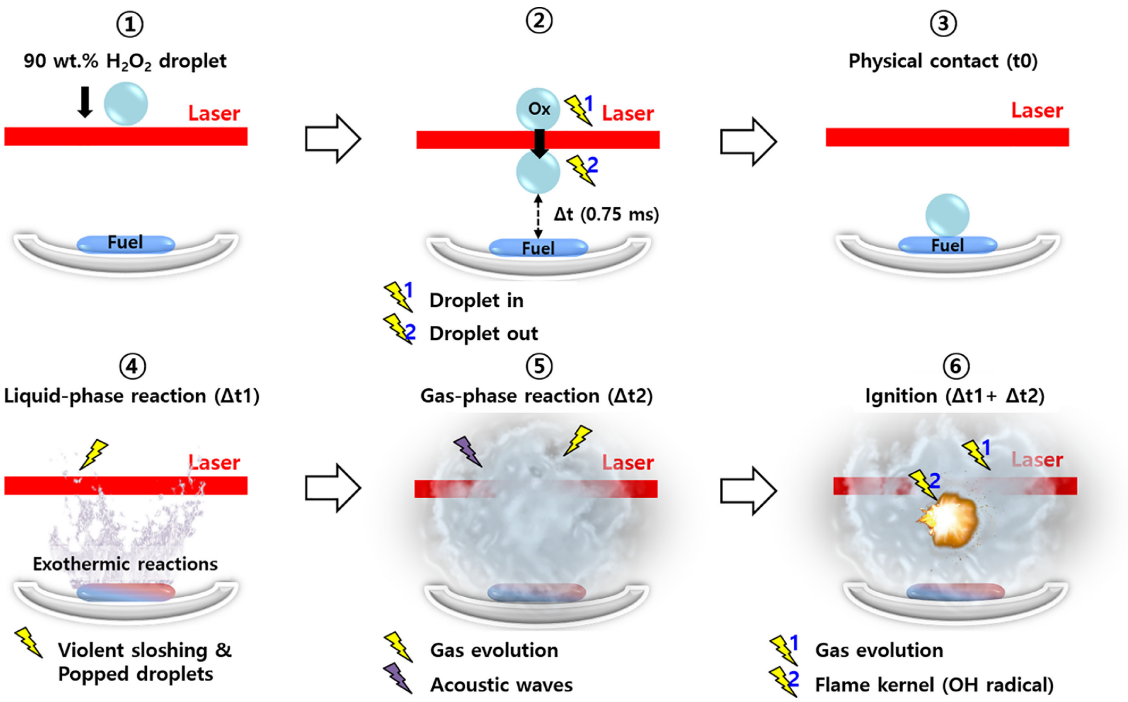

Figure 6.3: A schematic representation of the different steps of a drop test that can be measured with a laser/photodiode combination [14].

Some less used sensors for detecting ignition include a microphone, a photomultiplier tube (PMT), and thermocouples. These sensors can only detect the start of ignition but not the time of initial contact between the fuel and oxidizer. Therefore, if these sensors are to be used, it is in combination with a laser/photodiode setup. Both a microphone and a PMT were used in the drop test setup described by H. Kang et al [14]. The microphone was used during step 5 of Figure 6.3, where the quick expansion of the gas caused pressure waves in the air which would be picked up by the microphone. Step 6 made use of the PMT. It was setup to only capture light at a wavelength of 307 nm, which is the optical emission of hydroxyl OH radicals. A large amount of OH radicals is being produced during the ignition due to the decomposition of the oxidizer, hydrogen peroxide, which are picked up by the PMT. Finally, a thermocouple can be used for measuring ignition, as well as the temperature profile of the flame. By placing the thermocouple close to the point of ignition, a rapid rise in temperature can indicate the ignition.

The remaining equipment listed in Table 6.4 is regarded as secondary equipment. It includes a light source, an oscilloscope, and a syringe actuator, which are not a necessity for performing a drop test, but could be of added value. A syringe actuator, for example, can help to create a consistent droplet size and allows the researcher to place himself at a safe distance from the reaction vessel.

Based on this literature review the following equipment has been selected to be used in the drop test setup for this thesis: Computer system, light source, high-speed camera, laser, photodiode, reaction vessel, syringe, syringe actuator, and thermocouple. Section 6.2.2 will go more into detail about the specifications of the equipment used, and give an overview of the created drop test setup which is used in this thesis.

6.2. Experimental setup

The most important equipment to be used in the drop test setup was already pointed out in the previous section. On top of this there is some additional secondary equipment used. Subsection 6.2.1 lists the equipment used and gives a short description, then in subsection 6.2.2 an overview of the drop test setup is given.

6.2.1. Equipment list

A full inventory list can be found in Table 6.2. A description of each item is given below.

Table 6.2: A list of the equipment required for the drop test setup.

Inventory			
ID	**Item**	**ID**	**Item**
FH	Fume hood	DAQ-PD	DAQ NI-9215
LS	Light source	SYR	Syringe
HSC	High-speed camera	SYP	Syringe pump
PC	Computer system	CT	Capillary tube
LSR	Laser	RV	Reaction vessel
PD	Photodiodes	AT	Alignment tool
TC	Thermocouples	HTP	High test peroxide
DAQ-TC	DAQ NI-9219	Fuel	Fuel

The drop test setup was created in the chemical lab of the DASML in the Delft University of Technology. A fume hood was made available with a table inside on which the setup could be placed. The advantage of using a fume hood is that it provides a safe working environment, a safety glass could be brought down to protect from any splashing occurring during the experiments. On top of that it could be darkened. This, in combination with the light source, resulted in a constant light environment for each test. The light source is designed to cooperate well with the high speed camera. By dimming the light, the correct luminescence required by the camera could be reached, resulting in a clear captured image. The high-speed camera is a Photron mini AX200, which could be reserved from the DASML in combination with the light source. At its maximum resolution of 1024x1024 px it has a maximum frame rate of 6400 fps, other specifications can be found in Appendix B.3. Unfortunately, the images captured by the camera are black and white. This is sufficient for determining ignition delay but a color camera would give more insight into the effects happening before ignition. The HSC is connected to the PC through an Ethernet cable. On the PC Photron software package 4.0.4.1 is installed, which is required to operate the camera.

A class 2 laser was used with a maximum power output of <1mW. It produces a visible light beam with a wavelength of 650±10nm. Two FDS100 - Si photodiodes from Thorlabs were used. With a rise time of 10ns, they are fast enough to detect ID time since it is usually expressed in ms. Appendix B.1 contains the specification sheet of the used PDs. Wavelengths ranging from 350-1100nm can be detected, which includes light emitted by the laser, and visible light emitted by a combustion reaction. The specification sheet includes a recommended circuit for powering one PD. Since two are used the circuit is slightly modified and two PDs are placed in parallel. The resulting circuit can be seen in Figure 6.4.

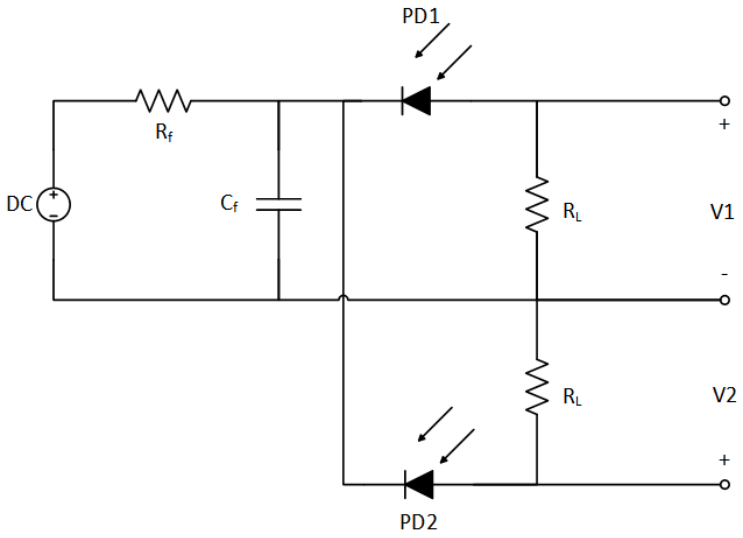

Figure 6.4: A drawing of the electrical circuit used to power the photodiodes. Adapted from [66].

A direct current of 1000 mA at 12 V is applied. A noise filter is implemented by use of a resistor R_f of 1 kΩ and a capacitor C_f of 0.1 μF. Both photodiodes require a load resistor from the anode to the circuit ground. This will convert the current produced by the PDs into a voltage which is used as the output of the circuit. Both load resistors R_L are 15 kΩ. The output voltages V_1 and V_2 are connected to a National Instruments (NI) Data Acquisition card (DAQ) with model number 9215. This model has a maximum sampling rate of 100 kS/s/ch which means that every single PD can be sampled at a frequency of 100 kHz. Translated this is 0.01 ms per sample showing that this is fast enough to detect ignition which is in the order of milliseconds.

Thermocouples used for this experiment are k-type (Nickel-Chromium / Nickel-Alumel) since they are inexpensive, accurate, reliable and have a wide temperature range. The TCs are manufactured by OMEGA are unsheathed and have a very fine diameter of 0.125 mm. Such fine diameter is desired since it results in a fast response of the temperature measured. Only small amounts of propellant are used during the drop test and the combustion only lasts for a time in the order of milliseconds. Within this short time the TC has to be able to heat up and record the temperature. For long term exposure the maximum working temperature of these TCs is 593^{o}C, however, for short term exposures temperatures of above 982^{o}C can be measured. Appendix B.2 contains a specification sheet for the used thermocouples. Before using the TCs they are calibrated using 0^{o}C and 20^{o}C water and insulated using shrink tubes. The insulation prevents the thermocouples from getting into contact with conductive materials, which can affect the measurement. Like the PDs the TCs are read using a DAQ from NI.

In this case model number 9219 is used which has 4 inputs especially designed for reading thermocouples. Each channel can be sampled at a frequency of 50 Hz which translates to an accuracy of 20 ms. This is not fast enough to determine ID time accurately but the TCs are mainly used to asses the flame temperatures reached during combustion.

A combination of a syringe pump, syringe, and capillary tube was used for droplet generation. The syringe pump used is model NE-1000 which has a programmable discharge rate which was set at 1.3 ml/min. A 2 ml plastic syringe was used with an internal diameter of 8.8 mm. The output of the syringe was connected to a capillary tube using a rubber tube. During the experiment the capillary tube was used to store and deposit the HTP. The droplets generated fell on the reaction vessel containing a fuel sample. A petridish was used as the reaction vessel. It has the advantages of easy placement of the TCs and allows the laser beam to be placed close above the fuel without interfering with the reaction vessel glass. As was learned from a graduated Master student who had also performed drop tests during his thesis, it can be challenging to accurately align all components of the setup. Therefore, an alignment tool was designed to aid in this process.

6.2.2. Setup

The final experimental setup used was placed on a table inside a fume hood of the DASML chemical lab. A picture of this setup can be found in Figure 6.5. Both the HSC and DAQ units are connected to the computer system for data recording. The syringe pump was placed such that is was easily operated and did not obstruct the view of the HSC. A 1x1 cm mesh was placed as a background for the recording to give some insight in the dimensions of the observed phenomena. The light source was setup to create a homogeneously lit up field of view for the camera.

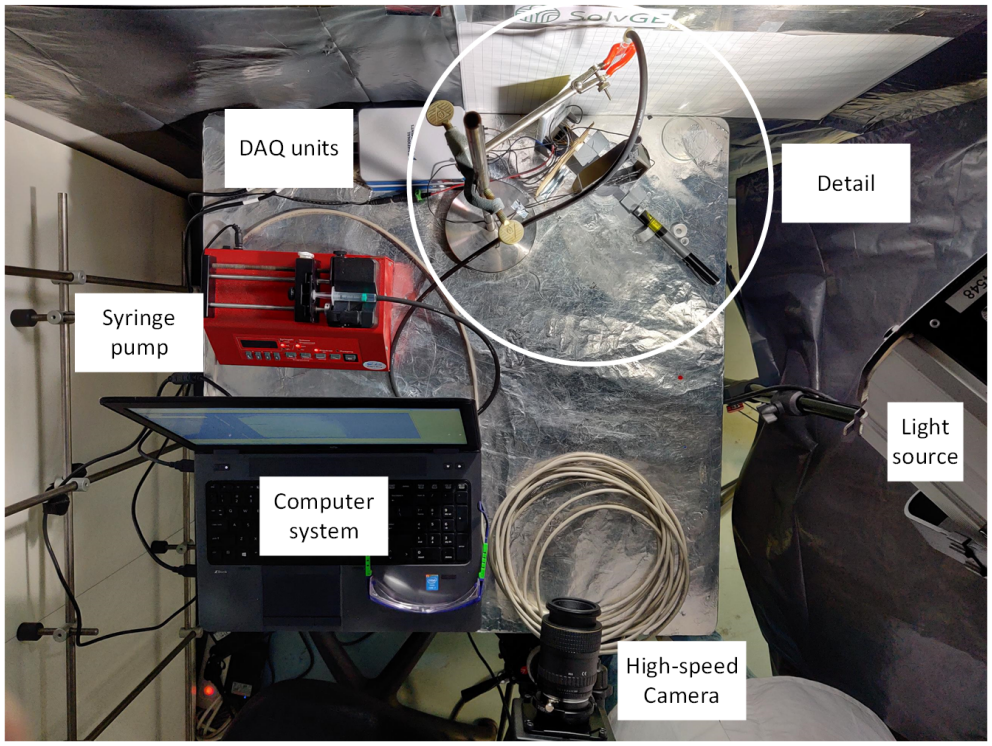

Figure 6.5: A picture of the drop test setup with components indicated.

A more detailed view of the reaction vessel and sensors can be seen in Figure 6.6. It shows the alignment tool which is 3D printed in house. It contains mounts for the laser, photodiodes, thermocouples, and reaction vessel. At the top of the alignment tool a cylinder is placed which can be used to position the capillary tube above the center of the reaction vessel, see Figure 6.6b. This ensures that droplets generated by it will always cross the laser beam and hit the reaction vessel in the center. The laser and PD mounts ensure that the laser crosses the center of the reaction vessel and hits the PD placed on the opposite side. Of the two PDs, the bottom one is aligned with the laser and used to detect the falling droplet, as well as gasses generated by initial reactions. The second PD is used to detect ignition. A special cap is designed for this PD, which can be seen as a white cylindrical part in Figure 6.6a. This cap shields off most light coming from the environment and limits the PDs field of view to the area where ignition will occur. The PDs are mounted on a breadboard which is used to create the electrical circuit that provides power. To protect this circuit from any splashing occurring during the experiment a cardboard shield is placed in front of it with holes for the PDs. This shield also helps the PDs stay in place. For the TCs several mounting places were included in the alignment tool. This allowed TCs to be placed at various heights from the reaction vessel. During the experiment they were placed at 7, 27 and 47 mm above the fuel surface. The TCs are placed 5 mm out of the center as to not interfere with the falling droplet.

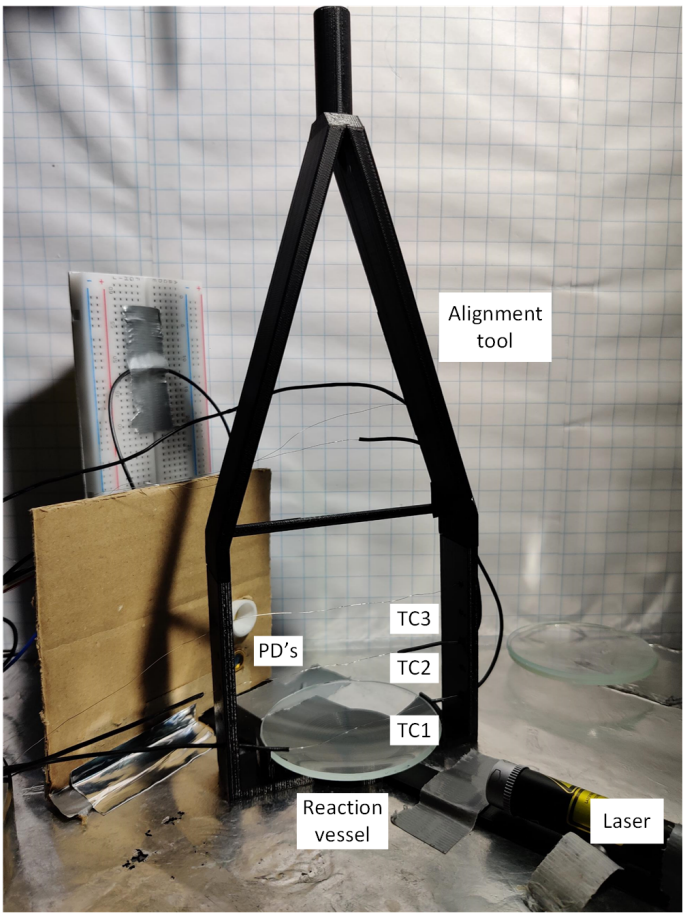

(a) Detailed image of the alignment tool with equipment mounted on it.

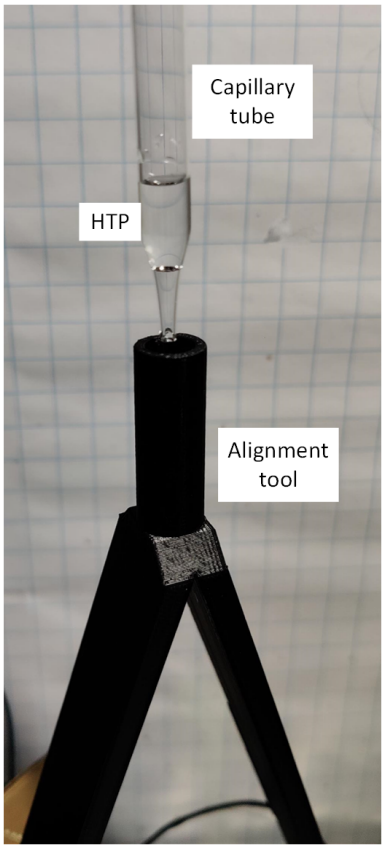

(b) Zoom in on the top of the alignment tool which guides the capillary tube in position.

Figure 6.6: Detailed images of the reaction vessel with sensors placed around it.

6.3. Test plan

In this section the test plan is described. First the different variations applied in the drop tests will be explained. Then an overview will be given on the procedure taken to perform a test.

6.3.1. Test variations

The goal of performing drop tests is not only to determine the ID time and temperature profile of the developed fuels, but also to assess how various parameters affect the ID time and temperature. The most promising propellant formulation resulting from the screening presented in Chapter 3 is used as a baseline for the experiments. A combination of viscous ethanol and MCAT showed the best results in terms of hypergolicity with HTP. Table 6.3 shows the parameters used during the baseline test.

Table 6.3: Parameters of the baseline drop test experiment.

Fuel	Catalyst	wt% Cat	%H2O2	Fuel volume	Fuel age	Drop height
Visc. Eth.	MCAT	3	97	0.1 ml	0	23 cm

Starting from the baseline the effect of various parameters on ID time and temperature will be studied. Every experiment only one parameter is changed with respect to the baseline. This will give an insight into the effect of each individual parameter. The parameters which are varied are listed below including a short description and expected results. A full list of performed drop tests can be found in Table 6.4.

Catalyst concentration: The wt% of MCAT in viscous ethanol decreased from 5%, to 3%, to 2%, to 1%, to finally 0.5%. Lowering the concentration is expected to increase the ID since less catalyst is available for the HTP to aid in its decomposition.

HTP concentration: The concentration of HTP is varied from 87.5%, to 90%, to 95%, to 97%. A high concentration of HTP is expected to result in a short ID since it has two benefits. It contains more H2O2, meaning there is more oxidizer available to react. And it contains less water, meaning less energy generated by the decomposition is wasted on heating up this water.

Liquid vs. Viscous ethanol: No thickening agent will be added to the ethanol, leaving it as a liquid. Then a similar study of varying catalyst concentration will be conducted, as was performed with viscous ethanol. Here a wt% of 10, 5, and 3 MCAT was used to create the propellant formulations. It is expected that, at equal concentrations of catalyst, liquid ethanol will show a shorter ID since it requires less energy to vaporize, in comparison to viscous ethanol. The viscous ethanol, however, is expected to show hypergolicity at lower concentrations of catalyst than is possible with liquid ethanol due to the energetic nature of the thickening agent.

Ethanol vs. Butanol: Butanol will be used for creating the propellant instead of ethanol. The butanol will be made viscous using the same wt% of thickening agent as was used for ethanol. MCAT will be added to the viscous butanol in concentrations of 5 wt% and 3 wt% to make it hypergolic with HTP. It is expected that changing from ethanol to butanol will result in an increase in ID based on a study by Shoaib et al. [67] on the effect of alcohol carbon chain length on ID.

MCAT vs. FCAT: A propellant will be formulated by combining viscous ethanol and FCAT. Two formulations are tested with a concentration of 5 wt% and 3 wt% FCAT. Based on the experiments performed in Chapter 3 it is expected that formulations containing FCAT show a

longer ID in comparison with MCAT formulations with the same concentration.

Fuel volume: The volume of fuel deposited on the reaction vessel is varied from 0.3 ml, to 0.2 ml, to 0.1 ml, to 0.05 ml. It is expected that a smaller volume of fuel results in a shorter ID. If less fuel is used less energy is required to vaporize it, which shortens the physical delay time.

Fuel age: The sample used for the baseline experiment was stored for 4 weeks. After this time period the ID will again be determined by performing a drop test. It is expected that the sample will show an increase in ID as it ages.

Drop height: The drop height can influence the ID since it affects the impact velocity of the droplet on the fuel pool. A higher drop height results in a higher impact velocity. It is expected that this will lead to better mixing conditions and atomization that will result in a decreased ID. The standard drop height for each test is 23 cm. To evaluate this effect tests are also performed with a drop height of 18 cm and 28 cm.

Table 6.4: Overview of all drop tests performed.

#	Fuel	Catalyst	wt% Cat	%H2O2	Fuel volume	Fuel age	Drop height
1	Visc. Eth.	MCAT	5	97	0.1 ml	0	23 cm
2	Visc. Eth.	MCAT	3	97	0.1 ml	0	23 cm
3	Visc. Eth.	MCAT	2	97	0.1 ml	0	23 cm
4	Visc. Eth.	MCAT	1	97	0.1 ml	0	23 cm
5	Visc. Eth.	MCAT	0.5	97	0.1 ml	0	23 cm
6	Visc. Eth.	MCAT	3	95	0.1 ml	0	23 cm
7	Visc. Eth.	MCAT	3	90	0.1 ml	0	23 cm
8	Visc. Eth.	MCAT	3	87.5	0.1 ml	0	23 cm
9	Liq. Eth.	MCAT	10	97	0.1 ml	0	23 cm
10	Liq. Eth.	MCAT	5	97	0.1 ml	0	23 cm
11	Liq. Eth.	MCAT	3	97	0.1 ml	0	23 cm
12	Visc. But.	MCAT	5	97	0.1 ml	0	23 cm
13	Visc. But.	MCAT	3	97	0.1 ml	0	23 cm
14	Visc. Eth.	FCAT	5	97	0.1 ml	0	23 cm
15	Visc. Eth.	FCAT	3	97	0.1 ml	0	23 cm
16	Visc. Eth.	MCAT	3	97	0.3 ml	0	23 cm
17	Visc. Eth.	MCAT	3	97	0.2 ml	0	23 cm
18	Visc. Eth.	MCAT	3	97	0.05 ml	0	23 cm
19	Visc. Eth.	MCAT	3	97	0.1 ml	4 weeks	23 cm
20	Visc. Eth.	MCAT	3	97	0.1 ml	0	18 cm
21	Visc. Eth.	MCAT	3	97	0.1 ml	0	28 cm

6.3.2. Test procedure

Every drop test is completed by performing the same sequence of steps. By adhering to the same procedure every time the chance of making mistakes as well as the variability between tests is reduced. The procedure can be divided into three phases: Preparation, execution, and post-processing.

During the preparation phase first the computer is setup. It is connected to the DAQ units and

the HSC. Then, all equipment (HSC, LS, LSR, DAQ, PD, SYP) is turned on. A script for reading PD and TC values is opened in Labview 2018 and the PFV program is opened to operate the HSC. The labview script can be found in Appendix C.3. The HSC is setup by focusing its lens on the beads of the TCs, setting the frame rate to 6400 fps, resolution to 768x768 px, and trigger mode to start. The resolution is reduced since it reduces the field of view to the area of interest and increases the recording time, which is limited by the internal storage of the camera. Then the fuel samples to be tested are formulated and the concentration of H_2O_2 is measured. Both in the same way as described in Chapter 3.

The execution phase starts by loading the HTP into the capillary tube, and depositing the correct amount of fuel on the reaction vessel. A pipette with an accuracy of 1μL is used to deposit an accurate volume of fuel. Then, with the help of the alignment tool, the capillary tube is positioned directly above the center of the reaction vessel. Labview is used to start the recording of the PDs and TCs. PFV is used to start the recording of the HSC. Then, by manually pressing a button on the syringe pump, a droplet of HTP is created which falls into the fuel pool, after which a reaction occurs.

After the reaction the post-processing phase starts. First, the data recording is stopped. In PFV the video captured by the HSC is watched back to see if it was successful in capturing all desired phenomena. If so, undesired parts of the video are cut off and the part containing the reaction is saved on an external hard drive. Data recorded by Labview is saved automatically. After each test the reaction vessel was cleaned with first acetone and then water, before it could be used for a new test.

To get a more reliable result at least a total of three drop tests are performed with each sample. After completion of three tests the sensor and camera data are preliminary analyzed. If something was missing or not measured correctly an additional drop test was performed. This was done until three drop tests were successful.

6.4. Results

In this section the results of the performed drop tests will be presented. First a characterization of the ignition profile will be described. Here the different phases leading up to ignition are discussed. Then the results regarding ID and temperature measurements are presented. These results are then used to analyse the effect of each parameter which was varied during the drop tests on the ID and temperature.

6.4.1. Ignition characterization

After completing all drop tests the data from the HSC, PDs, and TCs were analyzed. In almost all cases, the steps leading up to ignition were very similar. Only in the case where liquid ethanol was used, some major differences were found. Therefore, the ignition characterization will be done for two separate cases, viscous and liquid. Every test performed can be represented by one of these two cases. The fuel column of Table 6.4 shows which sample can be represented by which type of ignition.

Ignition of a viscous sample

For characterization of the ignition of a sample based on viscous ethanol the baseline experiment is used. Details of the sample used in this experiment can be found in Table 6.3. The characterization of ignition is based on data collected from the HSC as well as the PDs.

Data from both these sources clearly divide the ignition process into several phases. These phases of ignition will be discussed below and will be clarified using Figures 6.8 and 6.9 which visualize the HSC and PD data, respectively.

- **Point 1:** During the first phase the reaction vessel is filled with only fuel and the HTP droplet is about to make contact. Number 1 in Figures 6.8 and 6.9 correspond to this phase. The voltage output of PD1 is stable at 3 V, where the output of PD2 is stable around 0.1 V. This difference is due to the laser which illuminates the surface of PD1.

- **Point 2:** Here the HTP droplet makes contact with the fuel pool which is present in the reaction vessel. ID time is measured starting from this point. In Figure 6.8 frame 2 this point is indicated by a slight deformation of the HTP droplet. In case of the PD it is indicated by a drop in the output signal of PD1, indicated by a 2 in Figure 6.9. This short drop in signal is caused by the HTP droplet crossing the laser beam. Some of the light coming from the laser is reflected by the droplet and therefore does not reach the PD. Less light on the PD results in a lower output signal. Due to interference with the reaction vessel, the laser beam could not be placed closer to the fuel than 7.8 mm. This means that the drop in the PD signal does not exactly match with the time of contact. To correct for this, the time it takes for the droplet to fall from the bottom of the laser beam to the top of the fuel pool is calculated. This time depends on the drop height and is calculated using the Matlab script presented in Appendix C.2. For the nominal drop height of 23 cm the correction time is equal to 3.7 ms.

- **Point 3:** Point 3 marks the end of the physical delay time, which started at point 2. Gasses are starting to form coming from two different sources. Firstly, the HTP is decomposing into liquid water and oxygen gas, as it comes into contact with the catalyst which greatly speeds up the decomposition. This reaction is exothermic and releases enough thermal energy to heat up the ethanol above its boiling point and vaporize it. Due to the increased viscosity of ethanol the gasses are causing bubbles to form. The fuel pool swells up as the network structure created by the thickening agent in the ethanol tries to hold it together and the gasses created inside try to expand. To give a more clear view of this phenomena a close-up is shown in Figure 6.7. Figure 6.7a shows the size of the fuel pool right after impact with the HTP droplet, Figure 6.7b shows the swollen fuel bubble due to the decomposition of HTP. The size is clearly made visible by the fact that the bubble engulfs part of the TC, which is fully visible in Figure 6.7a. Gasses are released by bubbles popping. Since the HSC films black and white it is hard to visually detect these gasses. Here the laser beam offers some help by reflecting off the gasses into the lens of the camera. Frame 3 of Figure 6.8 shows this effect. Since the gasses reflect part of the laser beam into the camera, it must mean that less light is reaching the PD. When looking at Figure 6.9 this is clearly visible at point 3. Here the light received by the PD gradually decreases as more and more gasses block the laser beam.

- **Point 4:** Ignition takes place. Point 4 is the first frame that ignition is observed using the HSC. A small light point is visible in the fuel bubble indicated in frame 4 of Figure 6.8. It is unsure if this is the actual first ignition point since ignition might have happened in places not visible for the HSC. Since the light point is so small, and almost no light is emitted by it, the PD is unable to detect it. Locally the temperature has risen high enough to be over the auto-ignition point of ethanol. The vaporized ethanol then reacts with the oxygen gas created by the decomposition of HTP. Unfortunately, the conditions are not suitable for a sustainable combustion. This might be due to a lack of oxygen for the ethanol to combust with, or due to a loss of heat as a result of more ethanol vaporizing.

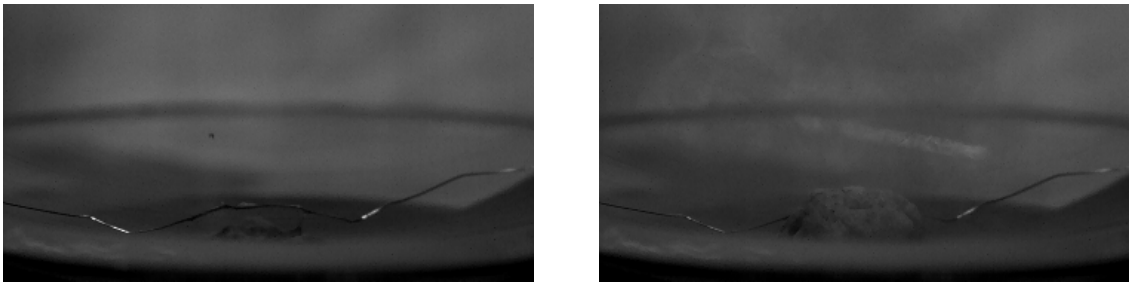

(a) Close-up of the fuel pool right after impact with the HTP droplet.

(b) Close-up of the fuel pool about 50ms after impact of the HTP droplet.

Figure 6.7: The bubbling effect created by the decomposition of HTP in viscous ethanol.

- **Point 5:** What happens at point 5 is similar to what happens in point 4 but occurs at multiple places inside the fuel bubble. Frame 5 of Figure 6.8 shows multiple points of ignition in the fuel bubble. Next to this also some sparks are created and expelled in all directions. Here the temperature has risen high enough to sustain a stable combustion. In the PD signal, Figure 6.9, this is indicated by number 5 and acts as the first increase in light received by the PDs.
- **Point 6:** The various sites of ignition have led to the ignition of the gas cloud above the fuel pool containing oxygen and vaporized ethanol. The flame spreads very rapidly and burns all available gasses in a short time. Due to this rapid expansion a shock wave is created which sounds like a loud bang. As can be seen in Figure 6.8 frame 6 this reaction releases a lot of light. The signal obtained from both PDs give a sudden large increase at this point, see Figure 6.9 point 6.
- **Point 7:** After the main combustion peak some unburned gasses might still be stored in bubbles. When these bubbles are popped they release these gasses which fuel the combustion and can slightly increase the light emitted by it. This phenomena can be seen in Figure 6.9 indicated by a 7. After this point the combustion dies out as there will be no more gasses left to burn.

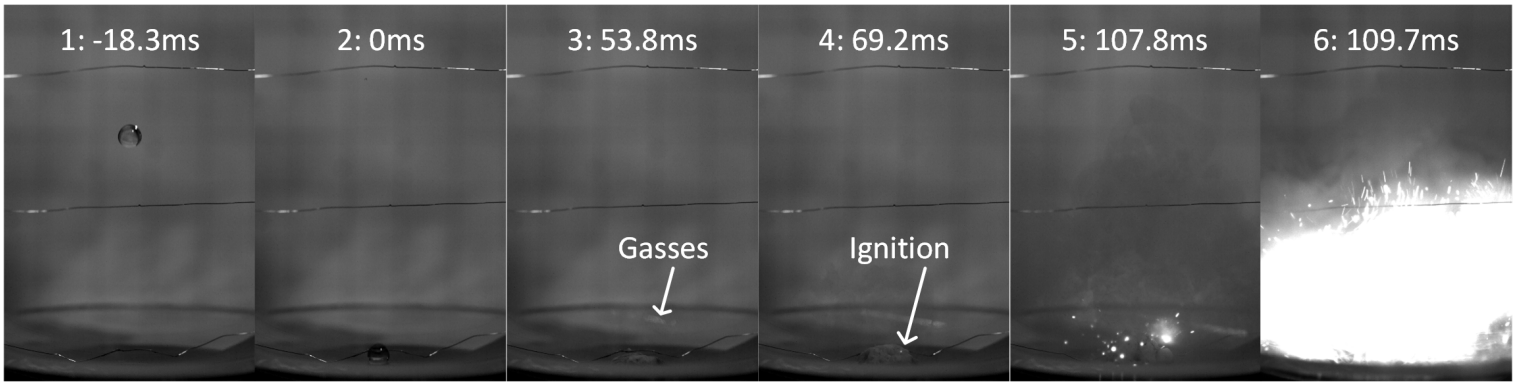

Figure 6.8: Ignition sequence of viscous ethanol with 3% MCAT in combination with 97% HTP. 1: HTP droplet falling (*t=-18.3ms*). 2: HTP droplet touches fuel pool (*t=0ms*). 3: Decomposition of HTP and vaporisation of fuel (*t=53.8ms*). 4: Start of ignition (*t=69.2ms*) 5: Ignition has progressed to multiple locations (*t=107.8ms*) 6: Full ignition of the vaporised gasses (*t=109.7ms*).

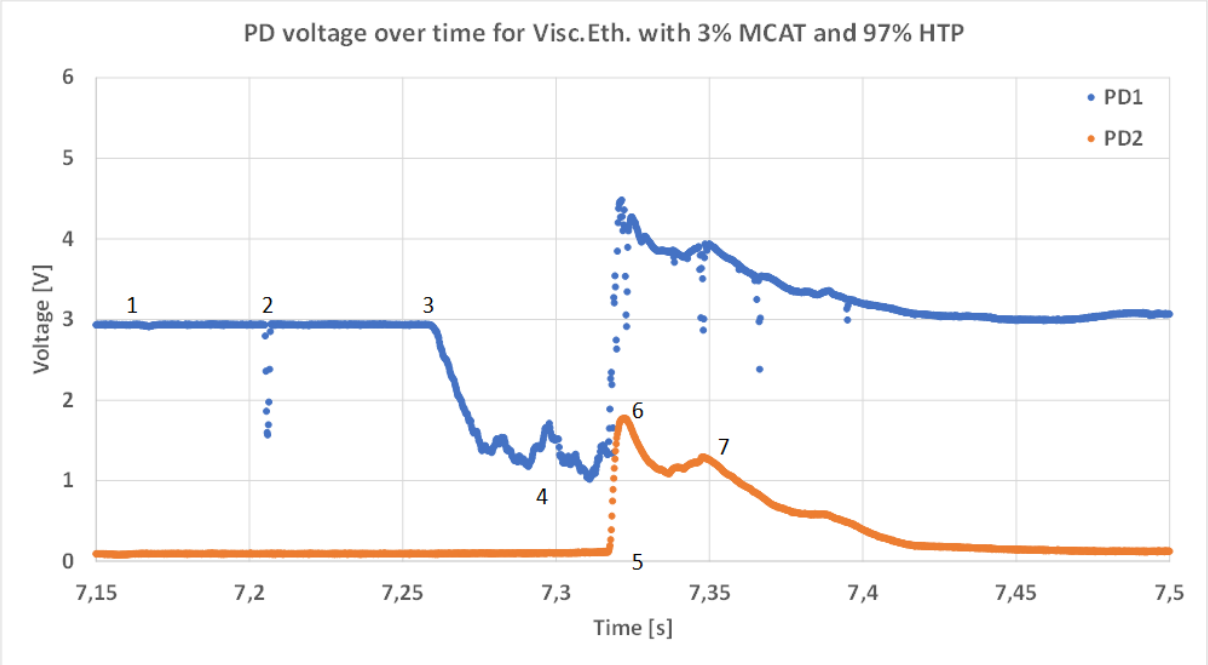

Figure 6.9: A plot of the PD voltage measured using two PDs during the baseline drop test. Numbers indicate the different phases of the ignition.

Ignition of a liquid sample

For characterization of the ignition of a sample based on liquid ethanol sample 9 from Table 6.4 is used. This sample contains 10% MCAT and is ignited with 97% HTP. Characterization for the liquid case is done in a similar manner to that of the viscous case. It is based on data collected from the HSC and PDs, which is again used to divide the ignition into several phases. There are, however, some important differences with respect to the viscous case. The phases of ignition will be discussed below and will be explained using Figures 6.10 and 6.11.

- **Point 1:** The first phase is exactly the same as for the viscous case. The HTP droplet is about to make contact to the fuel deposited in the reaction vessel. Both PDs give a stable output signal.
- **Point 2:** Also at point 2 nothing has changed yet with respect to the viscous case. Frame 2 of Figure 6.10 shows a slight deformation of the HTP droplet indicating contact with the fuel sample. Figure 6.11 shows a drop in the signal of PD1 indicating the droplet crossing the laser beam. Since the droplet is released from the same height as for the viscous case, the time correction required is also equal.
- **Point 3:** From this point on, differences are starting to occur. The impact of the HTP droplet on the liquid fuel sample causes it to break up into many small droplets which get expelled in all directions. For the viscous case, the viscosity was high enough to keep the fuel together during the impact, and prevent this from happening. Some of the fuel droplets cross the path of the laser, causing a scattering of light. This is caught by the HSC and can be seen in frame 3 of Figure 6.10. The droplets are also detected by PD1. When looking at the PD signal in Figure 6.11 there are multiple downwards peaks visible starting from number 3. Every single peak indicates a different droplet crossing the laser beam. Due to this effect it is harder to estimate when gasses are starting to form, as compared to the viscous case where it was very clear.

- **Point 4:** At point 4 gasses are starting to form. The gasses formed are exactly the same as for the viscous case, and come from the same source. The difference here is that the gasses are not trapped in the form of bubbles, as they were in the viscous case. One large cloud of gas is created which gradually increases in size and density. Since it starts with a low density it is hard to visually detect the gasses in the HSC images. Frame 4 of Figure 6.10 shows a background which is a bit darker and more blurry in comparison to the previous frames. This indicates that gasses have been formulated here. From the PD signal it is also not exactly clear when gasses are starting to form. This is due to the effect explained at point 3. An estimation has to be made based on the PD signal before and after the last fuel droplet crossed the laser beam.
- **Point 5:** Ignition takes place. A spark created in the fuel is lifted up slightly into the gasses and starts to ignite them, as can be seen in Figure 6.10 frame 5. This is different than the viscous case as here the ignition is not contained inside the fuel, but rather inside the gasses. For the viscous case multiple ignition points were required to fully ignite all the gasses created. Here one point is sufficient which results in a faster ignition.
- **Point 6:** Only 2 ms after ignition the majority of the gas cloud is burning. This releases enough light to get a fast increase in PD output signal, as is shown in Figure 6.11.
- **Point 7:** Due to the increase in temperature the still burning gas cloud is pushed up. This creating an even bigger volume of burning gas which translates to an increase in light released. Figure 6.11 clearly shows this as there is a rapid rise in light intensity quickly after point 6. After point 7 most gasses have been combusted and the light emitted by the reaction starts to drop.

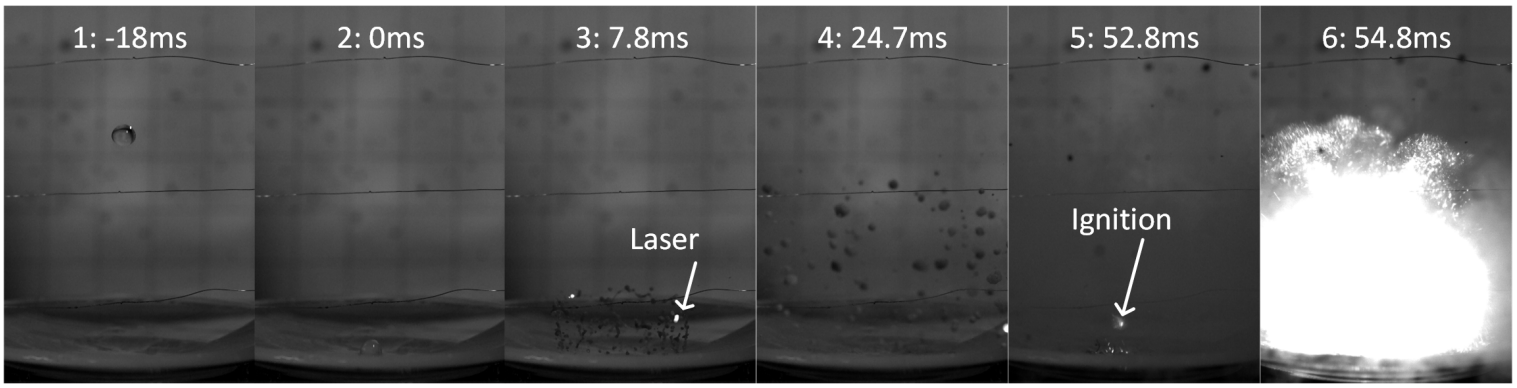

Figure 6.10: Ignition sequence of liquid ethanol with 10% MCAT in combination with 97% HTP. 1: HTP droplet falling (*t=-18ms*). 2: HTP droplet touches fuel pool (*t=0ms*). 3: Droplets of ethanol cross the laser beam (*t=7.8ms*). 4: Decomposition of HTP and vaporisation of fuel (*t=24.7ms*). 5: Ignition (*t=52.8ms*) 6: Full ignition of the vaporised gasses (*t=54.8ms*).

6.4.2. Ignition delay comparison

Using the data collected from the PDs and HSC during the drop tests both the physical, chemical, and total ignition delay are calculated for each sample which was tested. The results of these measurements can be found in Table 6.5. Values presented in this table are an average taken over at least three successful drop tests. Accompanied with each value is the standard deviation which gives some insight into the accuracy of the average delay times. It is chosen to present the PD and HSC data separately since there are some important differences between the delay times determined with them. However, by using two separate sources to calculate

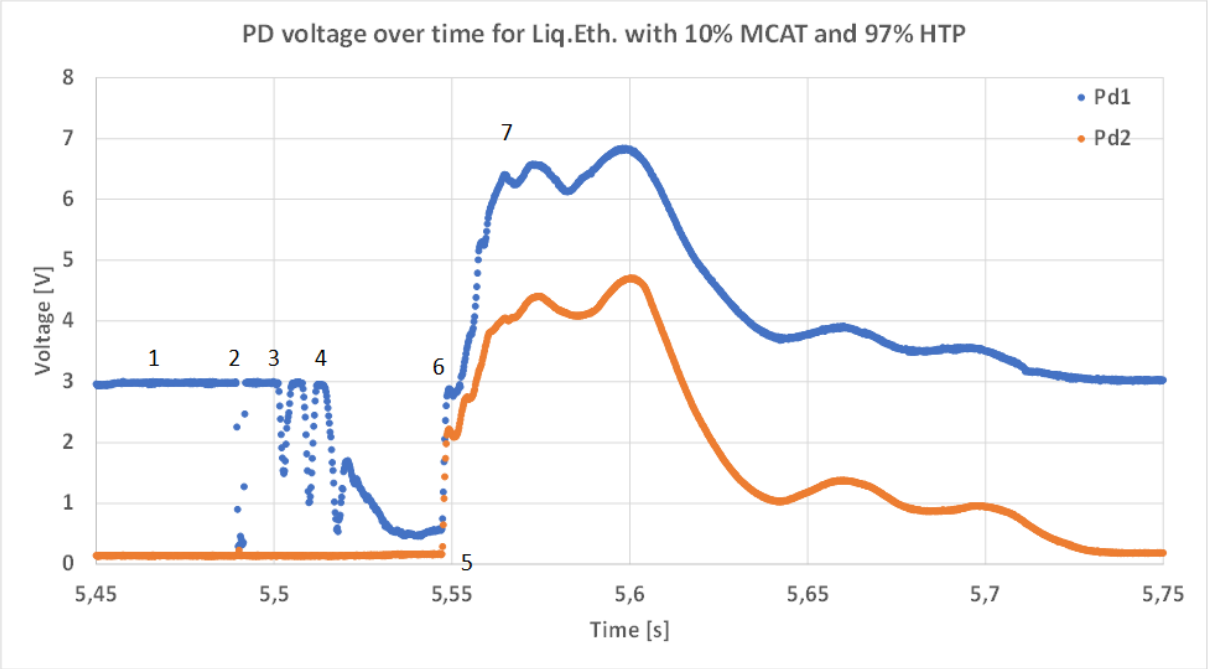

Figure 6.11: A plot of the PD voltage measured using two PDs during a drop test using liquid ethanol with 10% MCAT and 97% HTP. Numbers indicate the different phases of the ignition.

the delay times a stronger point can be made about their accuracy. All results are presented in ms. For the PD the physical delay is defined as the time between the HTP droplet crossing the laser, point 2 in Figure 6.9, and gasses starting to block the laser beam, point 3 in Figure 6.9 minus the time it takes for the droplet to travel from the bottom of the laser beam to the fuel surface. The chemical delay is defined as the time between the creation of gasses, point 3 in Figure 6.9, and ignition, point 5 in Figure 6.9. The total ignition delay is equal to the sum of the physical and chemical delay. In case of the HSC the physical delay is defined as the time between contact of the HTP droplet with the fuel, frame 2 in Figure 6.8, and the start of gasses being generated, frame 3 in Figure 6.8. Chemical delay is defined as the time between the generation of gasses, frame 3 in Figure 6.8, and the first sign of ignition, frame 4 in Figure 6.8. Similar as with the PD, here the total ignition delay is equal to the sum of the physical and chemical delay. Using Table 6.5 the effect of each variation made on the physical, chemical, and total ignition delay time is assessed. This is done for each parameter separately, as they were studied separately.

Catalyst concentration

The concentration of MCAT in the viscous ethanol fuel sample was varied from 5%, to 3%, to 2%, to 1%, to 0.5%. Rows 1 to 5 of Table 6.5 correspond to these fuel formulations and give the determined delay times. When looking at the total ID measured with both the PD and HSC it is clear that an increasing concentration of MCAT in ethanol results in a decreasing ID. This effect was expected since an increase in catalyst concentration results in a faster decomposition of HTP which in turn leads to a faster temperature rise and faster ignition. For higher concentrations a reduction in concentration only mildly affects the ID. A decrease from 5% to 3% only led to an increase of about 28% in ID. While at lower concentrations, a decrease from 2% to 1% led to an increase of almost 200% in ID. This shows that a concentration of 1% MCAT in viscous ethanol is close to its critical concentration, or minimum concentration of catalyst required for ignition. This point is confirmed by the results of the sample containing

Table 6.5: Average physical, chemical, and total ignition delay times measured using PDs and HSC for all samples presented in Table 6.4. All values are given in ms.

		Physical delay		Chemical delay		Total ignition delay	
#	Variant	PD	HSC	PD	HSC	PD	HSC
1	5% MCAT	43±12.3	51.6±9.8	45.5±9.8	23.8±4.2	89.5±3	75.4±5.6
2	3% MCAT	65.3±8.4	68.8±8.9	57.2±3.3	27.2±12.9	122.4±9.6	96.1±17.6
3	2% MCAT	82.1±2.4	84.6±4.1	62.7±27.7	46±17.3	144.8±26.4	130.6±13.5
4	1% MCAT	155.2±5.7	158.9±18.6	228.7±9.9	224.7±13.6	383.9±14.4	383.5±13.2
5	0.5% MCAT	430±41.8	445±26.3	627.2*	567*	1086.7*	1038.3*
6	95% HTP	74±1.8	78.3±4.7	77.3±4.7	45.2±6.7	151.4±4.7	123.4±3.9
7	90% HTP	86±9.7	87.9±12.2	83.1±12.3	67.6±7.5	169.1±3.6	155.5±5
8	87.5% HTP	112±8.1	118.5±4.7	**	**	**	**
9	Liq. 10% MCAT	13.9±3.6	16.8±3.9	40.3±5.3	35.5±4.4	54.2±21	52.3±1
10	Liq. 5% MCAT	14.7±4.1	14.9±4.6	46.2±20.6	35.7±17.7	60.9±16.6	50.6±13.1
11	Liq. 3% MCAT	22.2±1.3	23.6±1	**	**	**	**
12	But. 5% MCAT	42.4±4.1	43.3±3.5	38.9±7	20±1.7	81.4±9.7	63.3±5
13	But. 3% MCAT	61.5±4.9	62.8±4.1	77.6±23	29.5±2.7	141.9±19.4	94.8±0.2
14	5% FCAT	2161.2±970.8	1513.2±90.8	145±65.7	115±32.4	2306.2±91.4	1628.4±58.4
15	3% FCAT	3341.2±158.3	3374.1±163.3	153.4±19.5	92.8±38.6	3494.6±140.9	3466.9±137.3
16	0.3 ml fuel	48.2±17.5	53.7±15.2	84.3±18.8	36.4±4.8	132.6±2.4	90.1±10.7
17	0.2 ml fuel	50.7±8.8	55.6±7.9	58.5±9.3	29.4±3.8	109.2±2.7	85±9.6
18	0.05 ml fuel	65.3±5.5	68.6±6.5	53.5±6.2	19.7±3.4	118.8±3	88.2±4.1
19	4 weeks old	202.3±16.9	219.9±15.2	271.2±17.7	230.3±28.1	473.5±33.5	450.2±40.3
20	18 cm drop height	65.8±4.7	67±7	53.4±6.4	22.6±7	119.2±11	89.6±13.8
21	28 cm drop height	52.7±0.4	55.6±2.4	48.5±3.6	33.1±2.2	101.1±3.7	88.7±3.6

*Ignition was achieved only one out of three times. Therefore no standard deviation could be calculated.

**Ignition was not achieved in any case.

0.5% MCAT. Only one out of three drop tests resulted in an ignition. And in the case that an ignition occurred it took more than one second after droplet impact.

When comparing the data collected from the PDs with the HSC it is noticed that in all cases the HSC gives a shorter total ID. To find the cause of this discrepancy the physical and chemical delay data is compared between these two measurement devices. The difference does not seem to lie in the physical delay data. Here the delays measured by the PDs and HSC match and fall within their margin for each case. For the chemical delay, on the other hand, a large difference is found. This difference can be explained by the way the ignition point is defined for each measurement device. In case of the PDs it is defined as the point where the light intensity suddenly increases rapidly, as an effect of the light generated by the combustion. For the HSC it is defined as the first sign of ignition, the starting point. This point is so small and releases so little light that the PDs are not able to detect it. Due to the increased viscosity of the fuel the ignition source is temporarily captured inside the fuel and blocked from igniting the gasses which are present above the fuel pool. Only after several ms an ignition source manages to escape its bubble and create a full ignition of the gasses. The ignition of the gasses is what is captured by the PDs. The ID determined by the HSC gives a better representation of performance in a real combustion engine in comparison with the ID determined by the PDs. This is because in a combustion engine the fuel would be atomized by the injector, thereby creating fuel droplets which are too small to contain an ignition source. When an ignition occurs here

it would then immediately ignite the gasses surrounding it, without noticing the delay that is seen in these drop tests.

For higher concentrations of catalyst (5%, 3%, 2%) the physical delay makes up about 70% of the total delay time. This is a huge part. Physical delay includes the time for the oxidizer and fuel to properly mix, and for liquid phase reactions to take place that will vaporize the propellants. In a drop test the mixing conditions are far from ideal. In a combustion engine both the fuel and oxidizer would be atomized by an injector before coming into contact with each other. A proper injector can greatly decrease the time it takes to form a homogeneous mixture. Atomization of the propellants results in a large surface area available for reactions to occur, again speeding up the process. Using these propellant combinations in a combustion engine could therefore drastically decrease the physical delay, and thereby the total ID.

HTP concentration
The concentration of HTP was varied from 97%, to 95%, to 90%, to 87,5%. These samples correspond to rows 2 (Baseline, 97%) and 6 to 8 from Table 6.5. As was expected a decrease in HTP concentration results in an increased ID. A decreased concentration of HTP means that the oxidizer droplet contains a decreased amount of H_2O_2 and an increased amount of water. When the droplet makes contact with the fuel there is less H_2O_2 present to decompose, resulting in a slower increase in temperature. If the temperature increases too slow, too much heat can escape to the environment and the auto-ignition temperature is not reached. The increased amount of water is also a disadvantage. Water does not participate in the reaction, and is thus an undesired substance to be present. Heat created by the decomposition of H_2O_2, which is needed to heat up the fuel, is partially lost by heating up the water. At a HTP concentration of 87.5% this effect takes up too much of the heat resulting in no ignition in any of the three performed drop tests. Increasing the concentration HTP by 5%, from 90% to 95%, results in a 20% decrease in ID. Then by increasing the concentration for another 2%, from 95% to 97%, again a decrease of 20% is seen in total ID. This shows that to get an ID as low as possible it is essential to use HTP with an as high as possible concentration. Especially at high concentrations a small increase can have a big effect on ID.

Differences in data collected by the PDs and HSC is again seen here. This is due to the same effect as described in the part about catalyst concentration. The physical delay again makes up a big part of the total ID. It does, however, decrease with a decreasing HTP concentration. At 90% the physical delay only still represents 55% of the total ID. This again shows that using high HTP concentrations is more beneficial. When using a combustion engine high HTP concentrations result in a larger ID reduction with respect to low HTP concentrations.

Liquid vs. Viscous ethanol
Liquid ethanol fuel samples were formulated with 10%, 5% and 3% MCAT. The ID results from these samples can be found in rows 9 to 11 of Table 6.5 and give insight into the effect of adding thickening agent to ethanol on the ID. First the three liquid fuel samples are compared with each other. It is noticed that a concentration of 3% MCAT is not sufficient to achieve ignition. None out of three drop tests with this sample ignited. This shows that the critical MCAT concentration for liquid ethanol lies somewhere between 3 and 5%, which is significantly higher than for viscous ethanol, where it lies between 0.5 and 1%. This difference is caused by the addition of a thickening agent. Since the thickening agent is organic it participates in combustion. It adds a positive heat of formation to the ethanol, which in turn improves the hypergolicity [13].

The other two liquid fuel samples did both ignite. What stands out here is that their ID times are very similar. Both the sample with 10% and 5% MCAT showed an average total ID of around 50 ms. It was expected that, like with viscous ethanol, a higher concentration of catalyst would result in a lower ID. This effect might be explained by a saturation concentration which is reached. A certain catalyst concentration will be enough to cause a quick decomposition of all HTP present. Adding more catalyst will in this case not increase the decomposition rate, and therefore not significantly affect the ID. This saturation concentration could lay around 5% catalyst for this specific fuel formulation, as no effect on ID is noticed when increasing the catalyst concentration.

What also stands out it the physical delay compared to the chemical delay. For viscous ethanol cases the physical delay made up about 70% of the total ID. In case of liquid ethanol this is only around 30%. This difference can be explained by the difference in viscosity. As was already shown in Section 6.4.1 the viscous and liquid samples show a different ignition behavior. In case of the liquid sample, the impact of the HTP droplet caused the fuel to break up into smaller droplets. This increases the surface area, which means there is a large area for the oxidizer to react with the fuel, resulting in a fast reaction. For the viscous fuel sample this was not the case as the fuel remained in 'one piece'. Another effect of the increased viscosity is the energy required for vaporisation. The bonds created by the thickening agent need to be broken in order for the viscous fuel to evaporate. This requires more energy than vaporizing liquid ethanol, and thus takes more time. Due to these effects the liquid sample shows a much shorter physical delay in comparison to the viscous sample, which in turn results in a shorter total ID.

Ethanol vs. Butanol

To assess the effect of the fuel itself, ethanol was replaced by butanol. Like with viscous ethanol, the same concentration of thickening agent was added to butanol to make it more viscous. Two different fuel samples were formulated. One containing 5% of MCAT and one containing 3% of MCAT. Results of drop tests with these samples can be found in rows 12 and 13 of Table 6.5. The data does not show a significant difference between ethanol and butanol. In case of the 5% catalyst samples butanol shows a slightly lower ID, but for the 3% catalyst samples the ID is practically equal. Also the distribution of physical and chemical delay does not seem to vary between ethanol and butanol.

MCAT vs. FCAT

After MCAT, FCAT was the most promising catalyst resulting from the screening in Chapter 3. It was already noticed that its performance was worse than MCAT, but it is still used in a drop test to show the importance of catalyst choice. Two formulations were tested containing 5% and 3% FCAT mixed with viscous ethanol which correspond to rows 14 and 15 of Table 6.5 respectively. Both show a huge ID of 1,6 seconds for 5% and 3.5 seconds for 3% FCAT. An ID this high makes it unsuitable for use in a combustion engine since it is a cause of hard starts. Here propellants pile up in the combustion chamber and then ignite all at once, creating immense pressures which can damage or break the chamber. The large difference in ID with fuel samples containing MCAT can be caused by a difference in activation energy. If using FCAT to catalyse the decomposition of H_2O_2 requires a higher activation energy than when using MCAT it can explain the increased delay times. Another difference between FCAT and MCAT is that FCAT is purely catalytic, it acts only as an intermediate step in the reaction but overall does not change. MCAT, however, has an organic part which can participate in the combustion. This releases extra energy which speeds up the ignition process.

Fuel volume
For this set of drop tests the same fuel formulation as in the baseline test was used. Here the volume of fuel deposited in the reaction vessel was varied from 0.3 ml, to 0.2 ml, to 0.1 ml, to 0.05 ml. Results on ID can be found in rows 2 (baseline, 0.1 ml) and 16 to 18 of Table 6.5. When comparing the total ID as measured by the HSC there does not seem to be a large difference between them. In all cases the total ID is around 90 ms. However, when comparing the physical and chemical delay times something interesting is found. In the case where 0.3ml of fuel was used the physical delay was about 60% of the total ID. For the 0.05 ml case this was almost 80%. This can be explained by the area available for liquid phase reactions to occur. When more fuel is used (0.3 ml) there is a large surface area of fuel for the H_2O_2 to react with which causes a fast decomposition. However, the large amount of fuel also requires more energy to vaporize and heat up to the auto-ignition temperature which results in an increased chemical delay. In case of the 0.05 ml sample the opposite happens. Physical delay is long since there is only a small contact area between the H_2O_2 and fuel. But once decomposition has occurred, temperature rises quickly since only little heat is required to vaporize the ethanol. This results in a short chemical delay. Overall the physical and chemical delays seem to balance out. All cases were, however, fuel rich. There would almost always be some ethanol left. For further study it would be interesting to perform this test oxygen rich. This can be done by further decreasing the volume of the fuel pool or by switching the fuel and oxidizer. Since the droplet size created by the capillary tube is constant, it is hard to change the amount of HTP dropped. Instead the reaction vessel can be filled with a larger amount of HTP and a fuel droplet can be dropped in it.

Fuel age
The baseline fuel sample was used in drop tests on the day of production, and 4 weeks later to asses the effect of aging on ID. Results of the aged sample can be found in row 19 of Table 6.5. Even though the exact same sample was used, the total ID measured is about 4,5 times that of the day of production. This means that there is a slow reaction going on between the catalyst, ethanol, and thickening agent. The reaction was not only visible through ID data but also through visual observation. Figure 6.12 shows pictures taken of the fuel sample at the day of production and after 4 weeks. At the day of production the sample had a light brown color. In 4 weeks time this changed to a much darker brown/red color. It is unknown what reaction caused this color change and increase in ID. This reaction could be an interesting subject for further study. Some promising points found during this aging study are that in terms of viscosity nothing seemed to have changed. And there was also no catalyst sediment found on the bottom of the container after 4 weeks, which indicates that the viscosity is high enough to keep a homogeneous mixture for at least a month.

Drop height
Changing the drop height affects the impact velocity of the HTP droplet on the fuel pool. The change in impact velocity can have an effect on the mixing of the propellants, and therefore on the physical delay time. For this study the drop height was varied from 18 to 28 cm in steps of 5 cm. Results of the drop height variation can be found in rows 2 (baseline, 23 cm), 20 and 21 of Table 6.5. A drop height of 28, 23, and 18 cm corresponds to an impact velocity of about 2.33, 2,11, and 1.8 6m/s respectively. When looking at the results in terms of ID this change in impact velocity does not seem to have a large effect. In all cases the total ID measured by the HSC is around 90 ms. Also the distribution of physical and chemical delay is in the same range for all three cases. This can indicate that the change in impact velocity does not affect

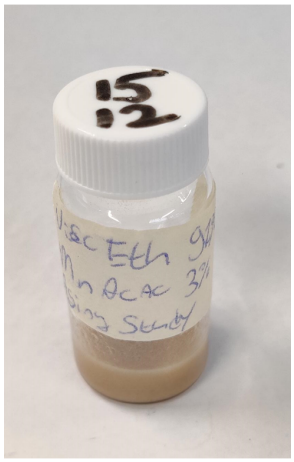

(a) Fuel sample at day of production

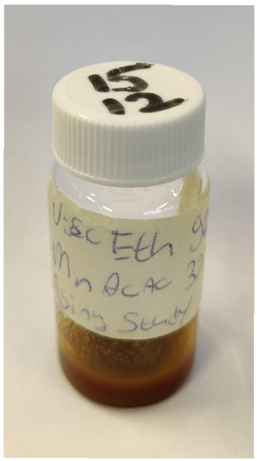

(b) Fuel sample after 4 weeks

Figure 6.12: The color change of the fuel sample after aging for 4 weeks.

the mixing of the propellants significantly, which is confirmed by the images captured with the HSC. In none of the three cases the impact velocity is high enough to break the fuel pool into smaller droplets. Mixing is thus very similar for all drop heights tested, and it does not affect the ID.

6.4.3. Temperature comparison

This section focuses on the analysis of the temperature data collected by the thermocouples. During the drop tests three TCs were used which were placed 7, 27, and 47 mm above the fuel surface. These TCs will be indicated as TC1, TC2, and TC3 respectively. Since data from the TCs was recorded at a sampling frequency of 50 Hz it cannot be used to determine ignition delay. The resolution of 20 ms is too large. Nevertheless, the TC data can be used to get insight in the energy which is released during ignition based on the maximum temperature that is reached. According to the manufacturers specifications, the response time of the thermocouple is in the range of 0.08 (in 18m/s air) to 1.0 (in still air) seconds. This is the time required to reach 63.2% of an instantaneous temperature change. Based on Figure 6.9 the total burn time of a drop test is estimated to be around 0.15 seconds (the time from the increase of light, ignition, until no more light is emitted). The short burn time is probably not enough for the thermocouple to reach the actual flame temperature. Figure 6.13 shows this effect. Here both the PD and TC data are plotted for the baseline drop test. As can be derived from the PD signal, the ignition occurs at about 7.3 seconds while the maximum temperatures for TC2 and TC3 are reached around 7.45 seconds. At the time that the maximum temperature is recorded, the combustion has already mostly stopped. For TC1 the maximum temperature is recorded at an even later time which can be explained by a small amount of combustion that is still going on at the fuel surface. This means that the TC data collected does not give information on the maximum temperature reached in the flame. However, since this is the case for all experiments, it does allow for qualitative comparison between drop test variations. Table 6.6 summarizes the temperature data. It contains the average maximum temperature measured over at least 3 drop tests and the TC which measured this temperature.

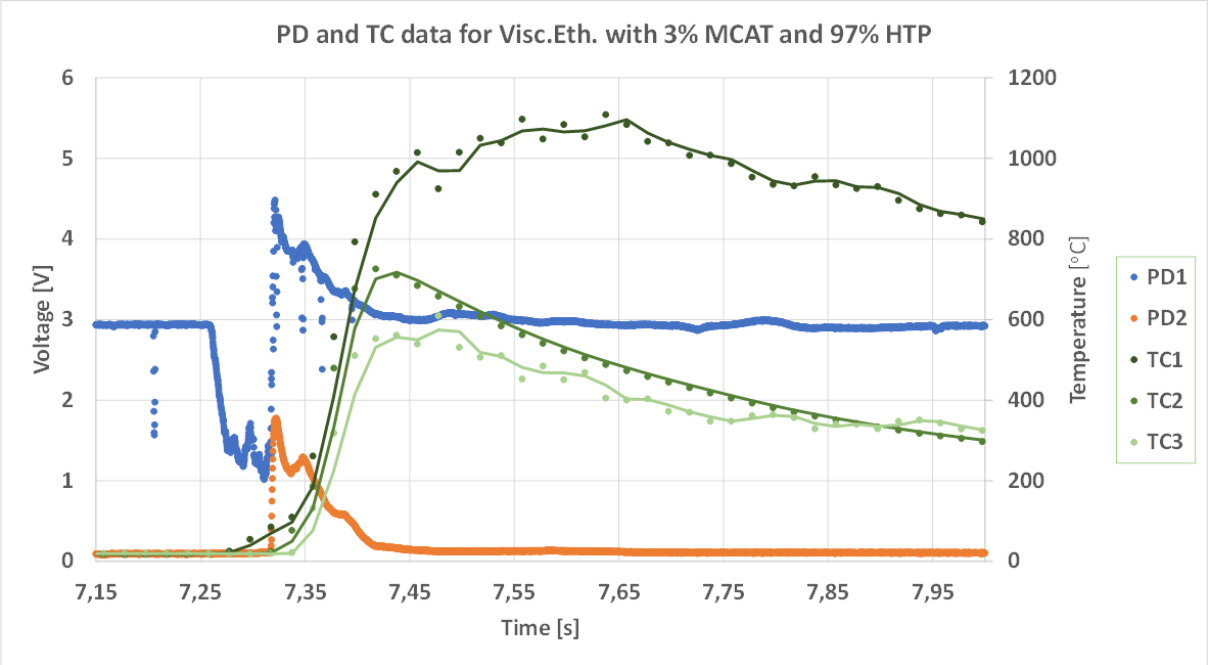

Figure 6.13: A plot of the PD and TC data of a drop test using viscous ethanol with 3% MCAT and 97% HTP.

The MCAT concentration seems to have an effect on temperature where a high catalyst concentration results in a higher temperature. Maximum temperatures reached with 5% and 3% MCAT are higher than those reached with 2% or 1% MCAT. The slightly higher temperature reached with 3% MCAT, compared to 5%, can be explained by the fact that TC1 was placed slightly closer to the fuel surface. What also stands out is that for 2% MCAT the highest temperature was measured at TC2 instead of TC1, which was the case for all other samples. When examining the high speed videos it is noticed that TC1 was placed out of center, resulting in a lower temperature measurement. Consequently, TC2 measured a higher temperature. In case of 0.5% no ignition was achieved, thus explaining the low temperature.

It was expected that a decrease in HTP concentration would result in a decrease in maximum temperature. This is because in low concentrations HTP more water is present which takes up more energy to heat up. At the same time less hydrogen peroxide is present, which is the main source of energy. Overall, the results follow this hypothesis. Drop tests performed with 95%, 90% and 87.5% HTP all showed a lower maximum temperature than the test using 97% HTP. However, there is one discrepancy at 95% HTP. This test was expected to show a higher temperature than the test using 90% HTP. It is unknown why it is lower, after checking the high speed videos no differences in TC placement or ignition location could be found. No ignition was achieved using 87.5% HTP hence the low temperature there.

When liquid ethanol was used instead of viscous ethanol the same effect with regard to catalyst concentration was found. A higher concentration MCAT resulted in a higher temperature. Overall the liquid samples created show a lower temperature than the viscous samples. An explanation can be the added energetic content of the thickening agent in the viscous fuel samples. Next to that the viscous samples showed a smaller volume where combustion occurred. More energy collected in a smaller volume results in a higher temperature. This effect is confirmed by the location where the maximum temperature was measured for the liquid samples. Here TC3 measured a higher temperature than TC1. This means that the flame has

spread over a much larger volume than when viscous ethanol was used. The low temperature measured at the liquid sample containing 3% MCAT can again be explained by the fact that it did not ignite.

Table 6.6: Average maximum temperature measured using a thermocouple for all samples presented in Table 6.4. All values are given in ^{o}C.

#	Variant	Max Temp	Location
1	5% MCAT	1023±241	TC1
2	3% MCAT	1062.5±45	TC1
3	2% MCAT	770.3±80	TC2
4	1% MCAT	803.3±99	TC1
5	0.5% MCAT	95.5±19.5	TC1
6	95% HTP	594.3±125	TC1
7	90% HTP	840.7±66	TC1
8	87.5% HTP	90±12	TC1
9	Liq. 10% MCAT	765±25	TC3
10	Liq. 5% MCAT	693±78	TC3
11	Liq. 3% MCAT	107.7±19	TC1
12	But. 5% MCAT	618±20	TC1
13	But. 3% MCAT	800±18	TC1
14	5% FCAT	887.3±88	TC1
15	3% FCAT	1293.5±38	TC1
16	0.3 ml fuel	929±328	TC1
17	0.2 ml fuel	631.3±260	TC1
18	0.05 ml fuel	886±188	TC1
19	4 weeks old	565.7±44	TC1
20	18 cm drop height	810.3±74	TC1
21	28 cm drop height	588±82	TC1

When comparing the viscous butanol samples with the viscous ethanol samples it is noticed that the ethanol samples show a higher temperature. The opposite was expected since the lower heating value (LHV) of butanol is with 33.1 MJ/kg higher than that of ethanol which is 26.7 MJ/kg [68]. Next to that the butanol sample containing 5% MCAT shows a lower temperature than the butanol sample containing 3% MCAT which is contradictory with data found in other cases. It is unknown why these differences are found since no significant differences in TC placement or ignition location could be found between measurements.

Drop test results using 5% FCAT showed a lower temperature than when 5% MCAT was used. An explanation for this effect could be that MCAT is partially organic. This means that it can partially participate in the combustion resulting in an increased temperature. FCAT does not have this feature as it is purely inorganic. When comparing the two FCAT samples it is noticed that the 3% FCAT sample shows a much higher temperature than the 5% FCAT sample. This can be explained by the fact that TC1 was placed directly on the fuel surface for 3% FCAT since it was expected to show decomposition and no ignition. The placement of TC1 for the 5% FCAT case is comparable to when MCAT was used.

For the 4 weeks old sample it was already observed that some unknown reaction had occurred in the sample which had a detrimental effect on the ignition delay time. When comparing the maximum temperatures measured it is noticed that the 4 weeks old sample shows a much

lower temperature than the original sample did. It is thought that this decrease in temperature is also a consequence of the slow reaction that occurred in the sample over time. No discrepancies were found in the placement of the thermocouples that could explain the large temperature difference.

When no ignition was expected TC1 was placed on the fuel surface to measure decomposition temperature. This was done for samples 5, 8, 11, and 15 from Table 6.6 where sample 15 did actually ignite. Between the other three samples the decomposition temperature was comparable and around 100^oC. Even though the measured temperature is lower than the actual temperature it is still too far below the auto-ignition point of ethanol, 363^oC, to achieve ignition.

Overall, there were too many cases where the measured temperature deviated from what was expected. Therefore, for further study a better setup has to be created where more reliable temperature measurements can be done. Also, to measure the actual flame temperature the burn time has to be increased which is not suitable for a drop test. More reliable temperature measurements could be performed using an injector test in a controlled chamber.

6.5. Conclusion

In this Chapter the ignition delay of various fuel samples was tested. This was done through a drop test where a droplet of oxidizer is dropped into a pool of fuel. The time between contact of the propellants and the ignition is defined as the ignition delay which is a crucial parameter in hypergolic propulsion systems. Based on a literature review an experimental setup was created. This setup used thermocouples for temperature measurement and contained two ways of measuring ID; using a high speed camera and using a laser-photodiode combination. To create consistent droplets a syringe pump in combination with a capillary tube was used. A baseline sample was created using viscous ethanol and 3% MCAT of which 0.1 ml was placed in the reaction vessel. A droplet of 97% HTP was dropped from a height of 23 cm. From this baseline test the following parameters were varied and their effects on ID and temperature were studied; catalyst concentration, HTP concentration, liquid vs. viscous ethanol, ethanol vs. butanol, MCAT vs. FCAT, fuel volume, fuel age, and drop height.

All samples could be characterized by one of two ignition profiles. This difference was clearly based on the use of viscous or a liquid fuel. In case of a viscous sample the fuel remained 'in one piece' after impact of the oxidizer droplet. No fuel droplets were expelled from the pool. Much of the gas created by the decomposition reaction of HTP was enclosed in the form of bubbles in the fuel pool. Every time a bubble pops some gasses were released. Ignition could occur inside a bubble without it resulting in ignition of the entire mixture. After a few ignition sources one succeeds to ignite the released gasses and thereby ignite the entire mixture. When a liquid sample was used the impact of the HTP droplet resulted in many small fuel droplets being expelled from the fuel pool. Decomposition gasses created were not trapped inside the fuel but immediately released resulting in a bigger gas cloud than was the case with a viscous fuel. Here a single ignition source is sufficient to ignite the whole mixture.

Based on data from the high speed camera and the photodiodes the ignition delay time could be calculated. Using this data the effect of each parameter mentioned above on the ID was determined. An increase in catalyst concentration results in a decrease in ID. More catalyst available results in an increased decomposition rate of hydrogen peroxide leading to a faster temperature increase and a faster ignition. From the variation of HTP concentration could be concluded that a high concentration of HTP results in a low ID. Since more hydrogen perox-

ide and less water is present, more energy is released and less energy is taken up by water. This results in a faster ignition. For an equal catalyst concentration samples based on liquid ethanol showed a lower ID time than samples based on viscous ethanol. This is mainly due to the much shorter physical delay for liquid samples. The low viscosity allows for easier mixing and better atomization. An advantage of viscous ethanol is, however, that ignition can be achieved at much lower catalyst concentrations. The critical concentration MCAT to achieve ignition lays between 0.5% and 1% for viscous ethanol and between 3% and 5% for liquid ethanol. This can be explained by the added energetic content of the thickening agent in viscous ethanol. No significant difference was found between the ID of ethanol and butanol samples. The use of MCAT resulted in much lower ID times than when FCAT was used. A factor contributing here is the fact that MCAT has an organic part which participates in the combustion where FCAT does not posses this. The fuel volume did not have an effect on the total ID. There were however some differences in physical and chemical delay. A larger volume of fuel resulted in a shorter physical delay since a larger surface area was available for decomposition reactions to occur. It, on the other hand, also resulted in a larger chemical delay due to the increased volume fuel that had to be evaporated. A fuel sample was tested on its production date as well as 4 weeks later. The 4 weeks old sample showed a large increase in ID of about 4.5 times the original. During storage a reaction occurred between the MCAT and ethanol which caused this effect. Nevertheless, the fuel still remained a homogeneous mixture and the catalyst particles did not separate from the fuel. A change in drop height did not have a significant effect on the ID.

Due to the response time of the thermocouples the actual flame temperature could not be measured. However, based on qualitative temperature data the following conclusions could be drawn. When MCAT is used a higher concentration of catalyst results in a higher temperature. Probably due to the decreased ID and the increased energetic content from the organic part of MCAT. Higher concentrations of HTP result in a higher temperature. This is because a high concentration of HTP contains little water which takes up energy in order to evaporate. Fuels based on viscous ethanol show a higher temperature than fuels based on liquid ethanol. Viscous ethanol contains a thickening agent which participates in combustion, thereby adding energy. Also the combustion of a viscous sample occurs in a smaller volume than the combustion of a liquid sample. The use of FCAT resulted in lower temperatures than the use of MCAT which can be explained by the partially organic nature of MCAT. Aging of a sample containing MCAT has a detrimental effect on its flame temperature. A slow reaction occurs between the catalyst and the ethanol during aging which causes this effect. When comparing butanol based samples to ethanol based samples it was found that when butanol was used a lower temperature was reached. This is in contradiction with what was expected since butanol has a higher LHV than ethanol. For further study a better setup has to be created for more reliable temperature measurement. To measure the actual flame temperature the burn time has to be increased.

7

Conclusions and Recommendations

The objective of this thesis was to develop two novel hypergolic bipropellant systems and their characterization. One system based on a negligible amount of catalyst and one based on a pyrophoric liquid. To reach this goal some research questions were formulated in Chapter 1. In this Chapter these questions will be answered and conclusions will be drawn in section 7.1. Then in section 7.2 recommendations will be given on what could have been done differently during this thesis and how one could continue the research presented in this report.

7.1. Conclusion

Four main research questions were presented. In Chapters 3 to 6 an effort was made to answer each of these, including their sub-questions. In Chapter 3 a study was performed to investigate which available catalyst could be used to induce hypergolicity between ethanol and hydrogen peroxide. Out of the thirteen tested catalysts one showed a very high potential and two showed a high potential. These catalysts were indicated as MCAT, FCAT and CCAT respectively and were further investigated. Due to the problem of sedimentation and to improve performance, a small amount of thickening agent was added to the ethanol. The negligible amount of 1% thickening agent was concluded to show the best balance in increased performance and low increase in viscosity. Fuels were formulated using the three most promising catalysts and viscous ethanol, (which contains 1% thickening agent). The goal here was to reduce the catalyst concentration as far as possible until no or very slow ignition is observed when 96%HTP was added. Results showed that a minimum of 3% FCAT, 5% CCAT, or 1% MCAT was required to achieve ignition. Finally an effort was made to further reduce the catalyst concentration required for hypergolic ignition by addition of energetic particles in the form of aluminum powder. This only resulted in minor improvement for 2 out of 6 tested samples and thus aluminum powder was not pursued as an option during this thesis.

In Chapter 4 the effects on rheological properties of adding 1% thickening agent to ethanol was studied. This study was split into four parts including viscosity study, yield point study, time dependent study and temperature dependent study. From the viscosity study can be concluded that the sample shows a shear thinning behavior. At low shear rates the viscosity is high which counteracts the sedimentation of particles in the sample. This means that when a catalyst is mixed with the sample the particles will stay distributed homogeneously for a much longer time than when a catalyst is added to pure (liquid) ethanol. This effect increases the life time of the catalytically enhanced ethanol fuel. Then at higher shear rates the viscosity decreases starting from the yield point. The yield point study shows a yield stress of about

0.078 Pa. By applying a shear stress of 0.078 Pa or higher the viscosity of the sample will decrease, causing the sample to flow and behave like a liquid. With increasing shear rate the sample will eventually reach a viscosity very close to that of pure (liquid) ethanol. For a propulsion application this means that by applying enough pressure the viscous ethanol will act like liquid ethanol and can be easily pumped through a feed and injection system. Results from the time dependent study showed that if the shear rate is increased in a short amount of time it results in a lower viscosity than when the same increase of shear rate is done over a longer duration. This effect makes the sample very suitable for use in pulse mode operation of a propulsion system. Here the propellant flow is started and stopped within a short duration of time. Under these conditions the sample shows the lowest viscosity. The second time dependent study showed that if a constant shear rate is applied, the viscosity decreases over time. This effect is more beneficial for propulsion applications with a longer burn time. Overall, the sample shows promising effects in both short and long burn time propulsion modes. Finally a temperature dependent study was performed. From the results can be concluded that an increase in temperature leads to a decrease in viscosity as well as a decrease in yield stress.

An effort to use a pyrophoric liquid to induce hypergolicity between ethanol and hydrogen peroxide was made in Chapter 5. For this study a 1.0M solution of triethylaluminum (TEA) in hexanes and a 1.0M solution of diethylzinc (DEZ) in hexanes was used. The addition of TEA or DEZ to viscous ethanol resulted in a reaction between the pyrophoric liquid and the thickening agent. The result was a rapid increase in viscosity, thereby forming a gel. This is undesired since it makes the fuel harder to pump and atomize. These gels contained around 1% pyrophoric liquid and did not react with air or hydrogen peroxide. Due to the incompatibility with viscous ethanol fuel samples were then formulated using liquid ethanol. Various concentrations of TEA solution were added to ethanol resulting in a seemingly homogeneous mixture. The mixtures were stable in air and a slow decomposition reaction occurred when 96% hydrogen peroxide was added. The same experiment was then repeated with the DEZ solution. Here, however, a problem occurred where the DEZ would react with oxygen still left in the mixing flask making the fuel useless. This oxygen was thought to be present due to a leak in the system. Due to this effect the exact concentration of pyrophoric liquid in the formulated fuels was unknown. This made it impossible to determine the minimum concentration required to achieve hypergolicity. Section 7.2 will give recommendations on how to mitigate the problems found here. A final experiment was performed where the TEA solution was directly mixed with 97% HTP. This resulted in ignition, thereby confirming the potential of these chemicals.

Finally in Chapter 6 drop tests were performed using only the developed catalyst based fuels. A baseline sample was created using viscous ethanol and 3% MCAT of which 0.1 ml was placed in the reaction vessel. A droplet of 97% HTP was dropped from a height of 23 cm. From this baseline test the following parameters were varied and their effects on ID and temperature were studied; catalyst concentration, HTP concentration, liquid vs. viscous ethanol, ethanol vs. butanol, MCAT vs. FCAT, fuel volume, fuel age, and drop height. All samples could be characterized by one of two ignition profiles. This difference was clearly based on the use of viscous or a liquid fuel. In case of a viscous sample the fuel remained 'in one piece' after impact of the oxidizer droplet. No fuel droplets were expelled from the pool. Much of the gas created by the decomposition reaction of HTP was enclosed in the form of bubbles in the fuel pool. Every time a bubble pops some gasses were released. Ignition could occur inside a bubble without it resulting in ignition of the entire mixture. After a few ignition sources one succeeds to ignite the released gasses and thereby ignite the entire mixture. When a liquid

sample was used the impact of the HTP droplet resulted in many small fuel droplets being expelled from the fuel pool. Decomposition gasses created were not trapped inside the fuel but immediately released resulting in a bigger gas cloud than was the case with a viscous fuel. Here a single ignition source is sufficient to ignite the whole mixture.

Using data from the HSC the effect of each parameter mentioned above on the ID was determined. The baseline fuel sample showed a total ID of around 90 ms. An increase in catalyst concentration results in a decrease in ID. From the variation of HTP concentration could be concluded that a high concentration of HTP results in a decreased ID. For an equal catalyst concentration, samples based on liquid ethanol showed a lower ID time than samples based on viscous ethanol. An advantage of viscous ethanol is, however, that ignition can be achieved at much lower catalyst concentrations. The critical concentration MCAT to achieve ignition lays between 0.5% and 1% for viscous ethanol and between 3% and 5% for liquid ethanol. No significant difference was found between the ID of ethanol and butanol samples. The use of MCAT resulted in much lower ID times than when FCAT was used. The fuel volume did not have an effect on the total ID. There were however some differences in physical and chemical delay. A larger volume of fuel resulted in a short physical delay, and a large chemical delay. The 4 weeks old sample showed a large increase in ID of about 4.5 times the original. During storage a reaction occurred between the MCAT and ethanol which caused this effect. Nevertheless, the fuel still remained a homogeneous mixture and the catalyst particles did not separate from the fuel. A change in drop height did not have a significant effect on the ID.

Overall, one of the two objectives for this thesis was reached. A fuel was created using a negligible amount of catalyst, >1%, which still achieved hypergolicity with hydrogen peroxide. Regarding the second objective, the work done can function as an initial study on this topic. Based on this work some recommendations can be given on what to do next, see section 7.2.

7.2. Recommendations

This section reflects on the work done by presenting some points of improvement as well as recommendations for future work in this field of study.

During the catalyst screening phase of this thesis, only catalysts available in the DASML were taken into account. This was done due to the limited funding and time resources that were available. Other catalysts that were not available might have shown more promising results than were found during this thesis. Therefore, it is recommended to explore a wider range of catalysts when resources are available.

Results obtained during the yield point study of the rheology study deviated from what was expected. The flow curve did not show a clear yield point. To improve this measurement next time it would be better to perform a measurement using a controlled shear stress instead of shear rate. Also, samples with a very low yield stress require the rheometer to operate close to the low-end torque specification. At these conditions the yield stress cannot be easily determined using the stress sweep method. Instead a test can be performed where the shear rate starts high and then logarithmically decreases. The yield point is then indicated by the yield stress which reaches a plateau at low shear rates.

When performing the experiments with pyrophoric liquids a reaction between the pyrophoric liquid and the thickening agent was observed. This caused a sudden increase in viscosity which was undesired since the goal was to create a fuel with properties close to that of

ethanol. For further study the use of other thickening agents in combination with pyrophoric liquids can be explored. Here the goal is to find a thickening agent which is compatible with the used pyrophoric liquids. This then has the potential to create a fuel with properties close to that of ethanol while at the same time trapping the pyrophoric liquid, thereby preventing it from reacting with the air. Another issue which caused the pyrophoric liquid to react with air was a possible leak in the experimental setup used to transfer the liquid. For further experimentation using pyrophoric liquids it is recommended to use a glovebox. A glovebox provides an inert atmosphere with a controllable humidity. This makes it much safer to handle these kinds of chemicals and prevents them from reacting prematurely. The use of a glovebox would also make it possible to use pure pyrophoric liquids instead of solutions. The hexane present in the used pyrophoric solutions is an undesired ingredient of the formulated fuels. Hexane is used in the solution since it prohibits the reactivity of the pyrophoric liquid. In a fuel this reactivity is required since it is the source of the hypergolic behavior. When using a pure pyrophoric liquid instead of a solution it is expected that a much smaller concentration is required to achieve hypergolicity. The downside is the increased risk when working with a pure pyrophoric liquid. Therefore the use of a glovebox is absolutely required.

Regarding the drop tests also some improvements could be made. In terms of the actual ignition delay measurement the laser/photodiode method showed to be less accurate in comparison to the use of a high speed camera. Therefore, the photodiode does not necessarily have to be used in further drop test experiments. When using a high speed camera it is recommended to use a color camera instead of a black/white one. This will give a better insight into the phenomena leading up to ignition. Unfortunately, a color high speed camera was not available for use during this thesis. The temperature measurements performed gave some contradictory and sometimes unreliable results. To improve on this a more controllable, constant environment has to be created in which the drop test can be performed. Also a drop test can be repeated for an additional number of times to increase the certainty of the measured values. Next to setup related improvement, some other recommendations can be given. First of all, drop tests should be performed with an O/F ratio close to the stoichiometric ratio or ratio with the highest specific impulse. This is because these mixture ratios are likely to be used in an actual propulsion system. Drop tests performed during this thesis made use of a fuel rich mixture ratio. Secondly, next to using hydrogen peroxide as an oxidizer it could also be interesting to investigate the hypergolicity with other common oxidizers. Especially if a fuel is formulated with the used of a pyrophoric liquid. If a fuel is hypergolic with a number of oxidizers this greatly increases its potential since it can be used for a large number of use cases. Finally, the aging effect observed in the fuel sample used for the drop test can be further investigated. It might be interesting to know how this effect behaves over time and what the cause is. Then, research could be done in search of a solution to this problem.

Bibliography

[1] S.M. Davis and N. Yilmaz. “Advances in Hypergolic Propellants: Ignition, Hydrazine, and Hydrogen Peroxide Research”. In: *Advances in Aerospace Engineering* (Sept. 2014).

[2] C.K. Law. “Fuel Options for Next-Generation Chemical Propulsion”. In: *AIAA Journal* 50.1 (2012).

[3] T. Edwards. “Liquid fuels and propellants for aerospace propulsion: 1903-2003”. In: *Journal of Propulsion and Power* 19.6 (2003), pp. 1089–1107.

[4] B.T.C. Zandbergen. *Thermal rocket propulsion*. 2018.

[5] J. Quesada. “Propellant grade hydrogen peroxide production and thermo pseudo hypergolicity investigation for dual mode green propulsion system”. Delft University of Technology, Jan. 2020.

[6] E.W. Schmidt and E.J. Wucherer. “Hydrazine(s) vs. Non-toxic propellants - where do we stand now?” In: *2nd international conference on green propellants for space propulsion* (2004).

[7] Q. Zhang and J.M. Shreeve. “Ionic liquid propellants: future fuels for space propulsion”. In: *Chemistry a European Journal* (2013), pp. 15446–15451.

[8] A.S. Gohardani, J. Stanojev, A. Demaire, K. Anflo, M. Persson, N. Wingborg, and C. Nilsson. “Green space propulsion: Opportunities and prospects”. In: *Progress in aerospace sciences* 71 (2014), pp. 128–149.

[9] C. Davis. “Overview of hydrazine fuels infrastructure”. In: (2012).

[10] Y. Cong, T. Zhang, T. Li, J. Sun, X. Wang, L. Ma, D. Liang and L. Lin. “Propulsive performance of a hypergolic H2O2/kerosene bipropellant”. In: *Journal of Propulsion and Power* 20.1 (2004).

[11] L.J. Maschio, L.G.F. Pereira, W.M. Meyer, R.I. Marques and R. Vieira. “A doe study on the hypergolicity of hydrogen peroxide with a rocket liquid fuel based on monoethanolamine and ethanol”. In: *International Journal of Energetic Materials and Chemical Propulsion* 17.2 (2018), pp. 137–145.

[12] D. Hasan, D. Grinstein, A. Kuznetsov, B. Natan, Z. Schlagman, A. Habibi, and M. Elyashiv. *Green Comparable Alternatives of Hydrazines-Based Monopropellant and Bipropellant Rocket Systems*. Aerospace Engineering, IntechOpen. Feb. 2019.

[13] M.S. Naseem, B.V.S. Jyoti, S.W. Baek, H.J. Lee and S.J. Cho. “Hypergolic studies of ethanol based gelled bi-propellant system for propulsion application”. In: *Propellants, Explosives, Pyrotechnics* 42 (2017).

[14] H. Kang, S. Park, Y. Park and J. Lee. “Ignition-delay measurements for drop test with hypergolic propellants: Reactive fuels and hydrogen peroxide”. In: *Combustion and Flame* 217 (2020), pp. 306–313.

[15] B. Natan, Y. Solomon, V. Perteghella. “Hypergolic ignition by fuel gellation and suspension of reactive or catalyst particles”. In: *Journal of Propulsion and Power* 27 (2011).

[16] W. Florczuk and G. Rarata. “Performance evaluation of hypergolic green propellants based on HTP for future next-generation spacecraft”. In: *53rd AIAA/SEA/ASEE Joint Propulsion Conference* (July 2017).

[17] T.W. Ryan, S.T. Schwab, and W.W. Harlowe. “Ignition delays, heats of combustion, and reaction rates of aluminum alkyl derivatives used as ignition and combustion enhancers for supersonic combustion”. In: *NASA Contractor Report* (1992).

[18] A.A. Kozlov, I.N. Borovik, A.A. Ermashkevich, V.P. Tashev, Sh.L. Guseinov, and V.A. Kosykh. “Self-ignition of fuel consisting of hydrogen peroxide, kerosine, and pyrophoric additives”. In: *Russian engineering research* 40.3 (2020), pp. 208–213.

[19] B.M. Melof and M.C. Grubelich. “Investigation of hypergolic fuels with hydrogen peroxide”. In: *37th AIAA/ASME/SAE/ASEE joint propulsion conference* (July 2001).

[20] B.V.S. Jyoti, M.S. Naseem and S.W. Baek. “Hypergolic and ignition delay study of pure and energized ethanol gel fuel with hydrogen peroxide”. In: *Combustion and flame* 176 (2017), pp. 318–325.

[21] J.John, P. Nandagopalan, S. Baek and S. Cho. “Hypergolic ignition delay studies of solidified ethanol fuel with hydrogen peroxide for hybrid rockets”. In: *Combustion and Flame* 212 (2020), pp. 205–215.

[22] A.J. Musker. “Highly stabilised hydrogen peroxide as a rocket propellant”. In: *AIAA/SAE/ASME 39th Joint Propulsion Conference* (2003).

[23] G.P. Sutton, O. Biblarz. *Rocket Propulsion Elements*. 7th. John Wiley & Sons, 2001.

[24] M. Ventura and G. Garboden. “A brief history of concentrated hydrogen peroxide uses”. In: *AIAA/SAE/ASME 35th Joint Propulsion Conference* (1999).

[25] N. Nimmerfroh, D. Pauls, and S. McMahon. “PROPULSE hydrogen peroxide: manufacture, quality, transportation and handling”. In: *AIAA/SAE/ASME 36th Joint Propulsion Conference* (2000).

[26] W.C. Schumb, S.N. Satterfield, and R.L. Wentworth. “Hydrogen peroxide”. In: *Reinhold, New York* (1955).

[27] United Nations. *European agreement concerning the international carriage of dangerous goods by road (adr)*. `https://adrbook.com`. 2021.

[28] Solvay Chemicals, Inc. *Hydrogen peroxide safety and handling information*. `https://www.solvay.com/sites/g/files/srpend221/files/2019-10/H2O2%20Safety%20and%20Handling%20of%20Hydrogen%20Peroxide.pdf`. 2021.

[29] E.J. Hopfinger and V. Baumback. “Liquid sloshing in cylindrical fuel tanks”. In: *Progress in Propulsion Physics* 1 (2009), pp. 1279–1292.

[30] M.B. Padwal, D. Natan, and D.P. Mishra. “Gel propellants”. In: *Progress in Energy and Combustion Science* 83 (2021).

[31] Y. Osada, K. Kajiwara, T. Fushimi, O. Irasa, Y. Hirokawa, T. Matsunaga, T. Shimomura, L. Wang, and H. Ishida. *Gels handbook fundamentals, properties and applications*. 1st ed. London: Academic Press, 2001.

[32] P.C. Pinto, N. Hopfe, J. Ramsel, W. Naumann, A. Thumann, G. Kurth. “Scalability of gelled propellant rocket motors”. In: *7th European conference for aeronautics and space sciences (EUCASS)* (2017).

[33] G. Nachmoni and B. Natan. “Combustion Characteristics of Gel Fuels”. In: *Combustion Science and Technology* 156 (2000), pp. 139–157.

[34] Polymer Properties Database. *Flow Properties of Polymers*. http://polymerdatabase.com/polymer%20physics/Viscosity2.html. 2021.

[35] S.Y. Jejurkar, G. Yadav, and D.P. Mishra. “Characterization of impinging jet sprays of gelled propellants loaded with nanoparticles in the impact wave regime”. In: *Fuel* 228 (2018), pp. 10–22.

[36] J.S. Mok, W.J. Welms, J.C. Sisco, and W.E. Anderson. “Thermal decomposition of Hydrogen Peroxide, Part 1: Experimental Results”. In: *Journal of Propulsion and Power* 21.5 (2005), pp. 942–953.

[37] Engineering Toolbox. *Fuels and Chemicals Auto-ignition Temperatures*. https://www.engineeringtoolbox.com/fuels-ignition-temperatures-d_171.html.

[38] Engineering Toolbox. *Heat of Combustion*. https://www.engineeringtoolbox.com/standard-heat-of-combustion-energy-content-d_1987.html.

[39] P. Pedziwiatr, F. Mikolajczyk, D. Zawadzki, K. Mikolajczyk, and A. Bedka. “Decomposition of hydrogen peroxide - kinetics and review of chosen catalysts”. In: *Acta Innovations* 26 (2018), pp. 45–52.

[40] J.J. Verendel. “Transition Metal Catalysis for Selective Synthesis and Sustainable Chemistry”. University of Uppsala, 2012.

[41] ICUMSA. *Relation between Brix value(%) and refractive index(nD)*. https://www.atago.net/en/databook-refractometer_relationship.php. 1974.

[42] P.A. Giguere and P.Geoffrion. “Refractive index of Hydrogen Peroxide”. In: *Canadian Journal of Research* 27 (1949), p. 168.

[43] C. Chen, H. Liaw, C. Shu, and Y. Hsieh. “Auto ignition Temperature Data for Methanol, Ethanol, Propanol, 2-Butanol, 1-Butanol, and 2-Methyl-2,4-pentanediol”. In: *Journal of Chemical and Engineering data* 55.11 (2010), pp. 5059–5064.

[44] M. Varma and B.V.S. Jyoti. “Ignition and combustion studies of heterogeneous UDMH-RFNA gel propellants”. In: *International journal of energetic materials and chemical propulsion* 10.3 (June 2011), pp. 259–275.

[45] B.V.S. Jyoti and S.W. Baek. “Formulation and comparative study of rheological properties of loaded and unloaded ethanol-based gel propellants”. In: *Journal of energetic materials* 33.2 (Apr. 2015), pp. 125–139.

[46] H. Peng, J.J. Zou, X.W. Zhang, and L. Wang. “Study on Al NPs-containing suspension as high-density liquid fuel”. In: *Journal of propulsion technology* 37.5 (May 2016), pp. 974–978.

[47] M. Negri and H.K. Ciezki. “Combustion of gelled propellants containing aluminum particles”. In: *49th AIAA/ASME/SAE/ASEE joint propulsion conference* (July 2013).

[48] L.T. De Luca, L. Galfetti, and F. Severini. “Burning of nano-aluminized composite rocket propellants”. In: *Combustion, explosion, and shock waves* 41.6 (2005), pp. 680–692.

[49] B. Palaszewski and J.S. Zakany. “Metallized gelled propellants - oxygen/rp-1/aluminum rocket heat transfer and combustion measurements”. In: *32nd AIAA/ASME/SAE/ASEE joint propulsion conference* (1996).

[50] R.H. Ewoldt. *Rheology theory and applications*. https://www.tainstruments.com/wp-content/uploads/Boston-Rheology-Training-2019.pdf.

[51] Kaye and Laby. *Viscosity of Ethanol*. https://wiki.anton-paar.com/en/ethanol/.

[52] Anton Paar. *Yield point, evaluation using the flow curve*. https://wiki.anton-paar.com/en/yield-point-evaluation-using-the-flow-curve/.

[53] T. Chen. *Rheological techniques for yield stress analysis*. http://www.tainstruments.com/pdf/literature/RH025.pdf.

[54] S.M. Davis and N. Yilmaz. “Thermochemical analysis of hypergolic propellants based on triethylalunimum/nitrous oxide”. In: *International journal of aerospace engineering* (2014).

[55] R.F.B. Goncalves, K. Iha, and J.A.F.F. Rocco. “Reactive molecular dynamics simulation and chemical kinetic evaluation of combustion of triehylaluninium (TEA)”. In: *Quimica Nova* 41.5 (2018), pp. 507–511.

[56] Y. Sato, K. Okada, M. Akiyoshi, K. Tokudome, and T. Matsunaga. “Reaction hazards of triethylaluminum under closed conditions”. In: *Journal of loss prevention in the process industries* 24 (2011), pp. 656–661.

[57] R. Sarpong. *Pyrophoric materials*. http://www.cchem.berkeley.edu/rsgrp/SOPs2017/Pyrophorics_Sarpong.pdf. 2016.

[58] VAC AERO International. *An introduction to vacuum pumps*. https://vacaero.com/information-resources/vacuum-pump-technology-education-and-training/1039-an-introduction-to-vacuum-pumps.html. 2016.

[59] T. Pourpoint and W.E. Anderson. “Physical and Chemical Processes Controlling Fuel Droplet Ignition”. In: *AIAA/SAE/ASME 40th Joint Propulsion Conference* (July 2004).

[60] T.L. Pourpoint and W. Anderson. “Hypergolic Reaction Mechanisms of Catalytically Promoted Fuels with Rocket Grade Hydrogen Peroxide”. In: *Combustion Science and Technology* (Jan. 2007), pp. 2107–2133.

[61] Z. Slocum-Wang, L.D. Felton, T.W. Turner, W.H. Stevenson. “Ignition delay screening techniques: drop testing vs. engine testing”. In: *AIAA/SAE/ASME 42nd Joint Propulsion Conference* (July 2006).

[62] J. Hollingshead, M. Ianuzzi, J. Moore, R. Yetter and G. Risha. “Investigation of ignition delay and combustion efficiency of TMEDA and various concentrations of nitric acid”. In: *AIAA Propulsion and Energy Forum* (2020). Virtual event.

[63] U. Swami, K. Senapathi, K.M. Srinivasulu, J. Desingu and A. Chowdhury. “Ignition delays of mixtures of the non-hypergolic energetic liquid hydroxyethylhydrazinium nitrate blended with unsymmetrical dimethylhydrazine”. In: *Propellants, Explosives, Pyrotechnics* 44 (2019), pp. 1139–1146.

[64] J. Li and W. Fan. “Experimental observation of hypergolic ignition of superbase-derived ionic liquids”. In: *Journal of propulsion and power* 34.1 (2018), pp. 125–132.

[65] A. Chowdhury, S. Thynell and S. Wang. “Ignition behavior of novel hypergolic materials”. In: *45th AIAA/ASME/SAE/ASEE Joint Propulsion Conference & Exhibit* (2009).

[66] Thorlabs. *Thorlabs FDS100 - Si Photodiode specification sheet*. https://www.thorlabs.com/thorproduct.cfm?partnumber=FDS100.

[67] M.N. Shoaib, B.V.S. Jyoti, S.W. Baek, and J. Huh. “Effect of alcohol carbon chain on enthalpy of combustion and ignition delay time for gelled hypergolic propellant system”. In: *Propellants, Explosives, Pyrotechnics* 43 (2018), pp. 453–460.

[68] NIST. *Chemistry WebBook*. https://webbook.nist.gov/chemistry/. 2018.

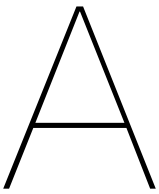

Safety plan pyrophoric liquids

This plan describes the purpose and the safety measures proposed for use of the following chemicals:

- Diethylzinc in a solution of hexanes 1.0M
- Triethylaluminum in a solution of hexanes 1.0M

Purpose
The goal of using the proposed chemicals is to create an ethanol-based fuel that is hypergolic with hydrogen peroxide, and other common oxidizers, by adding small amounts 0.5-1 wt% of this chemical to ethanol. Due to the low concentration of additive it is expected that this mixture will be stable under normal atmospheric conditions. After making the mixture a stability study will be performed to verify this.

Responsible People
Master student:
Pim van Dommelen - 4345673
Supervisor:
Dr. B.V.S. Jyoti

Safety Measures

- Never work alone
- Work in a fume hood with the sash as low as possible
- Use a syringe not bigger than 16 gauge to transfer the chemical
- Use plastic syringes and needles only once
- Perform a safety run using a solvent to practice the experiment
- All glassware used should be oven-dried before use
- Never return excess chemical to the original container
- Ensure access to an eyewash and safety shower
- Have a dry chemical extinguisher nearby

- Keep a container of dry sand nearby

Precautions

- Inform Durga when the experiments will take place
- Remove anything flammable from the work area
- Clean the workplace prior to use
- Wear PPE (glasses, lab coat, gloves, long pants, closed shoes)
- Always store the chemical under an inert atmosphere
- Do not eat or drink in the lab
- Wash hands after handling the chemicals

Materials

- Ethanol
- Diethylzinc in a solution of hexanes 1.0M
- Triethylaluminium in a solution of hexanes 1.0M
- Hexane
- Clamps
- 2 x Receiving bottle containing a seal
- Magnetic stirrer
- Magnetic stirring bar
- Schlenk line
- Bubbler
- Drying column
- Nitrogen supply
- Vacuum pump
- Fume hood
- 6 x Needle
- 2 x Syringe
- Dry sand

Setup

Figures A.1 and A.2 show a picture and schematic of the transfer setup used. In case of Figure A.1 the pyrophoric liquid is not shown since it is only taken out of storage when actually used.

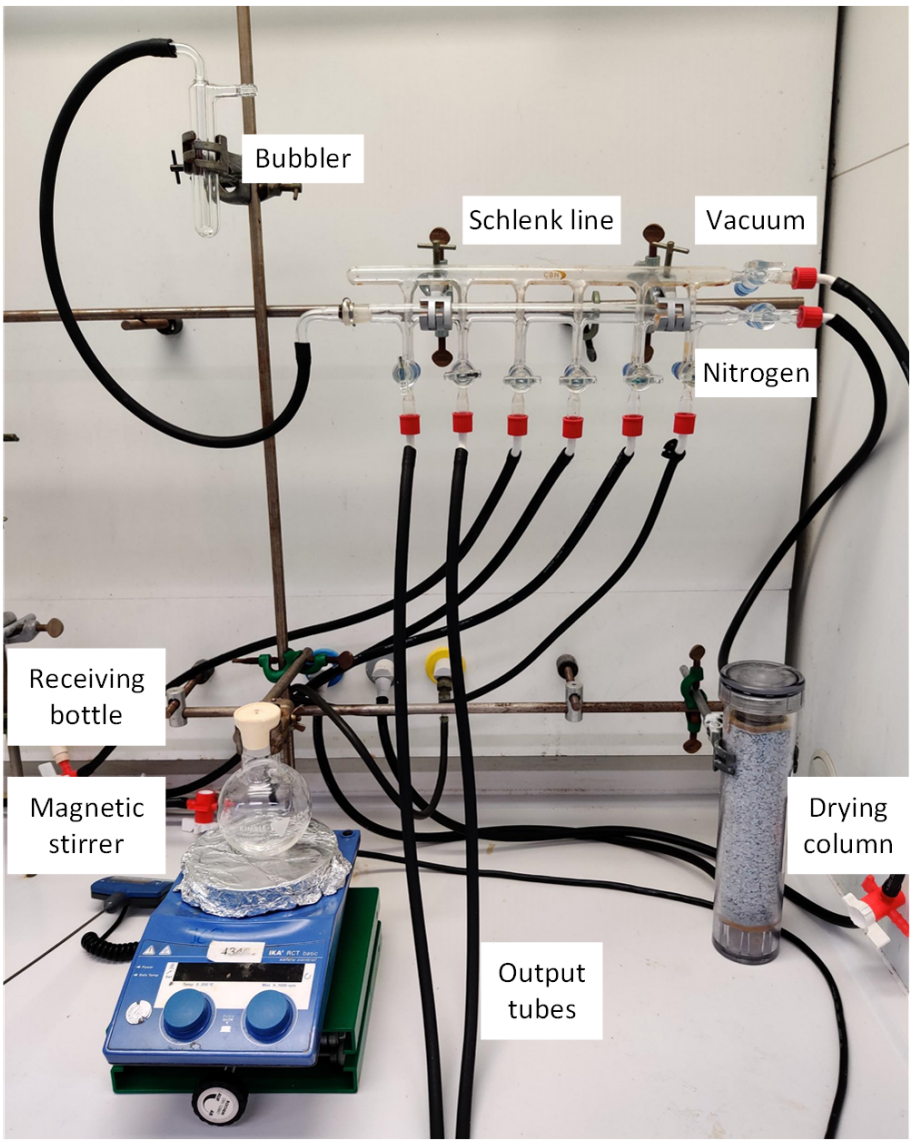

Figure A.1: A picture of the setup used for transferring a pyrophoric liquid.

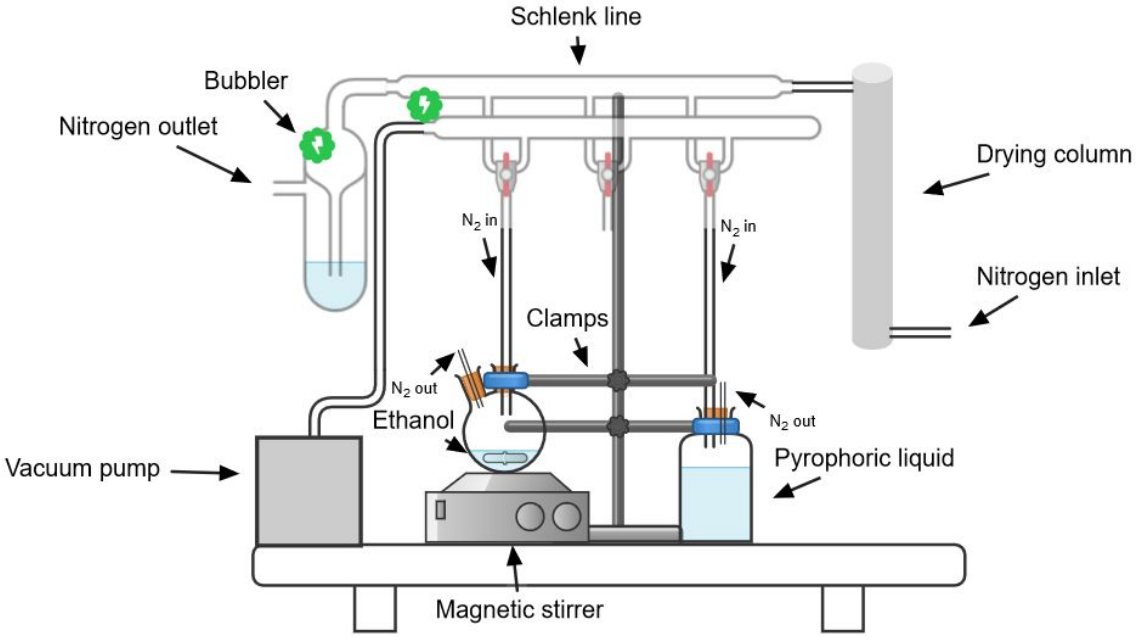

Figure A.2: A schematic representation of the setup used for transferring a pyrophoric liquid.

Procedure

Preparation:

- Clean all the glassware to be used.
- Dry the glassware in an oven on 120 ^{o}C for 4 hours. Then let it cool down under an inert atmosphere.
- Clean the workspace, remove flammable materials.
- Make sure that there is dry sand, an extinguisher, and an (eye) shower nearby.
- Make sure you are not alone. Inform other people of your experiment.
- Clamp the chemical bottle and receiving bottle in the fume hood to prevent them from moving.
- Place the receiving bottle on a magnetic stirrer and place a magnet inside. Seal the bottle using a septum.

Transfer:

- Flush the receiving bottle with alternating nitrogen and vacuum at least three times using the Schlenk line.
- Insert a needle with dry nitrogen from the Schlenk line into the receiving bottle.
- Insert a venting needle in the receiving bottle to prevent over pressurization.
- Use a syringe to transfer the desired amount of ethanol into the receiving bottle.
- Turn on the magnetic stirrer.
- Insert a needle with dry nitrogen from the Schlenk line into the chemical bottle.

- Insert a venting needle in the chemical bottle to prevent over pressurization.
- Flush a new syringe several times with nitrogen.
- Insert the needle of the syringe through the rubber of the chemical bottle.
- Gently pull liquid in the syringe. Never fill the syringe more than 50%. Only use small quantities <1 ml. Extract slightly more than required. The inflow of nitrogen and venting needle should prevent the syringe from creating a vacuum.
- While keeping the needle in the chemical bottle turn the syringe so the needle end points up. Now slowly push out the gas bubbles and excess liquid until the desired amount is still left in the syringe.
- Now pull in some inert gas so the needle does not contain any pyrophoric liquid.
- Remove the needle from the chemical bottle and insert it through the rubber of the receiving bottle.
- Deposit the desired amount of chemical into the receiving bottle.
- Remove the needle from the receiving bottle.
- Flush the syringe in hexane at least three times to clear it from the pyrophoric chemical.
- Remove the nitrogen supply and venting needle from the chemical bottle. Close it and store it.
- Remove the nitrogen supply and venting needle from the receiving bottle.
- Turn off the magnetic stirrer. -
- Study the stability of the mixture. Does any reaction occur? Does any phase separation occur?

Handling waste

- Propellants created using the pyrophoric liquid will be fully combusted in a fume hood.
- Materials that have come into contact with the pyrophoric liquid will be rinsed by hexane.
- The hexane will then be diluted by isopropanol until no reaction is observed. This is performed while mechanically stirring the hexane.
- The hexane/isopropanol mixture will then be diluted with methanol, while mechanically stirring it. The water is added very slowly.
- The hexane/isopropanol/methanol mixture will then be diluted with water, while mechanically stirring it. The water is added very slowly.
- The resulting solution is transferred to the aqueous organic waste.

Emergency procedure
In case of a spill:

- Announce the situation loudly
- Cover the spill with non-combustible material like dry sand

- Have a proper fire extinguisher ready in case of fire
- Use clean tools to clean up the absorbed material and place it into a metal or plastic container ready for disposal
- Do not use paper towels to clean up the spill
- Keep others from entering the area

In case of contact:

- If skin contact occurs, and/or skin or clothing are on fire, immediately drench in the safety shower with copious amounts of water for no less than 15 minutes to remove any remaining contaminants. If possible to do so without further injury, remove any remaining jewelry or clothing.
- If eye contact occurs, rinse thoroughly with plenty of water using an eyewash station for at least 15 minutes, occasionally lifting the upper and lower eyelids. Remove contact lenses if possible.
- If swallowed, do NOT induce vomiting unless directed otherwise by the SDS. Never give anything by mouth to an unconscious person. Rinse mouth with water.
- If inhaled, move into fresh air.

B

Instrumentation specification sheets

In this Chapter the full specification sheets of some instruments used can be found. Section B.1 shows the spec sheet of the photodiodes that were used, section B.2 contains the spec sheet for the k-type thermocouples and section B.3 displays the specifications of the high speed camera.

B.1. Photodiode datasheet

Si Photodiode

FDS100

Description

Thorlabs' FDS100 photodiode is ideal for measuring both pulsed and CW fiber light sources by converting optical power to electrical current. The detector is housed in a TO-5 package with an anode and cathode connection. The photodiode anode produces a current, which is a function of the incident light power and the wavelength. The responsivity $\Re(\lambda)$ can be read from the plot on the following page to estimate the amount of photocurrent. This can be converted to a voltage by placing a load resistor (R_L) from the photodiode anode to the circuit ground. Where P is the power, the output voltage is expressed as

$$V_o = P \times \Re \times R_L$$

The bandwidth, f_{BW}, and the rise time response, t_R, are determined from the diode capacitance, C_J, and the load resistance, R_L, as shown below. The diode capacitance can be lowered by placing a bias voltage from the photodiode cathode to the circuit ground.

$$f_{BW} = \frac{1}{(2\pi)R_L C_J},\ t_R = \frac{0.35}{f_{BW}}$$

Specifications

Specifications[a]		
Wavelength Range	λ	350 - 1100 nm
Peak Wavelength	λ_P	980 nm
Responsivity	$\Re(\lambda_p)$	0.65 A/W
Active Area		13 mm^2
Rise/Fall Time (632 nm, R_L=50 Ω, 20 V)	t_r/t_f	10 ns / 10 ns
NEP, Typical (900 nm, 20 V)	W/√Hz	1.2×10^{-14}
Dark Current (20V)	I_d	1.0 nA (Typ.) 20 nA (Max.)
Capacitance (20V)	C_j	24 pF (Typ.)
Package		TO-5
Sensor Material		Si

Maximum Rating	
Max Bias (Reverse) Voltage	25 V
Reverse Current	5 mA
Operating Temperature	-40 to 100 °C
Storage Temperature	-55 to 125 °C

a. Unless otherwise noted, all measurements are performed at 25 °C ambient temperature.

Recommended Circuit

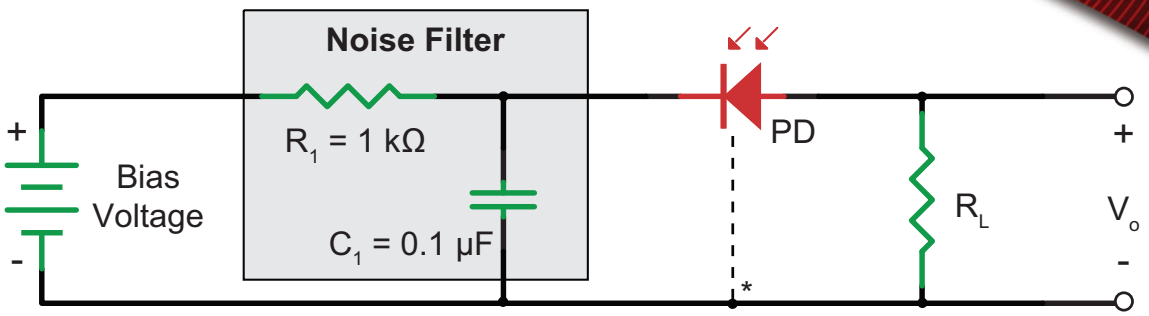

* Case ground for PD with a third lead.

Typical Spectral Intensity Distribution

The responsivity of a photodiode is a measure of its sensitivity to light and is defined as the ratio of the photocurrent I_P to the incident light power P at a given wavelength:

$$R_\lambda = \frac{I_P}{P}$$

In other words, it is a measure of the effectiveness of the conversion of light power into electrical current. Responsivity varies from lot to lot and with the wavelength of the incident light, applied reverse bias, and temperature. It increases slightly with applied reverse bias due to improved charge collection efficiency in the photodiode. The change in temperature increases or decreases the width of the band gap and varies inversely with the temperature.

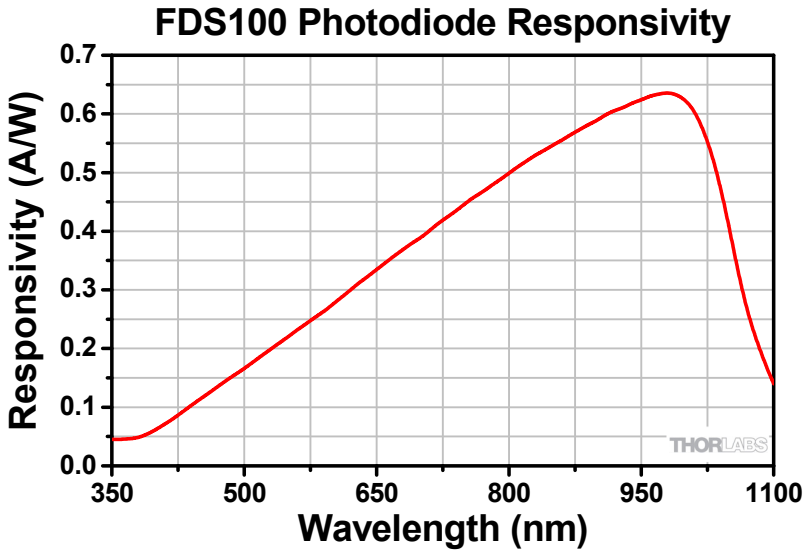

Drawing

Top View

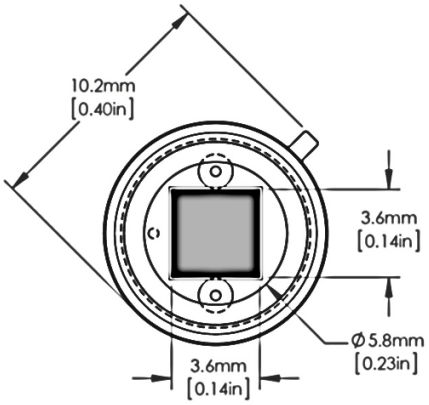

Top View

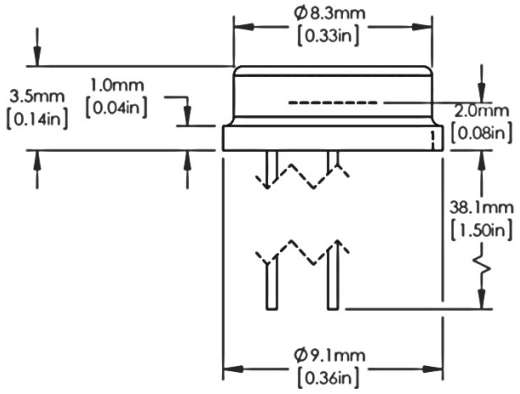

Bottom View

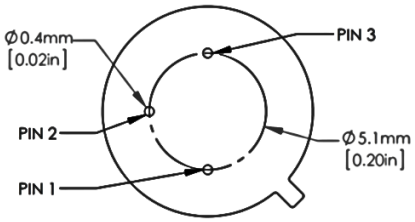

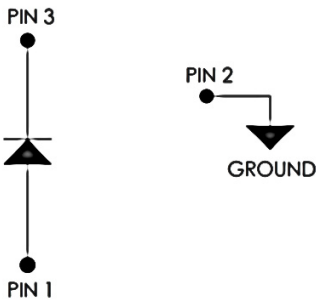

Precautions and Warranty Information

These products are ESD (electro static discharge) sensitive and as a result are not covered under warranty. In order to ensure the proper functioning of a photodiode care must be given to maintain the highest standards of compliance to the maximum electrical specifications when handling such devices. The photodiodes are particularly sensitive to any value that exceeds the absolute maximum ratings of the product. Any applied voltage in excess of the maximum specification will cause damage and possible complete failure to the product. The user must use handling procedures that prevent any electro static discharges or other voltage surges when handling or using these devices.

Thorlabs, Inc. Life Support and Military Use Application Policy is stated below:

THORLABS' PRODUCTS ARE NOT AUTHORIZED FOR USE AS CRITICAL COMPONENTS IN LIFE SUPPORT DEVICES OR SYSTEMS OR IN ANY MILITARY APPLICATION WITHOUT THE EXPRESS WRITTEN APPROVAL OF THE PRESIDENT OF THORLABS, INC. As used herein:

1. Life support devices or systems are devices or systems which, (a) are intended for surgical implant into the body, or (b) support or sustain life, and whose failure to perform, when properly used in accordance with instructions for use provided in the labeling, can be reasonably expected to result in a significant injury to the user.
2. A critical component is any component in a life support device or system whose failure to perform can be reasonably expected to cause the failure of the life support device or system or to affect its safety or effectiveness.
3. The Thorlabs products described in this document are not intended nor warranted for usage in Military Applications.

B.2. Thermocouple datasheet

Unsheathed Fine Gage Thermocouples

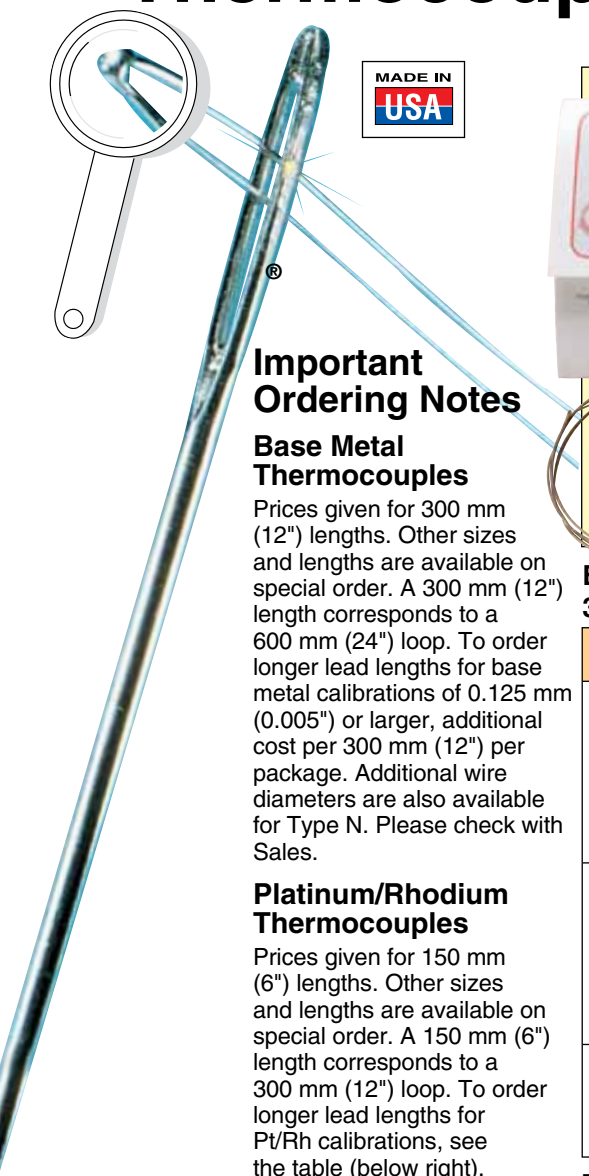

MADE IN USA

Convenient Packages of 5

Shown smaller than actual size.

Important Ordering Notes

Base Metal Thermocouples

Prices given for 300 mm (12") lengths. Other sizes and lengths are available on special order. A 300 mm (12") length corresponds to a 600 mm (24") loop. To order longer lead lengths for base metal calibrations of 0.125 mm (0.005") or larger, additional cost per 300 mm (12") per package. Additional wire diameters are also available for Type N. Please check with Sales.

Platinum/Rhodium Thermocouples

Prices given for 150 mm (6") lengths. Other sizes and lengths are available on special order. A 150 mm (6") length corresponds to a 300 mm (12") loop. To order longer lead lengths for Pt/Rh calibrations, see the table (below right).

Base Metal Calibrations: 300 mm (12") Length Standard–Package of 5

Calibration	Wire Dia. mm (in)	Model Number
J Iron-Constantan	0.025 (0.001)	IRCO-001
	0.050 (0.002)	IRCO-002
	0.075 (0.003)	IRCO-003
	0.125 (0.005)	IRCO-005
	0.25 (0.010)	IRCO-010
	0.38 (0.015)	IRCO-015
	0.5 (0.020)	IRCO-020
	0.81 (0.032)	IRCO-032
T Copper-Constantan	0.025 (0.001)	COCO-001
	0.050 (0.002)	COCO-002
	0.075 (0.003)	COCO-003
	0.125 (0.005)	COCO-005
	0.25 (0.010)	COCO-010
	0.38 (0.015)	COCO-015
	0.5 (0.020)	COCO-020
	0.81 (0.032)	COCO-032
N OMEGA-P®-OMEGA-N®	0.075 (0.003)	OPON-003
	0.125 (0.005)	OPON-005
	0.25 (0.010)	OPON-010
	0.50 (0.020)	OPON-020
	0.81 (0.032)	OPON-032

Calibration	Wire Dia. mm (in)	Model Number
K CHROMEGA®-ALOMEGA®	0.013 (0.0005)†	CHAL-0005
	0.025 (0.001)	CHAL-001
	0.050 (0.002)	CHAL-002
	0.075 (0.003)	CHAL-003
	0.125 (0.005)	CHAL-005
	0.25 (0.010)	CHAL-010
	0.38 (0.015)	CHAL-015
	0.50 (0.020)	CHAL-020
	0.81 (0.032)	CHAL-032
E CHROMEGA®-Constantan	0.013 (0.0005†)	CHCO-0005
	0.025 (0.001)	CHCO-001
	0.050 (0.002)	CHCO-002
	0.075 (0.003)	CHCO-003
	0.125 (0.005)	CHCO-005
	0.25 (0.010)	CHCO-010
	0.38 (0.015)	CHCO-015
	0.50 (0.020)	CHCO-020
	0.81 (0.032)	CHCO-032

† 0.013 mm (0.0005") diameter wires supplied with 200 mm (8") leads; maximum length 300 mm (12").
Note: *Shorter lead is negative lead.*

Pt/Rh Calibrations: 150 mm (6") Length Standard—Sold Individually

Calibration	Wire Dia. mm (in)	Model Number
R Pt/13%Rh-Pt	0.025 (0.001)	P13R-001
	0.050 (0.002)	P13R-002
	0.075 (0.003)	P13R-003
	0.125 (0.005)	P13R-005
	0.20 (0.008)	P13R-008
	0.25 (0.010)	P13R-010
	0.38 (0.015)	P13R-015
	0.50 (0.020)	P13R-020
	0.81 (0.032)	P13R-032

Calibration	Wire Dia mm (in)	Model Number
S Pt/10%Rh-Pt	0.025 (0.001)	P10R-001
	0.050 (0.002)	P10R-002
	0.075 (0.003)	P10R-003
	0.125 (0.005)	P10R-005
	0.20 (0.008)	P10R-008
	0.25 (0.010)	P10R-010
	0.38 (0.015)	P10R-015
	0.50 (0.020)	P10R-020
	0.81 (0.032)	P10R-032

Pt/Rh Calibrations: 150 mm (6") Length Standard—Sold Individually

Calibration	Wire Dia. mm (in)	Model Number
B Pt/30%Rh-Pt/6%Rh-	0.20 (0.008)	P30R-008
	0.25 (0.010)	P30R-010
	0.38 (0.015)	P30R-015
	0.50 (0.020)	P30R-020
	0.81 (0.032)	P30R-032

For Pricing and Details Visit omega.com/thermocouples

Wire Dia. mm (inches) Add'l Price/25 mm (1")
0.025 (0.001")
0.050 (0.002")
0.075 (0.003")
0.125 (0.005")
0.20 (0.008")
0.25 (0.010")
0.38 (0.015")
0.50 (0.020")
0.81 (0.032")

Discount Schedule Base Metal Thermocouples	
1 to 10 pkgs	Net
11 to 24 pkgs	5%
25 to 49 pkgs	10%
50 and up	15%

SPECIAL SIZES, ALLOYS OR ASSEMBLIES
Orders for special sizes, alloys or assemblies should be explicit and accompanied by a sketch or print, if possible.

Base metal thermocouples 0.125 mm (0.005") diameter and larger are made with Special Limits of Error wire.
Thermocouple insulator model nos. SH, DH, FS and OV also featured in this section.
Note: *Published price is based on market value at time of printing and is subject to change due to precious-metal market fluctuations.*

Ordering Example: CHAL-005, *package of five 300 mm (12") Type K thermocouples, 0.125 mm (0.005") diameter.*

MAXIMUM TEMPERATURE RANGE

Thermocouple Grade
– 328 to 2282°F
– 200 to 1250°C

Extension Grade
32 to 392°F
0 to 200°C

LIMITS OF ERROR
(whichever is greater)
Standard: 2.2°C or 0.75% Above 0°C
2.2°C or 2.0% Below 0°C
Special: 1.1°C or 0.4%

COMMENTS, BARE WIRE ENVIRONMENT:
Clean Oxidizing and Inert; Limited Use in Vacuum or Reducing; Wide Temperature Range; Most Popular Calibration

TEMPERATURE IN DEGREES °C
REFERENCE JUNCTION AT 0°C

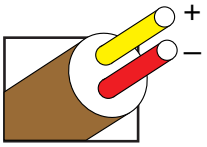

Thermocouple Grade

Nickel-Chromium vs. Nickel-Aluminum

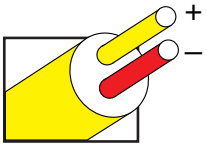

Extension Grade

Revised Thermocouple Reference Tables

TYPE K

Reference Tables
N.I.S.T. Monograph 175
Revised to ITS-90

Z

Thermoelectric Voltage in Millivolts

°C	-10	-9	-8	-7	-6	-5	-4	-3	-2	-1	0	°C
-260	-6.458	-6.457	-6.456	-6.455	-6.453	-6.452	-6.450	-6.448	-6.446	-6.444	-6.441	-260
-250	-6.441	-6.438	-6.435	-6.432	-6.429	-6.425	-6.421	-6.417	-6.413	-6.408	-6.404	-250
-240	-6.404	-6.399	-6.393	-6.388	-6.382	-6.377	-6.370	-6.364	-6.358	-6.351	-6.344	-240
-230	-6.344	-6.337	-6.329	-6.322	-6.314	-6.306	-6.297	-6.289	-6.280	-6.271	-6.262	-230
-220	-6.262	-6.252	-6.243	-6.233	-6.223	-6.213	-6.202	-6.192	-6.181	-6.170	-6.158	-220
-210	-6.158	-6.147	-6.135	-6.123	-6.111	-6.099	-6.087	-6.074	-6.061	-6.048	-6.035	-210
-200	-6.035	-6.021	-6.007	-5.994	-5.980	-5.965	-5.951	-5.936	-5.922	-5.907	-5.891	-200
-190	-5.891	-5.876	-5.861	-5.845	-5.829	-5.813	-5.797	-5.780	-5.763	-5.747	-5.730	-190
-180	-5.730	-5.713	-5.695	-5.678	-5.660	-5.642	-5.624	-5.606	-5.588	-5.569	-5.550	-180
-170	-5.550	-5.531	-5.512	-5.493	-5.474	-5.454	-5.435	-5.415	-5.395	-5.374	-5.354	-170
-160	-5.354	-5.333	-5.313	-5.292	-5.271	-5.250	-5.228	-5.207	-5.185	-5.163	-5.141	-160
-150	-5.141	-5.119	-5.097	-5.074	-5.052	-5.029	-5.006	-4.983	-4.960	-4.936	-4.913	-150
-140	-4.913	-4.889	-4.865	-4.841	-4.817	-4.793	-4.768	-4.744	-4.719	-4.694	-4.669	-140
-130	-4.669	-4.644	-4.618	-4.593	-4.567	-4.542	-4.516	-4.490	-4.463	-4.437	-4.411	-130
-120	-4.411	-4.384	-4.357	-4.330	-4.303	-4.276	-4.249	-4.221	-4.194	-4.166	-4.138	-120
-110	-4.138	-4.110	-4.082	-4.054	-4.025	-3.997	-3.968	-3.939	-3.911	-3.882	-3.852	-110
-100	-3.852	-3.823	-3.794	-3.764	-3.734	-3.705	-3.675	-3.645	-3.614	-3.584	-3.554	-100
-90	-3.554	-3.523	-3.492	-3.462	-3.431	-3.400	-3.368	-3.337	-3.306	-3.274	-3.243	-90
-80	-3.243	-3.211	-3.179	-3.147	-3.115	-3.083	-3.050	-3.018	-2.986	-2.953	-2.920	-80
-70	-2.920	-2.887	-2.854	-2.821	-2.788	-2.755	-2.721	-2.688	-2.654	-2.620	-2.587	-70
-60	-2.587	-2.553	-2.519	-2.485	-2.450	-2.416	-2.382	-2.347	-2.312	-2.278	-2.243	-60
-50	-2.243	-2.208	-2.173	-2.138	-2.103	-2.067	-2.032	-1.996	-1.961	-1.925	-1.889	-50
-40	-1.889	-1.854	-1.818	-1.782	-1.745	-1.709	-1.673	-1.637	-1.600	-1.564	-1.527	-40
-30	-1.527	-1.490	-1.453	-1.417	-1.380	-1.343	-1.305	-1.268	-1.231	-1.194	-1.156	-30
-20	-1.156	-1.119	-1.081	-1.043	-1.006	-0.968	-0.930	-0.892	-0.854	-0.816	-0.778	-20
-10	-0.778	-0.739	-0.701	-0.663	-0.624	-0.586	-0.547	-0.508	-0.470	-0.431	-0.392	-10
0	-0.392	-0.353	-0.314	-0.275	-0.236	-0.197	-0.157	-0.118	-0.079	-0.039	0.000	0
0	0.000	0.039	0.079	0.119	0.158	0.198	0.238	0.277	0.317	0.357	0.397	0
10	0.397	0.437	0.477	0.517	0.557	0.597	0.637	0.677	0.718	0.758	0.798	10
20	0.798	0.838	0.879	0.919	0.960	1.000	1.041	1.081	1.122	1.163	1.203	20
30	1.203	1.244	1.285	1.326	1.366	1.407	1.448	1.489	1.530	1.571	1.612	30
40	1.612	1.653	1.694	1.735	1.776	1.817	1.858	1.899	1.941	1.982	2.023	40
50	2.023	2.064	2.106	2.147	2.188	2.230	2.271	2.312	2.354	2.395	2.436	50
60	2.436	2.478	2.519	2.561	2.602	2.644	2.685	2.727	2.768	2.810	2.851	60
70	2.851	2.893	2.934	2.976	3.017	3.059	3.100	3.142	3.184	3.225	3.267	70
80	3.267	3.308	3.350	3.391	3.433	3.474	3.516	3.557	3.599	3.640	3.682	80
90	3.682	3.723	3.765	3.806	3.848	3.889	3.931	3.972	4.013	4.055	4.096	90
100	4.096	4.138	4.179	4.220	4.262	4.303	4.344	4.385	4.427	4.468	4.509	100
110	4.509	4.550	4.591	4.633	4.674	4.715	4.756	4.797	4.838	4.879	4.920	110
120	4.920	4.961	5.002	5.043	5.084	5.124	5.165	5.206	5.247	5.288	5.328	120
130	5.328	5.369	5.410	5.450	5.491	5.532	5.572	5.613	5.653	5.694	5.735	130
140	5.735	5.775	5.815	5.856	5.896	5.937	5.977	6.017	6.058	6.098	6.138	140
150	6.138	6.179	6.219	6.259	6.299	6.339	6.380	6.420	6.460	6.500	6.540	150
160	6.540	6.580	6.620	6.660	6.701	6.741	6.781	6.821	6.861	6.901	6.941	160
170	6.941	6.981	7.021	7.060	7.100	7.140	7.180	7.220	7.260	7.300	7.340	170
180	7.340	7.380	7.420	7.460	7.500	7.540	7.579	7.619	7.659	7.699	7.739	180
190	7.739	7.779	7.819	7.859	7.899	7.939	7.979	8.019	8.059	8.099	8.138	190
200	8.138	8.178	8.218	8.258	8.298	8.338	8.378	8.418	8.458	8.499	8.539	200
210	8.539	8.579	8.619	8.659	8.699	8.739	8.779	8.819	8.860	8.900	8.940	210
220	8.940	8.980	9.020	9.061	9.101	9.141	9.181	9.222	9.262	9.302	9.343	220
230	9.343	9.383	9.423	9.464	9.504	9.545	9.585	9.626	9.666	9.707	9.747	230
240	9.747	9.788	9.828	9.869	9.909	9.950	9.991	10.031	10.072	10.113	10.153	240
°C	0	1	2	3	4	5	6	7	8	9	10	°C

°C	0	1	2	3	4	5	6	7	8	9	10	°C
250	10.153	10.194	10.235	10.276	10.316	10.357	10.398	10.439	10.480	10.520	10.561	250
260	10.561	10.602	10.643	10.684	10.725	10.766	10.807	10.848	10.889	10.930	10.971	260
270	10.971	11.012	11.053	11.094	11.135	11.176	11.217	11.259	11.300	11.341	11.382	270
280	11.382	11.423	11.465	11.506	11.547	11.588	11.630	11.671	11.712	11.753	11.795	280
290	11.795	11.836	11.877	11.919	11.960	12.001	12.043	12.084	12.126	12.167	12.209	290
300	12.209	12.250	12.291	12.333	12.374	12.416	12.457	12.499	12.540	12.582	12.624	300
310	12.624	12.665	12.707	12.748	12.790	12.831	12.873	12.915	12.956	12.998	13.040	310
320	13.040	13.081	13.123	13.165	13.206	13.248	13.290	13.331	13.373	13.415	13.457	320
330	13.457	13.498	13.540	13.582	13.624	13.665	13.707	13.749	13.791	13.833	13.874	330
340	13.874	13.916	13.958	14.000	14.042	14.084	14.126	14.167	14.209	14.251	14.293	340
350	14.293	14.335	14.377	14.419	14.461	14.503	14.545	14.587	14.629	14.671	14.713	350
360	14.713	14.755	14.797	14.839	14.881	14.923	14.965	15.007	15.049	15.091	15.133	360
370	15.133	15.175	15.217	15.259	15.301	15.343	15.385	15.427	15.469	15.511	15.554	370
380	15.554	15.596	15.638	15.680	15.722	15.764	15.806	15.849	15.891	15.933	15.975	380
390	15.975	16.017	16.059	16.102	16.144	16.186	16.228	16.270	16.313	16.355	16.397	390
400	16.397	16.439	16.482	16.524	16.566	16.608	16.651	16.693	16.735	16.778	16.820	400
410	16.820	16.862	16.904	16.947	16.989	17.031	17.074	17.116	17.158	17.201	17.243	410
420	17.243	17.285	17.328	17.370	17.413	17.455	17.497	17.540	17.582	17.624	17.667	420
430	17.667	17.709	17.752	17.794	17.837	17.879	17.921	17.964	18.006	18.049	18.091	430
440	18.091	18.134	18.176	18.218	18.261	18.303	18.346	18.388	18.431	18.473	18.516	440
450	18.516	18.558	18.601	18.643	18.686	18.728	18.771	18.813	18.856	18.898	18.941	450
460	18.941	18.983	19.026	19.068	19.111	19.154	19.196	19.239	19.281	19.324	19.366	460
470	19.366	19.409	19.451	19.494	19.537	19.579	19.622	19.664	19.707	19.750	19.792	470
480	19.792	19.835	19.877	19.920	19.962	20.005	20.048	20.090	20.133	20.175	20.218	480
490	20.218	20.261	20.303	20.346	20.389	20.431	20.474	20.516	20.559	20.602	20.644	490
500	20.644	20.687	20.730	20.772	20.815	20.857	20.900	20.943	20.985	21.028	21.071	500
510	21.071	21.113	21.156	21.199	21.241	21.284	21.326	21.369	21.412	21.454	21.497	510
520	21.497	21.540	21.582	21.625	21.668	21.710	21.753	21.796	21.838	21.881	21.924	520
530	21.924	21.966	22.009	22.052	22.094	22.137	22.179	22.222	22.265	22.307	22.350	530
540	22.350	22.393	22.435	22.478	22.521	22.563	22.606	22.649	22.691	22.734	22.776	540
550	22.776	22.819	22.862	22.904	22.947	22.990	23.032	23.075	23.117	23.160	23.203	550
560	23.203	23.245	23.288	23.331	23.373	23.416	23.458	23.501	23.544	23.586	23.629	560
570	23.629	23.671	23.714	23.757	23.799	23.842	23.884	23.927	23.970	24.012	24.055	570
580	24.055	24.097	24.140	24.182	24.225	24.267	24.310	24.353	24.395	24.438	24.480	580
590	24.480	24.523	24.565	24.608	24.650	24.693	24.735	24.778	24.820	24.863	24.905	590
600	24.905	24.948	24.990	25.033	25.075	25.118	25.160	25.203	25.245	25.288	25.330	600
610	25.330	25.373	25.415	25.458	25.500	25.543	25.585	25.627	25.670	25.712	25.755	610
620	25.755	25.797	25.840	25.882	25.924	25.967	26.009	26.052	26.094	26.136	26.179	620
630	26.179	26.221	26.263	26.306	26.348	26.390	26.433	26.475	26.517	26.560	26.602	630
640	26.602	26.644	26.687	26.729	26.771	26.814	26.856	26.898	26.940	26.983	27.025	640
650	27.025	27.067	27.109	27.152	27.194	27.236	27.278	27.320	27.363	27.405	27.447	650
660	27.447	27.489	27.531	27.574	27.616	27.658	27.700	27.742	27.784	27.826	27.869	660
670	27.869	27.911	27.953	27.995	28.037	28.079	28.121	28.163	28.205	28.247	28.289	670
680	28.289	28.332	28.374	28.416	28.458	28.500	28.542	28.584	28.626	28.668	28.710	680
690	28.710	28.752	28.794	28.835	28.877	28.919	28.961	29.003	29.045	29.087	29.129	690
700	29.129	29.171	29.213	29.255	29.297	29.338	29.380	29.422	29.464	29.506	29.548	700
710	29.548	29.589	29.631	29.673	29.715	29.757	29.798	29.840	29.882	29.924	29.965	710
720	29.965	30.007	30.049	30.090	30.132	30.174	30.216	30.257	30.299	30.341	30.382	720
730	30.382	30.424	30.466	30.507	30.549	30.590	30.632	30.674	30.715	30.757	30.798	730
740	30.798	30.840	30.881	30.923	30.964	31.006	31.047	31.089	31.130	31.172	31.213	740
750	31.213	31.255	31.296	31.338	31.379	31.421	31.462	31.504	31.545	31.586	31.628	750
760	31.628	31.669	31.710	31.752	31.793	31.834	31.876	31.917	31.958	32.000	32.041	760
770	32.041	32.082	32.124	32.165	32.206	32.247	32.289	32.330	32.371	32.412	32.453	770
780	32.453	32.495	32.536	32.577	32.618	32.659	32.700	32.742	32.783	32.824	32.865	780
790	32.865	32.906	32.947	32.988	33.029	33.070	33.111	33.152	33.193	33.234	33.275	790
°C	0	1	2	3	4	5	6	7	8	9	10	°C

Revised Thermocouple Reference Tables

TYPE K

Reference Tables
N.I.S.T. Monograph 175
Revised to ITS-90

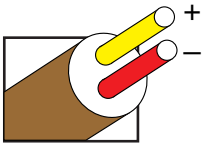

Thermocouple Grade

Nickel-Chromium vs. Nickel-Aluminum

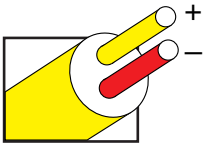

Extension Grade

MAXIMUM TEMPERATURE RANGE
Thermocouple Grade
– 328 to 2282°F
– 200 to 1250°C
Extension Grade
32 to 392°F
0 to 200°C

LIMITS OF ERROR
(whichever is greater)
Standard: 2.2°C or 0.75% Above 0°C
2.2°C or 2.0% Below 0°C
Special: 1.1°C or 0.4%

COMMENTS, BARE WIRE ENVIRONMENT:
Clean Oxidizing and Inert; Limited Use in Vacuum or Reducing; Wide Temperature Range; Most Popular Calibration

TEMPERATURE IN DEGREES °C
REFERENCE JUNCTION AT 0°C

Thermoelectric Voltage in Millivolts

°C	0	1	2	3	4	5	6	7	8	9	10	°C
800	33.275	33.316	33.357	33.398	33.439	33.480	33.521	33.562	33.603	33.644	33.685	800
810	33.685	33.726	33.767	33.808	33.848	33.889	33.930	33.971	34.012	34.053	34.093	810
820	34.093	34.134	34.175	34.216	34.257	34.297	34.338	34.379	34.420	34.460	34.501	820
830	34.501	34.542	34.582	34.623	34.664	34.704	34.745	34.786	34.826	34.867	34.908	830
840	34.908	34.948	34.989	35.029	35.070	35.110	35.151	35.192	35.232	35.273	35.313	840
850	35.313	35.354	35.394	35.435	35.475	35.516	35.556	35.596	35.637	35.677	35.718	850
860	35.718	35.758	35.798	35.839	35.879	35.920	35.960	36.000	36.041	36.081	36.121	860
870	36.121	36.162	36.202	36.242	36.282	36.323	36.363	36.403	36.443	36.484	36.524	870
880	36.524	36.564	36.604	36.644	36.685	36.725	36.765	36.805	36.845	36.885	36.925	880
890	36.925	36.965	37.006	37.046	37.086	37.126	37.166	37.206	37.246	37.286	37.326	890
900	37.326	37.366	37.406	37.446	37.486	37.526	37.566	37.606	37.646	37.686	37.725	900
910	37.725	37.765	37.805	37.845	37.885	37.925	37.965	38.005	38.044	38.084	38.124	910
920	38.124	38.164	38.204	38.243	38.283	38.323	38.363	38.402	38.442	38.482	38.522	920
930	38.522	38.561	38.601	38.641	38.680	38.720	38.760	38.799	38.839	38.878	38.918	930
940	38.918	38.958	38.997	39.037	39.076	39.116	39.155	39.195	39.235	39.274	39.314	940
950	39.314	39.353	39.393	39.432	39.471	39.511	39.550	39.590	39.629	39.669	39.708	950
960	39.708	39.747	39.787	39.826	39.866	39.905	39.944	39.984	40.023	40.062	40.101	960
970	40.101	40.141	40.180	40.219	40.259	40.298	40.337	40.376	40.415	40.455	40.494	970
980	40.494	40.533	40.572	40.611	40.651	40.690	40.729	40.768	40.807	40.846	40.885	980
990	40.885	40.924	40.963	41.002	41.042	41.081	41.120	41.159	41.198	41.237	41.276	990
1000	41.276	41.315	41.354	41.393	41.431	41.470	41.509	41.548	41.587	41.626	41.665	1000
1010	41.665	41.704	41.743	41.781	41.820	41.859	41.898	41.937	41.976	42.014	42.053	1010
1020	42.053	42.092	42.131	42.169	42.208	42.247	42.286	42.324	42.363	42.402	42.440	1020
1030	42.440	42.479	42.518	42.556	42.595	42.633	42.672	42.711	42.749	42.788	42.826	1030
1040	42.826	42.865	42.903	42.942	42.980	43.019	43.057	43.096	43.134	43.173	43.211	1040
1050	43.211	43.250	43.288	43.327	43.365	43.403	43.442	43.480	43.518	43.557	43.595	1050
1060	43.595	43.633	43.672	43.710	43.748	43.787	43.825	43.863	43.901	43.940	43.978	1060
1070	43.978	44.016	44.054	44.092	44.130	44.169	44.207	44.245	44.283	44.321	44.359	1070
1080	44.359	44.397	44.435	44.473	44.512	44.550	44.588	44.626	44.664	44.702	44.740	1080
1090	44.740	44.778	44.816	44.853	44.891	44.929	44.967	45.005	45.043	45.081	45.119	1090
°C	0	1	2	3	4	5	6	7	8	9	10	°C

°C	0	1	2	3	4	5	6	7	8	9	10	°C
1100	45.119	45.157	45.194	45.232	45.270	45.308	45.346	45.383	45.421	45.459	45.497	1100
1110	45.497	45.534	45.572	45.610	45.647	45.685	45.723	45.760	45.798	45.836	45.873	1110
1120	45.873	45.911	45.948	45.986	46.024	46.061	46.099	46.136	46.174	46.211	46.249	1120
1130	46.249	46.286	46.324	46.361	46.398	46.436	46.473	46.511	46.548	46.585	46.623	1130
1140	46.623	46.660	46.697	46.735	46.772	46.809	46.847	46.884	46.921	46.958	46.995	1140
1150	46.995	47.033	47.070	47.107	47.144	47.181	47.218	47.256	47.293	47.330	47.367	1150
1160	47.367	47.404	47.441	47.478	47.515	47.552	47.589	47.626	47.663	47.700	47.737	1160
1170	47.737	47.774	47.811	47.848	47.884	47.921	47.958	47.995	48.032	48.069	48.105	1170
1180	48.105	48.142	48.179	48.216	48.252	48.289	48.326	48.363	48.399	48.436	48.473	1180
1190	48.473	48.509	48.546	48.582	48.619	48.656	48.692	48.729	48.765	48.802	48.838	1190
1200	48.838	48.875	48.911	48.948	48.984	49.021	49.057	49.093	49.130	49.166	49.202	1200
1210	49.202	49.239	49.275	49.311	49.348	49.384	49.420	49.456	49.493	49.529	49.565	1210
1220	49.565	49.601	49.637	49.674	49.710	49.746	49.782	49.818	49.854	49.890	49.926	1220
1230	49.926	49.962	49.998	50.034	50.070	50.106	50.142	50.178	50.214	50.250	50.286	1230
1240	50.286	50.322	50.358	50.393	50.429	50.465	50.501	50.537	50.572	50.608	50.644	1240
1250	50.644	50.680	50.715	50.751	50.787	50.822	50.858	50.894	50.929	50.965	51.000	1250
1260	51.000	51.036	51.071	51.107	51.142	51.178	51.213	51.249	51.284	51.320	51.355	1260
1270	51.355	51.391	51.426	51.461	51.497	51.532	51.567	51.603	51.638	51.673	51.708	1270
1280	51.708	51.744	51.779	51.814	51.849	51.885	51.920	51.955	51.990	52.025	52.060	1280
1290	52.060	52.095	52.130	52.165	52.200	52.235	52.270	52.305	52.340	52.375	52.410	1290
1300	52.410	52.445	52.480	52.515	52.550	52.585	52.620	52.654	52.689	52.724	52.759	1300
1310	52.759	52.794	52.828	52.863	52.898	52.932	52.967	53.002	53.037	53.071	53.106	1310
1320	53.106	53.140	53.175	53.210	53.244	53.279	53.313	53.348	53.382	53.417	53.451	1320
1330	53.451	53.486	53.520	53.555	53.589	53.623	53.658	53.692	53.727	53.761	53.795	1330
1340	53.795	53.830	53.864	53.898	53.932	53.967	54.001	54.035	54.069	54.104	54.138	1340
1350	54.138	54.172	54.206	54.240	54.274	54.308	54.343	54.377	54.411	54.445	54.479	1350
1360	54.479	54.513	54.547	54.581	54.615	54.649	54.683	54.717	54.751	54.785	54.819	1360
1370	54.819	54.852	54.886									1370
°C	0	1	2	3	4	5	6	7	8	9	10	°C

B.3. High speed camera datasheet

Photron

Datasheet

Compact high-speed cameras with high light sensitivity

The FASTCAM Mini AX is Photron's highest performance model within the FASTCAM Mini series of high-speed cameras. The Mini AX delivers exceptional light sensitivity, excellent image quality and flexible region of interest (ROI) features for customers who do not require the ultimate frame rate performance of the FASTCAM SA-Z, but would benefit from the same high-end camera image sensor features.

Three performance level models - Mini AX50, AX100 and AX200 - deliver 1-megapixel image resolution (1024 x 1024 pixels) at frame rates up to 2,000fps, 4,000fps and 6,400fps respectively. All three Mini AX models offer a minimum exposure duration of 1µs as standard with recording memory options up to 32GB providing extended recording times and triggering flexibility.

Subject to export approval the Mini AX100 can be offered with maximum frame rates up to 540,000fps and the Mini AX200 with maximum frame rates up to 900,000fps with a minimum exposure time of 260 nanoseconds.

Standard operational features of the FASTCAM Mini AX include a mechanical shutter to allow remote system calibration, Gigabit Ethernet Interface for reliable system control with high-speed data transfer to PC, and the ability to remotely switch off cooling fans to eliminate vibration when recording at high magnifications.

With the combination of high frame rates, high image quality and exceptional light sensitivity contained within a 120mm x 120mm x 94mm rugged camera body weighing just 1.5kg, the FASTCAM Mini AX is ideally suited for use in a wide range of demanding scientific and industrial applications.

FASTCAM Mini AX

Model AX50 / AX100 / AX200

1-Megapixel CMOS Image Sensor:
1024 x 1024 pixels at 2,000fps (Mini AX50)
1024 x 1024 pixels at 4,000fps (Mini AX100)
1024 x 1024 pixels at 6,400fps (Mini AX200)

Maximum Frame Rate:
170,000fps (Mini AX50 type 170K)
212,500fps (Mini AX100 type 200K)
540,000fps (Mini AX100 type 540K)
216,000fps (Mini AX200 type 200K)
540,000fps (Mini AX200 type 540K)
900,000fps (Mini AX200 type 900k)

Class Leading Light Sensitivity:
ISO 40,000 monochrome
ISO 16,000 color

Global Electronic Shutter:
1ms to 1µs independent of frame rate
(Mini AX200 model 900K only: 260ns shutter available subject to export control)

Dynamic Range (ADC):
12-bit monochrome, 36-bit color

Compact and Lightweight:
120mm (H) x 120mm (W) x 94mm (D)
4.72″ (H) x 4.72″ (W) x 3.70″ (D)
Weight: 1.5Kg (3.30 lbs.)

Internal Recording Memory:
8GB, 16GB, or 32GB

Fast Gigabit Ethernet Interface:
Provides high-speed image download to standard notebook/PC

Flexible Frame Synchronization:
Frame rate may be synchronized to external unstable frequencies

High-G Rated:
Suitable for application in high-G environments; operation tested to 100G, 10ms, 6-axes

Fan Stop Function:
Remotely switch off cooling fans to eliminate vibration

Image Sensor Technical Data

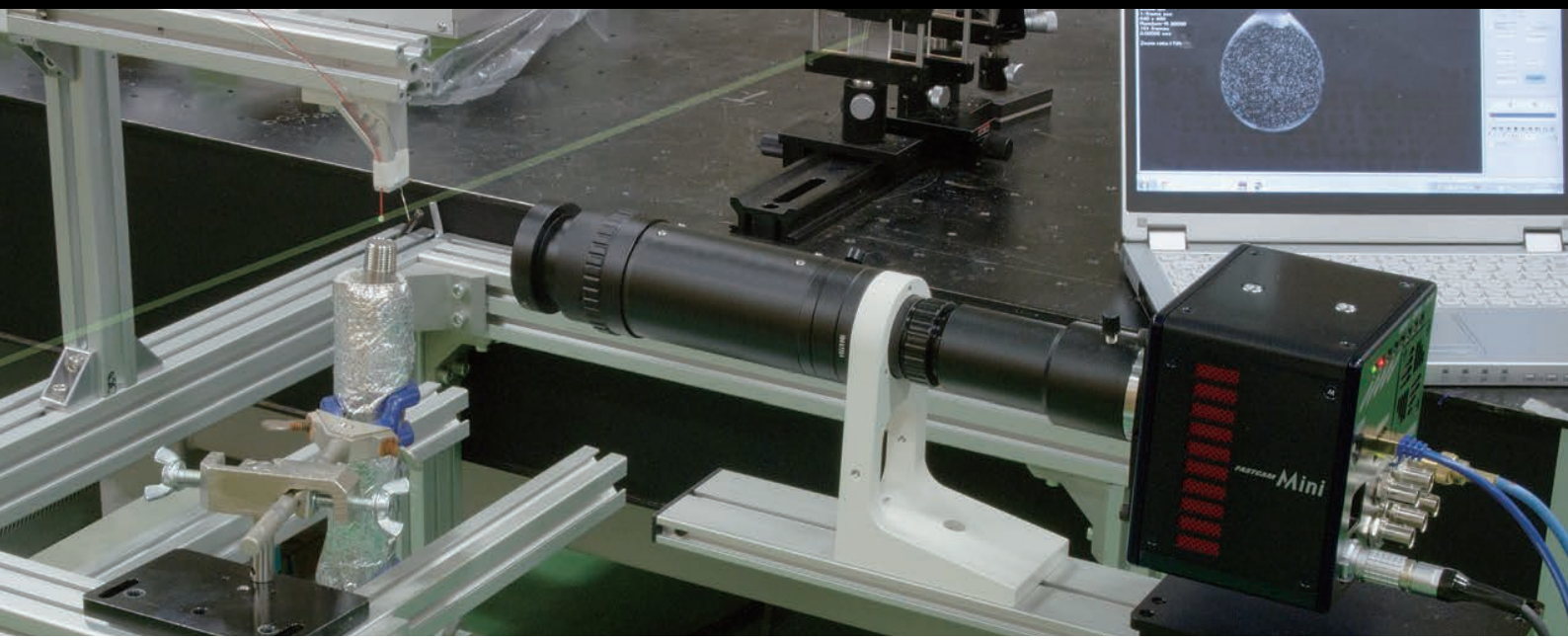

Light Sensitivity:

FASTCAM MINI AX	
Monochrome models	ISO 40,000
Color models	ISO 16,000

Monochrome sensors used in the FASTCAM Mini AX cameras are supplied without an IR absorbing filter, extending the camera spectral response beyod 900nm. When the sensitivity of the FASTCAM Mini AX camera is measured to tungsten light including near IR response an equivalent value of ISO 100,000 is obtained.

Image Sensor:

The FASTCAM Mini AX system uses an advanced CMOS image sensor optimized for light sensitivity and high image quality that is unique to Photron.

A 20-micron pixel pitch gives a sensor size at full image resolution of 20.48 x 20.48mm (diagonal 28.96mm).

Lenses designed for both FX (35mm full frame) and also DX (APS-C digital SLR) formats are fully compatible with the FASTCAM Mini AX at full image resolution.

Sensor Type	Proprietary Design Advanced CMOS
Maximum Resolution (pixels)	1024 x 1024 pixels
Sensor Size / Diagonal	20.48 x 20.48mm / 28.96mm
Pixel Size (microns)	20µm x 20µm
Quantum Efficiency	46% at 630nm
Fill Factor	58%
Color Matrix	Bayer CFA (single sensor)
Light Sensitivity	ISO 40,000 monochrome ISO 16,000 color (monochrome sensor equivalent ISO 100,000 including near IR response)
Shutter	Global Electronic Shutter 1ms to 1µs independent of frame rate (Mini AX200 model 900K only: 260ns shutter available subject to export control)

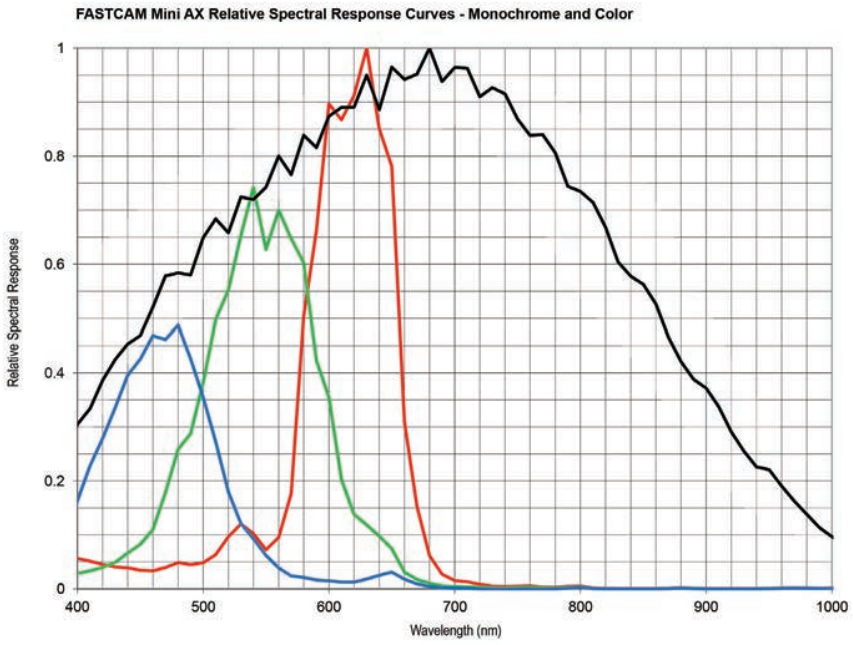

Camera Performance Specifications

Camera Performance Specifications

Model	Mini AX50	Mini AX100	Mini AX200
Full Frame Performance	2,000fps 1024 x 1024 pixels	4,000fps 1024 x 1024 pixels	6,400fps 1024 x 1024 pixels
Maximum Frame Rate	Type 170K: 170,000fps (128 x 16 pixels)	Type 200K: 212,500fps (128 x 16 pixels) Type 540K: 540,000fps* (128 x 16 pixels)	Type 200K: 216,000fps (128 x 16 pixels) Type 540K: 540,000fps* (128 x 16 pixels) Type 900K: 900,000fps* (128 x 16 pixels)
Minimum Exposure Time	Global electronic shutter to 1.05µs selectable independent or frame rate (260ns option available with Mini AX200 type 900K only) *		
Inter Frame Time (for PIV)	1.71µs		
Ruggedized Mechanical Calibration Shutter	Standard feature		
Dynamic Range (ADC)	12-bit monochrome 36-bit color		
Memory Capacity Options	8GB: 5,457 frames at full resolution 16GB: 10,918 frames at full resolution 32GB: 21,841 frames at full resolution		
Memory Partitions	Up to 64 memory segments		
Region of Interest	Selectable in steps of 128 pixels (horizontal) x 16 pixels (vertical)		
Trigger Inputs	Selectable +/- TTL 5V and switch closure		
Trigger Delay	Programmable on selected input / output triggers: 100ns resolution		
Input / Output	Input: Trigger (TTL/Switch), sync, ready, event, IRIG Output: trigger, sync, ready, rec, exposure		
Trigger Modes	Start, end, center, manual, random, random reset, image trigger, time lapse		
Time Code Input	IRIG-B		
External Sync	+/- TTL 5Vp-p Variable frequency sync		
Camera Control Interface	High-speed Gigabit Ethernet		
Image Data Display	Frame rate, shutter speed, trigger mode, date/time, status, real time / IRIG time, frame count, resolution		
Saved Image Formats	BMP, TIFF, JPEG, PNG, RAW, RAWW, MRAW, AVI, WMV, FTIF, MOV - Images can be saved with or without image data and in 8-bit, 16-bit or 36-bit depth of sensor where supported		
Supported OS	Microsoft Windows operating system including: 7, 8, 8.1, 10 (32/64-bit)		

* Frame rates above 225,000fps and exposure times below 1µs may be subject to export control regulations in some areas

High-Speed Gigabit Ethernet Interface:

The FASTCAM Mini AX camera system is equipped with a high-speed Gigabit Ethernet Interface to provide reliable network communication and fast download of image data.

Dedicated I/O:

A dedicated BNC connection for a contact closure hardware trigger input is provided. In addition, two programmable inputs and two programmable output channels provide direct connection for common tasks such as synchronization of multiple cameras and operation in conjunction with Data Acquisition (DAQ) hardware.

High-G Mechanical Calibration Shutter:

The ruggedized mechanical shutter fitted as standard to the FASTCAM Mini AX camera allows sensor black balance calibration to be carried out remotely from the system control software.

Nikon G-Type Compatible Lens Fitting:

The FASTCAM Mini AX camera is equipped with an objective lens mount compatible with readily available Nikon G-type lenses. Controls provided within the lens mount allow the control of lens aperture on lenses without external iris control.

Camera Operation Features

Frame Synchronization	Accurate frame synchronization with other cameras and with external and unstable frequencies.
Dual Slope Shutter (Extended Dynamic Range)	Selectable in 20 steps (0 to 95% in 5% increments) to prevent pixel overexposure without post processing.
Memory Partitions	Up to 64 memory segments allow multiple events to be stored in camera memory before downloading, with automatic progression to the next available partition.
Low Light Mode	Operation at minimum frame rate with separately adjustable shutter time to allow easy camera set-up and focus in ambient lighting.
IRIG Phase Lock	Enables multiple cameras to be synchronized together with other instrumentation equipment or to a master external time source.
Internal Time Delay Generator	Allows programmable delays to be set on input and output triggers; 100ns resolution.
Event Markers	Up to ten user-entered event markers to define specific events within the recorded image sequence .
Download While Recording	FASTCAM Mini AX supports Partition Recording Mode, allowing image data captured in one memory partition to be downloaded while at the same time recording into another partition.
Automatic Download	The system can be set to automatically download image data to the control PC and, when download is complete to re-arm in readiness for the next trigger with automatically incremented file names.
Software Binning	Virtual pixel binning (2x2, 4x4 etc.) allows increased light sensitivity with reduced image resolution without changing camera field of view.

Operation Software Features

Image Calibration	2D image calibration allows the measurement of distance and angle from the image. A calibration grid overlay can be superimposed on the image.
Image Overlay	A stored reference image may be overlaid on the live image to allow accurate camera positioning to achieve the same view as a previous test.
Import of Multiple Image Sequences	Multiple image sequences can be loaded and simultaneously replayed. Timing of image sequences can be adjusted to create a common time reference. Time based synchronization allows images captured at different frame rates to be synchronized.
High Dynamic Range Mode	Making use of the full sensor dynamic range, HDR mode allows enhanced detail in both light and dark areas of an image to be displayed simultaneously.
Motion Detector	In order to highlight subtle changes in an image, Motion Detector allows a reference image to be subtracted from a recorded sequence. Details including propagation of shock waves and surface changes during impact can be visualized using the feature.
Line Profile	A line profile representing grey levels along a line drawn across any region of the image is displayed. In live mode the Line Profile can be used to ensure optimum image focus is achieved.
Histogram	A histogram displaying grey levels within a user-defined image area is displayed. In live mode the Histogram can be used to ensure that optimum exposure levels are set for the scene being recorded.

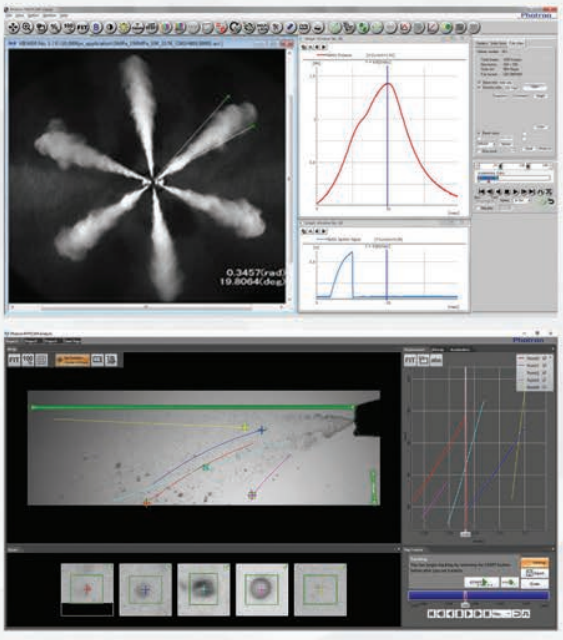

Photron FASTCAM Viewer:
Photron FASTCAM Viewer software (PFV) has been designed to provide an intuitive and feature rich user interface for the control of Photron high-speed cameras, data saving, image replay and simple motion analysis. Advanced operation menus provide access to features for advanced camera operation and image enhancement. Tools are provided to allow image calibration and easy measurement of angles and distances from image data. Also included are a C++ SDK and wrappers for LabView and MATLAB ®.

An optional software plug-in module provides synchronisation between Photron high- speed cameras and data acquired through National Instruments data acquisition systems. Synchronised data captured by the DAQ system provides waveform information which can be viewed alongside high-speed camera images.

Photron FASTCAM Analysis:
PFV software allows image sequences to be exported directly to optional Photron FASTCAM Analysis (PFA) Motion Analysis software. This entry level Motion Analysis software with an on screen 'step by step guide' function launches automatically from Photron FASTCAM Viewer software, and provides automated tracking of up to 5 points using feature or correlation tracking algorithms for the automated analysis of motion within an image sequence.

Frame Rate / Image Resolution

Variable Region of Interest:
Region of Interest (ROI) or sub-windowing allows a user-specified portion of the sensor to be defined to capture images. By using a reduced portion of the image area, the frame rate at which images are recorded can be increased. FASTCAM Mini AX allows the ROI to be set in increments of 128 pixels horizontal and 16 pixels vertical.

Square Image Sensor Format:
Unlike broadcast and media applications where image formats such as 16:9 have now become standard, in scientific and industrial imaging applications an image sensor with a 1:1 image format is generally accepted to be advantageous. To capture the maximum useful image data in applications including microscopy, detonics, combustion imaging and many others, a 1:1 sensor format provides greater flexibility than 'letterbox' image formats. The FASTCAM Mini AX image sensor allows the user to choose either square or rectangular image formats in order to obtain the maximum subject information.

External Frame Synchronization:
The FASTCAM Mini AX camera can be fully synchronized with an external event to allow the timing of when each individual image is captured to be precisely referenced. The camera can be accurately synchronized to unstable frequencies allowing complex events such as combustion in rapidly accelerating or decelerating engines to be recorded and studied.

Record During Download Operation:
FASTCAM Mini AX recording memory can be divided into multiple active sections. The user can record an on-going event in one memory partition while at the same time downloading a previously recorded image sequence in order to improve workflow and optimize camera operation.

Mini AX200

Resolution	Frame Rate	8GB		16GB		32GB	
(h x v pixels)	Max fps	Frames	Time (sec)**	Frames	Time (sec)**	Frames	Time (sec)**
1024 x 1024	6,400	5,457	0.85	10,918	1.71	21,841	3.41
1024 x 896	7,200	6,236	0.87	12,478	1.73	24,961	3.47
896 x 896	8,100	7,127	0.88	14,261	1.76	28,527	3.52
768 x 768	10,800	9,701	0.90	19,410	1.80	38,829	3.60
512 x 512	22,500	21,829	0.97	43,674	1.94	87,365	3.88
512 x 256	43,200	43,658	1.01	87,349	2.02	174,730	4.04
256 x 256	67,500	87,317	1.29	174,698	2.59	349,461	5.18
256 x 128	120,000	174,634	1.46	349,397	2.91	698,922	5.82
128 x 128	162,000	349,269	2.16	698,794	4.31	1,397,845	8.63
128 x 64	259,200	698,538	2.69	1,397,589	5.39	2,795,690	10.79
128 x 32	360,000	1,397,077	3.88	2,795,178	7.76	5,591,381	15.53
128 x 16	540,000	2,794,154	5.17	5,590,357	10.35	11,182,762	20.71
128 x 16	900,000						

Mini AX100

Resolution	Frame Rate	8GB		16GB		32GB	
(h x v pixels)	Max fps	Frames	Time (sec)**	Frames	Time (sec)**	Frames	Time (sec)**
1024 x 1024	4,000	5,457	1.36	10,918	2.73	21,841	5.46
1024 x 896	4,500	6,236	1.39	12,478	2.77	24,961	5.55
896 x 896	5,400	7,127	1.32	14,261	2.64	28,527	5.28
768 x 768	6,800	9,701	1.43	19,410	2.85	38,829	5.71
512 x 512	13,600	21,829	1.61	43,674	3.21	87,365	6.42
512 x 256	25,500	43,658	1.71	87,349	3.43	174,730	6.85
256 x 256	37,500	87,317	2.33	174,698	4.66	349,461	9.32
256 x 128	61,200	174,634	2.85	349,397	5.71	698,922	11.42
128 x 128	76,500	349,269	4.57	698,794	9.13	1,397,845	18.27
128 x 64	127,500	698,538	5.48	1,397,589	10.96	2,795,690	21.93
128 x 32	170,000	1,397,077	8.22	2,795,178	16.44	5,591,381	32.89
128 x 16	540,000	2,794,154	5.17	5,590,357	10.35	11,182,762	20.71

Mini AX50

Resolution	Frame Rate	8GB		16GB		32GB	
(h x v pixels)	Max fps	Frames	Time (sec)**	Frames	Time (sec)**	Frames	Time (sec)**
1024 x 1024	2,000	5,457	2.73	10,918	5.46	21,841	10.92
1024 x 896	2,500	6,236	2.49	12,478	4.99	24,961	9.98
896 x 896	2,500	7,127	2.85	14,261	5.70	28,527	11.41
768 x 768	3,600	9,701	2.69	19,410	5.39	38,829	10.79
512 x 512	7,200	21,829	3.03	43,674	6.07	87,365	12.13
512 x 256	13,600	43,658	3.21	87,349	6.42	174,730	12.85
256 x 256	20,400	87,317	4.28	174,698	8.56	349,461	17.13
256 x 128	37,500	174,634	4.66	349,397	9.32	698,922	18.64
128 x 128	45,900	349,269	7.61	698,794	15.22	1,397,845	30.45
128 x 64	76,500	698,538	9.13	1,397,589	18.27	2,795,690	36.54
128 x 32	127,500	1,397,077	10.96	2,795,178	21.92	5,591,381	43.85
128 x 16	170,000	2,794,154	16.44	5,590,357	32.88	11,182,762	65.78

* Specifications subject to change without notice.

** Recording time is an estimate and may be different depending on recording conditions and settings.

Photo
Schlieren imaging of fuel injection and engine combustion
20,000fps

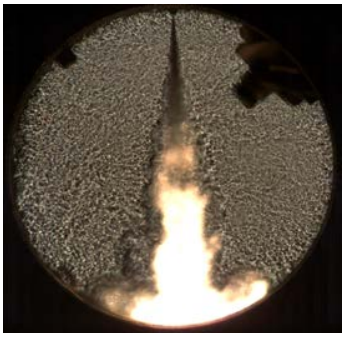

Mechanical & Environmental Specifications

Compatibility with Specialist Lens Systems:
A combination of small physical size, low weight and high light sensitivity allows the FASTCAM Mini AX to be coupled to a range of optical systems such as scientific and long distance microscopes, rigid endoscopes or borescopes, and image intensifiers for applications ranging from imaging flows in microfluidic devices to combustion diagnostics.

PIV and DIC Requirements:
FASTCAM Mini AX specifications match with the requirements for optical measurement techniques such as Particle Image Velocimetry (PIV) and Digital Image Correlation (DIC). The FASTCAM Mini AX has many key performance specifications desired for these measurement systems.

In PIV the detection of low light levels from small particles is fundamental. A high sensitivity image sensor allows the use of smaller tracer particles and/or lower laser power.

For DIC applications a highly sensitive camera allows the use of smaller objective lens apertures yielding greater depth of field and enhanced measurement of out of plane displacements.

Small Physical Size:
The small physical size and weight of the Mini camera range allows the use of conventional opto-mechanical hardware for rigid and stable mounting of multiple cameras, and for the location of cameras in space limited locations.

Specifications subject to change without notice.

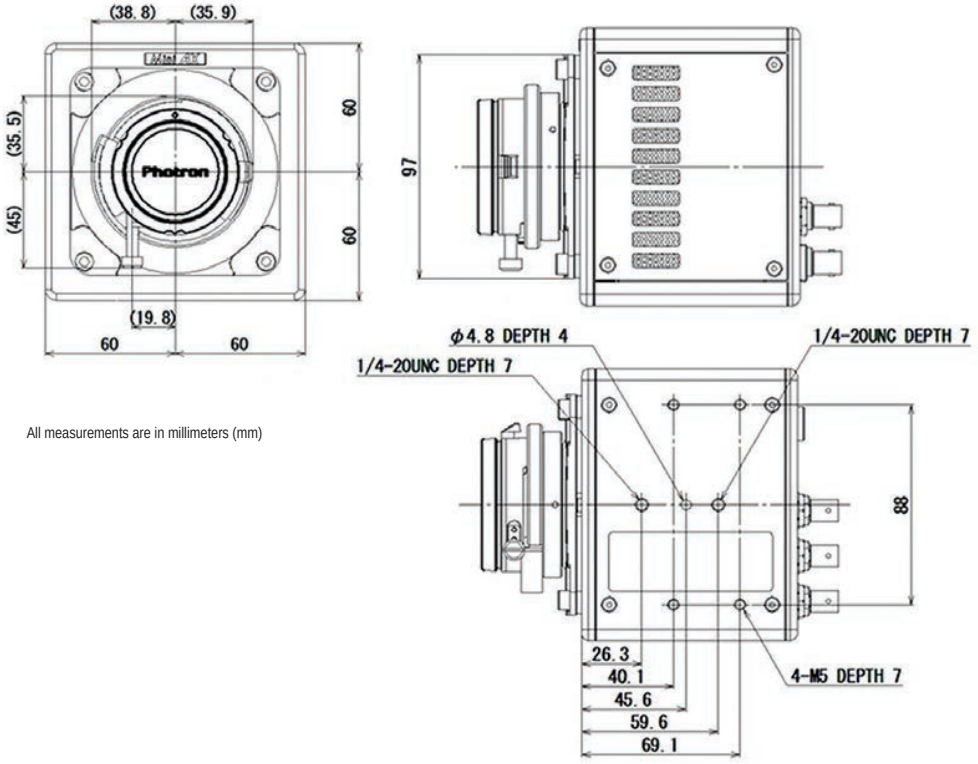

All measurements are in millimeters (mm)

Mechanical and Environmental Specifications

Mechanical	
Lens Mount	F-mount (G-type lens compatible) and C-mount provided - Optional lens mounts available include M42 adapter
Camera Mountings	4 x 1/4 - 20 UNC (base and top), 4 x M5 (base)
External Dimensions	
Camera Body (excluding protrusions)	120mm (H) x 120mm (W) x 94mm (D) 4.72" (H) x 4.72" (W) x 3.70" (D)
Weight	
Camera Body	1.5kg (3.30lbs)
Environmental	
Operating Temperature	0 to 40C, 32˚ to 104˚F
Storage Temperature	-20 to 60C, -4˚ to 140˚F
Humidity	85% or less (non-condensing)
Cooling	Internal fan cooling (fan-off mode supported)
Operational Shock	100G, 10ms, 6-axes
Power	
AC Power (with supplied adapter)	100 to 240V, 50 to 60Hz
DC Power	22 to 32V, 55VA

PHOTRON USA, INC.
9520 Padgett Street, Suite 110
San Diego, CA 92126
USA

Tel: 858.684.3555 or 800.585.2129
Fax: 858.684.3558
Email: image@photron.com
www.photron.com

PHOTRON EUROPE LIMITED
The Barn, Bottom Road
West Wycombe
Bucks. HP14 4BS
United Kingdom

Tel: +44 (0) 1494 481011
Fax: +44 (0) 1494 487011
Email: image@photron.com
www.photron.com

PHOTRON (Shanghai)
Room 20C, Zhao-Feng
World Trade Building
No. 369, JiangSu Road
Chang Ning District
Shanghai, 200050 China
Tel: +86 (21) 5268-3700
Fax: +86 (21) 5268-3702
Email: info@photron.cn.com
www.photron.cn.com

PHOTRON LIMITED
21F, Jinbocho Mitsui Bldg.
1-105 Kanda Jimbocho
Chiyoda-ku, Tokyo 101-0051
Japan

Tel: +81 (3) 3518-6271
Fax: +81 (3) 3 3518-6279
Email: image@photron.co.jp
www.photron.co.jp

REV# 21.01.04

C

Codes

C.1. Brix to H_2O_2 concentration

This section contains the data used to relate refractive index to H_2O_2 concentration. The refractometer used displays a value of ^{o}Brix. Using data from ICUMSA, [41], a relationship can be determined between ^{o}Brix and refractive index. The data used is displayed in Table C.1 which is used to make the plot in Figure C.1. From the plot Equation C.1 is derived where a ^{o}Brix value can be filled in for x, resulting in a y value which is the refractive index.

$$y = 7 \cdot 10^{-6}x^2 + 0.0014x + 1.3331 \tag{C.1}$$

Table C.1: Relationship between brix and refractive index [41].

^{o}Brix	Refractive index	^{o}Brix	Refractive index	^{o}Brix	Refractive index
0	1.33299	16	1.35729	31	1.38296
1	1.33442	17	1.35891	32	1.38478
2	1.33586	18	1.36054	33	1.38661
3	1.33732	19	1.36218	34	1.38846
4	1.33879	20	1.36384	35	1.39032
5	1.34026	21	1.36551	36	1.3922
6	1.34175	22	1.3672	37	1.39409
7	1.34325	23	1.36889	38	1.396
8	1.34477	24	1.3706	39	1.39792
9	1.34629	25	1.37233	40	1.39986
10	1.34782	26	1.37406	41	1.40181
11	1.34937	27	1.37582	42	1.40378
12	1.35093	28	1.37758	43	1.40576
13	1.3525	29	1.37936	44	1.40776
14	1.35408	30	1.38115	45	1.40978
15	1.35568				

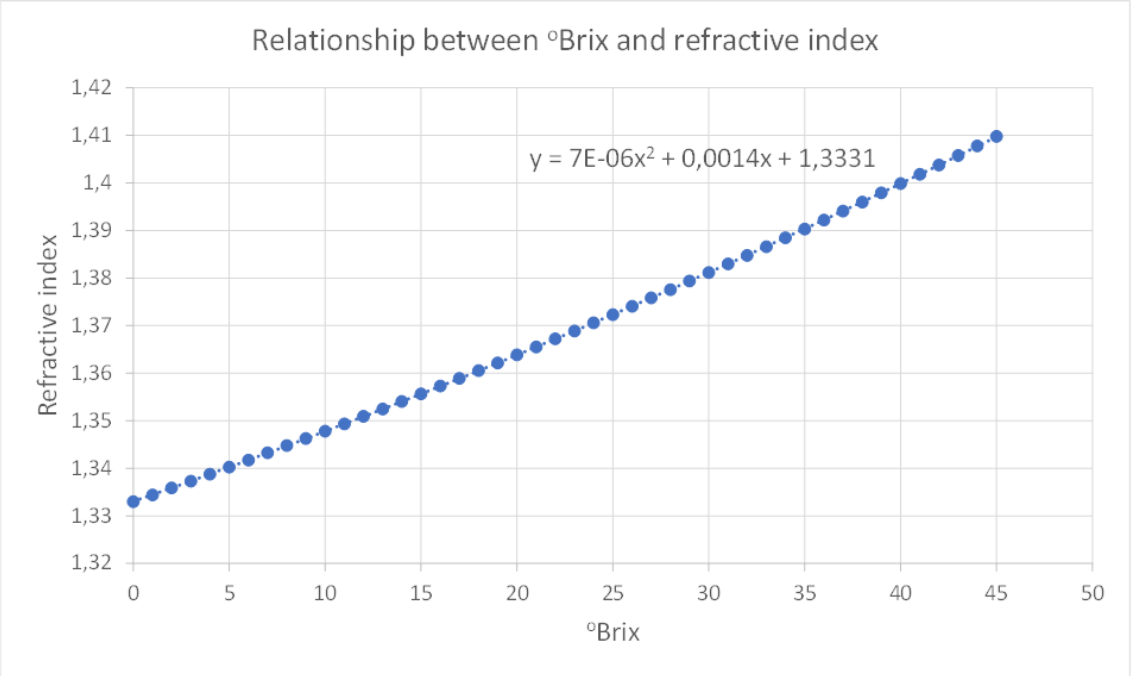

Figure C.1: Relationship between °Brix and refractive index plotted.

Then in a similar way the concentration of hydrogen peroxide is determined. Here data collected by P.A. Giguere and P. Geoffrion, [42], is used. Table C.2 shows this data. The data is plotted in Figure C.2 and a relationship is determined from it. Equation C.2 shows this relationship. The refractive index calculated using Equation C.1 can be filled in here as x, the resulting y value is equal to the concentration hydrogen peroxide.

$$y = -3329.4x^2 + 10452x - 8016.9 \tag{C.2}$$

Table C.2: Relationship between refractive index and concentration hydrogen peroxide [42].

wt% H_2O_2	**Refractive index**
0	1.33299
10.1	1.33946
19.98	1.34603
30.11	1.35296
40.03	1.35986
50.1	1.36724
60.66	1.37508
70.15	1.38284
79.86	1.39072
92.36	1.40157
96.26	1.40495
99.3	1.40774

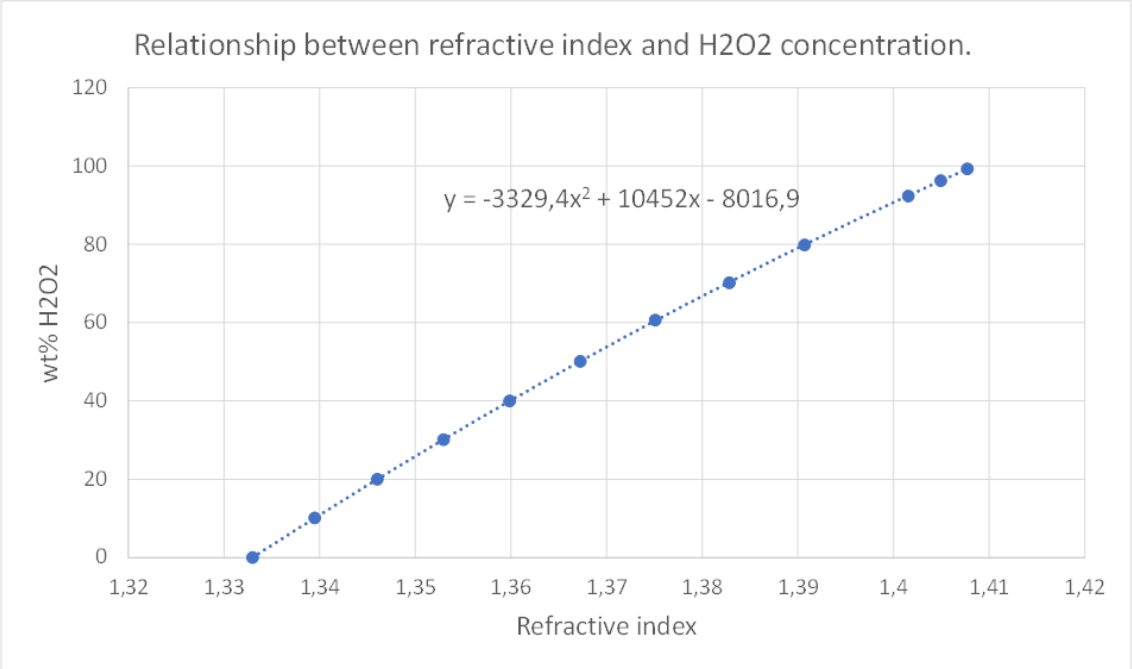

Figure C.2: Relationship between refractive index and concentration hydrogen peroxide plotted.

C.2. Additional delay for laser measurement

This section contains the matlab code used to calculate the time it takes for the droplet to travel from the laser beam to the top of the fuel pool. This time has to be subtracted from the delay measured by the laser/pd system.

```
clc
clear all

g = 9.81;                   %Gravitational acceleration [m/s^2]
Hd = 0.235;                 %Drop height from table in [m]
Tt = 0.004;                 %Thickness of the 3d printed structure [m]
Tp = 0.002;                 %Thickness of the petridish [m]
Tf = 0.0024;                %Height of the fuel drop [m] for 0.2ml of
    viscous fuel
Dl = 0.002;                 %Diameter of the laser beam [m]
Hl = 0.0142;                %Distance between the table and the bottom
    of the laser beam [m]

Ll = Hd - Hl - Dl;          %Distance the drop has to travel to the top
    of the laser beam [m]
Lf = Hd - Tt - Tp - Tf; %Distance the drop has to travel to the top
    of the fuel drop [m]

tl = sqrt(2*Ll/g);          %Time it takes for the drop to reach the top
     of the laser beam [s]
tf = sqrt(2*Lf/g);          %Time it takes for the drop to reach the top
     of the fuel drop [s]

```

```
18 Delay = tf-tl;           %Time it takes for the drop to pass through
    the laser and hit the fuel [s]
```

C.3. Labview script

This section contains the labview script used for collecting the photodiode and thermocouple data. The script is shown in Figure C.3. The DAQ assistant is used to collect data from the DAQ cards. A separate function is used for the photodiodes and thermocouples. This is necessary since data is collected at a different frequency. Then for both sensors a real time plot is presented. Collected data is written to a text file. This is also done separately due to the difference in sampling frequency.

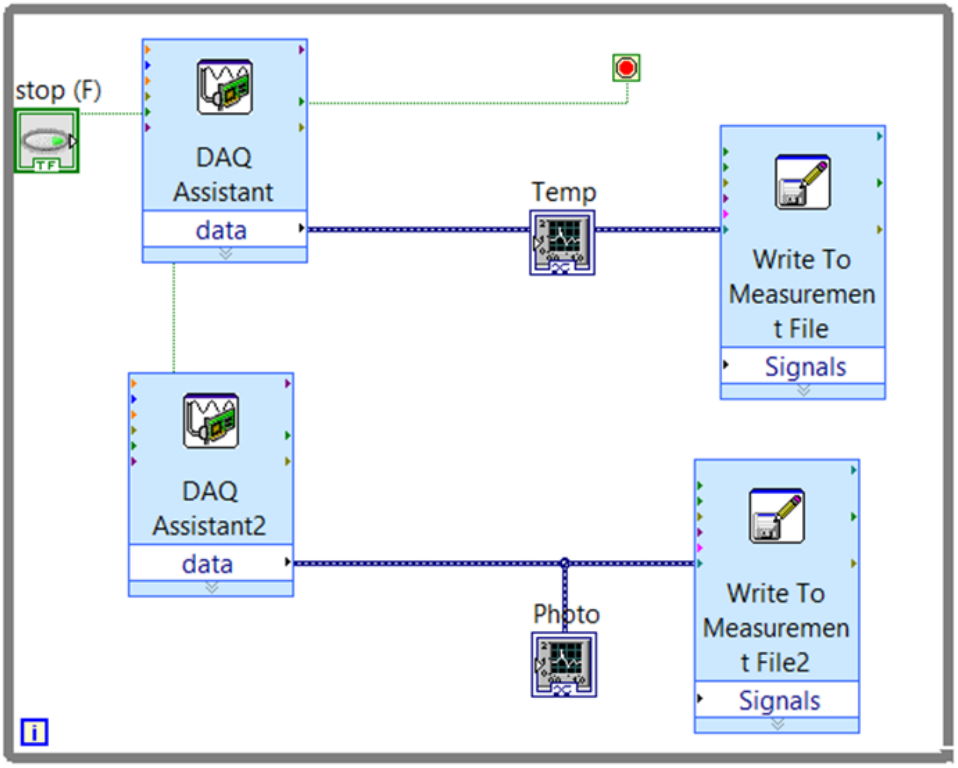

Figure C.3: Screenshot of the labview script used for data acquisition.